VOL.107 NO.HY10. OCT. 1981

JOURNAL OF THE HYDRAULICS DIVISION

PROCEEDINGS OF
THE AMERICAN SOCIETY
OF CIVIL ENGINEERS

VOL.107 NO.HY10. OCT. 1981

JOURNAL OF THE HYDRAULICS DIVISION

PROCEEDINGS OF THE AMERICAN SOCIETY OF CIVIL ENGINEERS

ISSN 0044-796X

Melvin W. Anderson, Editor
University of South Florida

AMERICAN SOCIETY OF CIVIL ENGINEERS

CONTENTS

The Journal of the Hydraulics Division (ISSN 0044-796X) is published monthly by the American Society of Civil Engineers. Publications office is at 345 East 47th Street, New York, N.Y. 10017. Address all ASCE correspondence to the Editorial and General Offices at 345 East 47th Street, New York, N.Y. 10017. Allow six weeks for change of address to become effective. Subscription price to members is $16.50. Nonmember subscriptions available; prices obtainable on request. Second-class postage paid at New York, N.Y. and at additional mailing offices. HY.

POSTMASTER: Send address changes to American Society of Civil Engineers, 345 East 47th Street, New York, NY 10017.

The Society is not responsible for any statement made or opinion expressed in its publications.

TECHNICAL NOTES

Proc. Paper 16531

DISCUSSION

Proc. Paper 16526

[a]Discussion period closed for this paper. Any other discussion received during this discussion period will be published in subsequent Journals.

INFORMATION RETRIEVAL

The key words, abstract, and reference "cards" for each article in this Journal represent part of the ASCE participation in the EJC information retrieval plan. The retrieval data are placed herein so that each can be cut out, placed on a 3 × 5 card and given an accession number for the user's file. The accession number is then entered on key word cards so that the user can subsequently match key words to choose the articles he wishes. Details of this program were given in an August, 1962 article in CIVIL ENGINEERING, reprints of which are available on request to ASCE headquarters.

*Discussion period closed for this paper. Any other discussion received during this discussion period will be published in subsequent Journals.

16552 SETTLING VELOCITY OF SPHERICAL PARTICLES IN CALM WATER

KEY WORDS: Drag; Experimental data; **Particles;** Sediment transport; **Settling velocity; Spheres;** Turbulence

ABSTRACT: The settling velocities of round and smooth spherical particles in calm water at 200 /LT R /LT 6,000 were analysed utilizing modern measuring techniques. When the present results are compared with the "standard" CTS = f(R) curve, they fall on the average 20 percent higher. However, the "standard" curve was established with the majority of data derived from fixed spheres tested in wind tunnels. Because the experiments are limited, a new drag coefficient cannot be made. To settle the existing discrepancy between "fixed" and "falling" spheres, it will be necessary to do further research, Possibly focusing on the effect of the Strouhal number on the drag of freely falling spheres.

REFERENCE: Boillat, Jean L. (Research Asst., Lab. D'Hydraulique, Ecole Polytechnique Federal, CH-1015 Lausanne, Switzerland), and Graf, Walter H., "Settling Velocity of Spherical Particles in Calm Water," *Journal of the Hydraulics Division,* ASCE, Vol. 107, No. HY10, **Proc. Paper 16552**, October, 1981, pp. 1123-1131

16549 LENGTH OF FLOW SEPARATION OVER DUNES

KEY WORDS: Bed roughness; **Dimensional analysis; Dunes; Dune sands; Flow separation;** Flow visualization; Grain size; **Open channel flow; Sands;** Two dimensional flow; Uniform flow

ABSTRACT: Dimensional analysis was used to define the length of the flow saparation for the case of two-dimensional, uniform flow over dunes, which was expressed in terms of bed-form geometry and the sand size of the bed material. Experiments were conducted in a rectangular flume using artificial dunes and a flow visualization method to measure the flow separation length. When dunes are flat, length of the flow separation is affected by the sand-grain roughness. When dunes are steep, the length of the flow separation is due mainly to the bed-form geometry and is relatively constant. The reverse rectangular steps can be considered as dunes of infinite length, and the length of the flow separation for such steps will always be greater than that obtained for dunes of finite length.

REFERENCE: Engel, Peter (Research Engr., Environmental Hydr. Sect., Hydr. Div., National Water Research Inst., Canada Center for Inland Waters., P.O. Box 5050, Burlington, Ontario, Canada L7R 4A6), "Length of Flow Separation over Dunes," *Journal of the Hydraulics Division,* ASCE, Vol. 107, No. HY10, **Proc. Paper 16549**, October, 1981, pp. 1133-1143

16541 ALGORITHMS FOR PIPE NETWORK ANALYSIS

KEY WORDS: **Algorithms;** Convergence; Converging flow; **Network analysis;** Network analyzers; **Piping systems;** Reliability; **Water distribution**

ABSTRACT: Algorithms for analyzing steady-state flow conditions in pipe networks are described for general applications. The algorithms are based on both loop equations expressed in terms of unknown flowrates and node equations expressed in terms of unknown heads. Five methods, which represent those in significant use today, are included. Using an extensive data base, describing a variety of pipe networks, the reliabilities of these algorithms for pipe network analysis were investigated. Numerous convergence and reliability problems were documented. Two methods based on loop equations have superior convergence characteristics. Methods based on node equations were less reliable; single adjustment methods must be employed with caution.

REFERENCE: Wood, Don J. (Prof., Dept. of Civ. Engrg., Univ. of Kentucky, Lexington, Ky. 40506), and Rayes, A. G., "Reliability of Algorithms for Pipe Network Analysis," *Journal of the Hydraulics Division,* ASCE, Vol. 107, No. HY10, **Proc. Paper 16541**, October, 1981, pp. 1145-1161

16540 SLUICE AND SPILLWAY FLOWS

KEY WORDS: **Boundary conditions;** Calculations; Contraction; Discharge (water); **Flow characteristics; Laplace equation;** Numerical analysis; **Sluice gates; Spillways**

ABSTRACT: The classical problems of steady-state flow under a sluice gate and over a spillway are solved by the boundary integral equation method. In both cases an iterative methods is used to adjust the free-surface profiles until they satisfy both the kinematic and dynamic boundary conditions. In the case of sluice gate flow, a point by point adjustment method is used which quickly converges to the correct solution within three to six iterations. The results closely check previous, less efficient calculations. Some of the variation is past experimental results is explained by calculations in which the geometry of the gate is altered slightly near the tip. Even a small change from the ideal geometry can have a major effect on the contraction coefficient. Flow over a spillway is a more difficult problem due to poor convergence properties in the free-surface profile behind the spillway crest.

REFERENCE: Cheng, Alexander H-D. (Grad. Student, School of Civ. and Environmental Engrg., Cornell Univ., Ithaca, N.Y. 14853), Liggett, James A., and Liu, Philip L-F., "Boundary Calculations of Sluice and Spillway Flows," *Journal of the Hydraulics Division,* ASCE, Vol. 107, No. HY10, **Proc. Paper 16540**, October, 1981, pp. 1163-1178

16535 JET INJECTIONS FOR OPTIMUM MIXING IN PIPE FLOW

KEY WORDS: **Diffusion; Discharge measurement;** Discharge (water); Injection; Jet flow; **Mixing;** Optimization; **Pipe flow;** Secondary flow; Solutes

ABSTRACT: The use of jet injections, as contrasted to injections with no momentum, can help to reduce the pipe flow distance required for the mixing of injected and ambient fluids without requiring appurtenances or devices inside the pipe. For uniform, turbulent flow, experiments were conducted to determine the optimum injection conditions for a single jet at the pipe wall at 90° to 150° relative to the ambient flow, and for two jets at 90°. Depending on the type of injection and the desired degree of mixing, the required flow distance can be reduced up to 70 percent compared to injection with no momentum. For uniform flow, there are only small benefits from using more than two injection points. However, the two experiments which were conducted with a secondary current in the pipe flow indicated greater benefits from using multiple-point injection.

REFERENCE: Fitzgerald, Steven D. (Sr. Grad. Engr., Turner Collie & Braden Inc., Houston, Tex.), and Holley, Edward R., "Jet Injections for Optimum Mixing in Pipe Flow," *Journal of the Hydraulics Division,* ASCE, Vol. 107, No. HY10, **Proc. Paper 16535**, October, 1981, pp. 1179-1195

16539 EQUATION FORMULATION FOR GROUND-WATER FLOW

KEY WORDS: **Boundary value problems;** Boundary values; Computation; Computers; **Ground water;** Numerical analysis; **Porous media; Porous media flow; Seepage; Two dimensional flow**

ABSTRACT: Advantages of boundary integral equation methods (BIEM) for the analysis of two-dimensional flows through porous media are numerous. The data required and the number of unknowns are significantly fewer than for other general, numerical methods such as finite differences of finite element methods. A BIEM based on the Cauchy integral equation is developed. This formulation has the advantage that the equation used for any unknown is a Fredholm equation of the second kind which results in well-conditioned equations and allows nodes to be closely spaced in the region of singularities. The method is extended to the analysis of multizone, anisotropic flows. Computational algorithms for solution of the equations by a simple iterative method and by direct solution of the full set of simultaneous linear equations are developed.

REFERENCE: Hunt, Bruce (Reader in Civ. Engrg., Univ. of Canterbury, Christchurch, 1 New Zealand), and Isaacs, Lewis T., "Integral Equation Formulation for Ground-Water Flow," *Journal of the Hydraulics Division,* ASCE, Vol. 107, No. HY10, **Proc. Paper 16539**, October, 1981, pp. 1197-1209

16587 EROSION RESISTANCE OF COHESIVE SOILS

KEY WORDS: **Clays; Cohesive soils; Erosion; Rheology;** Salinity; **Soil erosion; Soil mechanics;** Soil strength; Temperature; Velocity; Water content (soils)

ABSTRACT: An experimental study is described that concerned the surface erosion of an illitic silty clay (Grundite) at selected salinities and water contents; the study was designed to test the applicability of rate process and double layer theories. Both velocity increment and temperature increment tests were run in a refrigerated water tunnel. Experimental activation energies and flow volumes were computer from test results. Values for experimental activation energies range from 14 to 32 kcal/mole, suggesting that interparticle contacts are essentially solid to solid as for soil deformation at higher stress levels. The mechanisms controlling resistance to surface erosion are fundamentally similar to the mechanisms controlling soil strength.

REFERENCE: Kelly, William E. (Assoc. Prof., Dept. of Civ. Engrg., Univ. of Rhode Island, Kingston, R. I.), and Gularte,, "Erosion Resistance of Cohesive Soils," *Journal of the Hydraulics Division,* ASCE, Vol. 107, No. HY10, **Proc. Paper 16587**, October, 1981, pp. 1211-1224

16602 ICE COVER EFFECTS ON STREAM FLOWS AND MIXING

KEY WORDS: **Channels (waterways); Computation; Dispersion;** Equivalence; Flow charting; **Flow rate;** Free surfaces; **Ice cover;** Numerical analysis; **Stream flow; Turbulent flow; Velocity**

ABSTRACT: The distributions of velocity, turbulent eddy, and mass diffusivities were computed for three pairs of free-surface and ice-covered flows using the k-ϵ turbulence model. The flow rate, channel slope, and bottom roughness values were kept the same for each pair of flows and the flow depths were computed. The resulting flow depths for ice-covered flows were 15 to 30 percent higher than the depths for free-surface flows. The computed velocity and eddy viscosity distributions do not follow the conventional logarithmic and parabolic distributions for the whole depth of flow. Concentration distributions resulting from the introduction of a neutrally buoyant tracer were computed for all the flows.

REFERENCE: Lau, Y. Lam (Head, Environmental Hydr. Section, Hydr. Research Div., National Water Research Inst., Canada Centre for Inland Waters, Burlington, Ontario, Canada, L7R 4A6), and Krishnappan, Bommanna G., "Ice Cover Effects on Stream Flows and Mixing," *Journal of the Hydraulics Division,* ASCE, Vol. 107, No. HY10, **Proc. Paper 16602**, October, 1981, pp. 1225-1242

16603 COMPARISON OF FREE SURFACE VORTICES

KEY WORDS: **Field tests;** Free surfaces; **Inlets (waterways); Models;** Prototypes; Scale effect; **Vortices; Waterways**

ABSTRACT: A Comparison between model and prototype observations of vortex intensity is used to investigate potential scale effects of modeling free surface vortices. Due to the inherent difficulty with field observations, a reasonably large number of such comparisons are needed prior to reaching conclusions. To this end, a survey of available model-prototype data is made and presented in summary form for a variety of intake types. Based on this comparison summary, and referring to previously published research on this subject, some scale effects may exist when modeling air core vortices, and some increase in model flow may compensate for such effects. Little or no scale effect is evident for weak vortices or dimples. Recommendations are made for conducting model tests.

REFERENCE: Hecker, George E. (Dir., Alden Research Lab.; also, Assoc. Prof., Civ,. Engrg. Dept., Worcester Polytechnic Inst., Holden, Mass. 01520), "Model-Prototype Comparision of Free Surface Vortices," *Journal of the Hydraulics Division,* ASCE, Vol. 107, No. HY10, **Proc. Paper 16603**, October, 1981, pp. 1243-1259

U.S. Customary-SI Conversion Factors

In accordance with the October, 1970 action of the ASCE Board of Direction, which stated that all publications of the Society should list all measurements in both U.S. Customary and SI (International System) units, the following list contains conversion factors to enable readers to compute the SI unit values of measurements. A complete guide to the SI system and its use has been published by the American Society for Testing and Materials. Copies of this publication (ASTM E-380) can be purchased from ASCE at a price of $3.00 each; orders must be prepaid.

All authors of *Journal* papers are being asked to prepare their papers in this dual-unit format. To provide preliminary assistance to authors, the following list of conversion factors and guides are recommended by the ASCE Committee on Metrication.

To convert	To	Multiply by
inches (in.)	millimeters (mm)	25.4
feet (ft)	meters (m)	0.305
yards (yd)	meters (m)	0.914
miles (miles)	kilometers (km)	1.61
square inches (sq in.)	square millimeters (mm^2)	645
square feet (sq ft)	square meters (m^2)	0.093
square yards (sq yd)	square meters (m^2)	0.836
square miles (sq miles)	square kilometers (km^2)	2.59
acres (acre)	hectares (ha)	0.405
cubic inches (cu in.)	cubic millimeters (mm^3)	16,400
cubic feet (cu ft)	cubic meters (m^3)	0.028
cubic yards (cu yd)	cubic meters (m^3)	0.765
pounds (lb) mass	kilograms (kg)	0.453
tons (ton) mass	kilograms (kg)	907
pound force (lbf)	newtons (N)	4.45
kilogram force (kgf)	newtons (N)	9.81
pounds per square foot (psf)	pascals (Pa)	47.9
pounds per square inch (psi)	kilopascals (kPa)	6.89
U.S. gallons (gal)	liters (L)	3.79
acre-feet (acre-ft)	cubic meters (m^3)	1,233

SETTLING VELOCITY OF SPHERICAL PARTICLES IN CALM WATER

By Jean L. Boillat[1] and Walter H. Graf,[2] M. ASCE

INTRODUCTION

During a study on the effect of turbulence on the settling velocity by the writers (4), some interesting experimental observations have become evident on the settling velocity of spheres in a calm, thus nonturbulent, water. The writers would like to communicate these findings herewith.

EXPERIMENTAL SETUP

The experimental installation was described in detail in Refs. 2 and 3; it should suffice to give but a brief review. The *spheres* being perfectly spherical and smooth, had diameters of $0.200 \text{ cm} \leq D \leq 1.905 \text{ cm}$ and densities of $1.018 \text{ g/cm}^3 \leq \rho_s \leq 2.700 \text{ g/cm}^3$. They were freely-falling in a rectangular and transparent *container* having the dimensions of 130 cm × 130 cm × 80 cm; the latter was filled with water of a temperature of $17.6° \leq T° \leq 24.1°$, thus of quasiconstant density of $\rho \simeq 0.9983 \text{ g/cm}^3$ and of a viscosity of $0.0106 \text{ cm}^2/\text{s} \leq \nu \leq 0.0091 \text{ cm}^2/\text{s}$. The experiments covered a Reynolds number range of $140 \leq R \leq 13{,}394$, with $R = v_{ss}D/\nu$. To ensure that the particle's settling velocity, v_{ss}, is not influenced by boundary effects such as the surrounding walls, the particle's departure and arrival, a prestudy (see Ref. 2) was performed which rendered that measurements should only be taken in the zone called DEC (domaine expérimental confiné), to be seen schematically in Fig. 1.

Special attention was taken that the spheres were introduced, with zero departure velocity, without rotation and without air bubbles being attached. The spheres were released 5 cm or more underneath the ceiling, using a special spring-clamp device to achieve this. In order to measure the *time of settling* accurately, the following system was developed: 2 cameras and a video recorder were employed to film (1) The entrance and exit respectively of the sphere

[1]Research Asst., Lab. d'hydraulique, Ecole Polytechnique Federale, CH-1015 Lausanne, Switzerland.

[2]Prof. and Dir., Lab. d'hydraulique, Ecole Polytechnique Federale, CH-1015 Lausanne, Switzerland.

Note.—Discussion open until March 1, 1982. To extend the closing date one month, a written request must be filed with the Manager of Technical and Professional Publications, ASCE. Manuscript was submitted for review for possible publication on December 10, 1980. This paper is part of the Journal of the Hydraulics Division, Proceedings of the American Society of Civil Engineers, ©ASCE, Vol. 107, No. HY10, October, 1981. ISSN 0044-796X/81/0010-1123/$01.00.

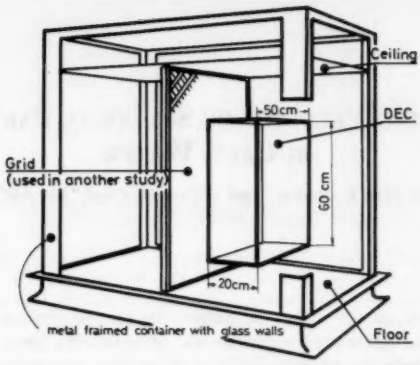

FIG. 1.—Schema of Container; Showing Zone DEC, where Measurements Are Performed

in the measuring zone (DEC); and (2) the clock indicating entrance and exit time respectively. The entire process was also restituated on a TV monitor. Subsequently the taped images were analysed by reading the time of passage of the sphere into and out of the measuring zone. In this way a precision in the time measurement of 1/40 sec was achieved.

Experimental Results

All of the present experimental data are plotted on the conventional drag coefficient, CT, versus Reynolds number, R, diagram in Fig. 2(*a*).

In Fig. 2, one immediately observes that the present data do not fall on the "standard" CTS = $f(R)$ curve as given, e.g., by Schlichting (Ref. 8, p. 17). Since the experiments were performed under extreme experimental control the writers exclude, for the time being, that these deviations could be attributed to experimental errors.

However, it became evident that a repeated experiment, with the same sphere and under identical experimental conditions, showed a certain scattering. It is therefore that the "median" of each set is more representative; see Fig. 2(*b*). In Table 1 these "median" data are listed, with all the experimental information.

A polynomial regression fit to the present data amounted to a new "reference" CTR = $f(R)$ curve, which is given in Fig. 3. The dotted lines, at the CTR = $f(R)$ curve on the two extreme ends of the experimental range, indicate that due to lack of sufficient data, a certain caution is in place. Nevertheless within the zone of $2 \times 10^2 < R < 6 \times 10^3$, the ratio of CTR/CTS is always higher than 1.10 and may get as high as 1.3. Furthermore, it will not escape to the observer that in the CTR = $f(R)$ plot at $R \leq 2 \times 10^3$ there exists a distinguishable hump.

Before the writers' results are considered, it seems in place to review whether similar observations on deviation from the standard curve have been made before.

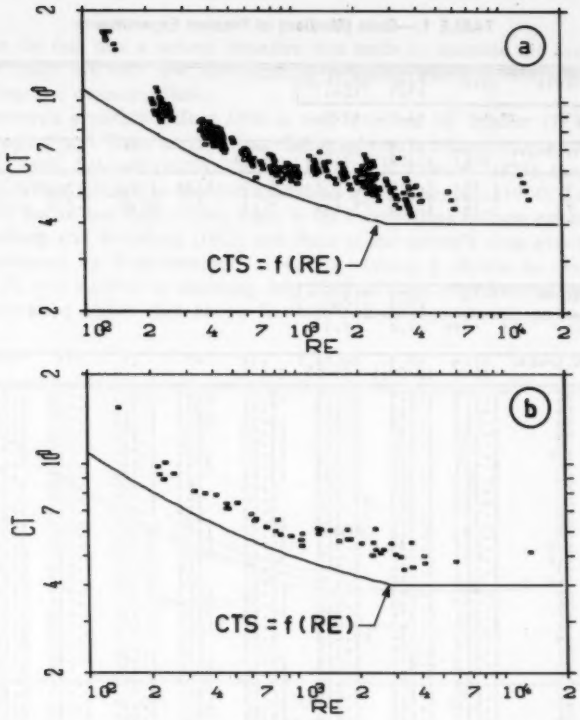

FIG. 2.—Experimental Results Compared with Standard Curve, CTS = f(R): (*a*) All Data; (*b*) Median of all Data

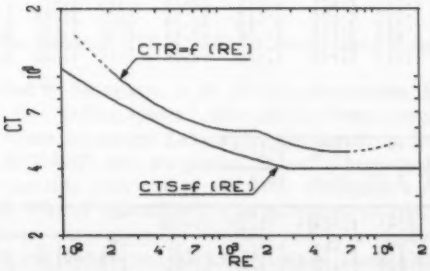

FIG. 3.—Representation of Curves: CTS = f(R) and CTR = f(R)

TABLE 1.—Data (Median) of Present Experiments

SERIE	DATE	TEMP (°C)	DELTA_L (CM)
15	17 10 77	17.6	60.0

N.SPHERE	DIAM (CM)	RO_S (G/CM3)	DELTA_T (SEC)	VSS (CM/S)	RE	CT	CTS	CTA
1G	1.303	2.155	[illegible]	75.50	13344	[illegible]	[illegible]	[illegible]
1A	0.531	1.068	6.425	9.75	521	0.735	0.533	0.627
7J	0.299	1.146	7.900	7.69	216	0.976	0.745	1.030

SERIE	DATE	TEMP (°C)	DELTA_L (CM)
16	18 7 79	20.0	60.0

N.SPHERE	DIAM (CM)	RO_S (G/CM3)	DELTA_T (SEC)	VSS (CM/S)	RE	CT	CTS	CTA
2G	1.273	1.129	3.175	18.96	2393	[illegible]	[illegible]	[illegible]
1A	1.270	1.019	3.100	7.41	935	0.575	0.438	0.598
3G	0.640	1.180	3.650	16.44	1049	0.562	0.445	0.590
4G	0.505	1.157	4.750	12.63	636	0.657	0.551	0.648
5G	0.397	1.191	5.150	11.65	461	[illegible]	[illegible]	0.716
12G	0.297	1.382	4.350	13.79	409	0.786	0.629	0.760
5G	0.801	1.446	2.000	30.00	2346	0.521	0.411	0.534
6G	0.302	1.368	4.400	13.64	411	0.796	0.627	0.748
7G	0.300	1.175	6.950	8.63	259	0.927	0.735	0.931
7Z	0.301	1.083	12.875	4.66	140	1.535	0.537	1.373
8G	0.405	1.050	11.000	5.45	220	0.920	0.730	1.019
9G	0.305	2.157	2.150	27.91	435	[illegible]	[illegible]	[illegible]
7B	0.400	2.162	1.900	31.58	1253	0.611	0.486	0.641
10G	0.502	2.138	1.650	36.36	1820	0.566	0.432	0.580
11G	0.601	2.147	1.425	42.11	2525	0.510	0.408	0.527
3J	0.421	1.376	3.350	17.91	716	0.617	0.534	0.629
4J	0.400	1.100	7.400	8.11	323	0.812	0.679	0.831
8S	0.799	1.143	3.750	16.00	1275	0.598	0.465	0.581
8G	0.800	1.099	4.500	13.33	1064	0.559	0.444	0.589
9J	1.001	1.374	1.900	31.58	3154	0.494	0.400	0.502
9J	0.999	1.143	3.400	17.65	1758	0.608	0.435	0.641
9J	0.609	1.034	10.000	6.00	364	0.797	0.652	0.787
9J	0.498	1.035	7.975	7.52	376	0.685	0.554	0.656
9J	1.210	1.343	1.750	34.29	4137	0.471	0.400	0.492
9Z	1.507	1.361	1.550	38.71	5818	0.477	0.400	0.472
9J	1.201	1.193	2.430	25.00	2933	0.502	0.405	0.517
9J	1.199	1.161	3.500	17.14	2051	0.549	0.423	0.558
9S	1.506	1.186	2.200	27.27	4095	0.437	0.400	0.443
9S	1.500	1.100	3.150	19.05	2844	0.544	0.430	0.512
3POM	0.300	1.450	3.800	15.79	472	0.712	0.521	0.725
4POM	0.400	1.450	3.025	19.83	791	0.601	0.520	0.616
6POM	0.600	1.450	2.475	24.24	1450	0.604	0.452	0.579
8POM	0.800	1.450	2.050	29.27	2335	0.552	0.413	0.537
3PA	0.301	1.157	7.650	7.84	235	1.004	0.761	0.941
5PA	0.500	1.157	4.750	12.63	630	0.649	0.552	0.649
12PA	1.200	1.157	2.750	21.82	2611	0.522	0.405	0.522
15PA	1.500	1.157	2.525	23.76	3554	0.555	0.430	0.492
9PUR	0.900	1.260	2.725	22.02	1757	0.565	0.435	0.581
3V	0.300	2.700	1.700	35.29	1056	0.537	0.445	0.590
4V	0.400	2.700	1.500	40.00	1596	0.557	0.443	0.579
5V	0.501	2.700	1.310	46.15	2321	0.523	0.414	0.540
6V	0.600	2.700	1.100	54.55	3264	0.449	0.400	0.499

SERIE	DATE	TEMP (°C)	DELTA_L (CM)
17	18 7 79	20.2	60.0

N.SPHERE	DIAM (CM)	RO_S (G/CM3)	DELTA_T (SEC)	VSS (CM/S)	RE	CT	CTS	CTA
2POM	0.200	1.449	5.200	11.54	231	0.886	0.766	0.993
4PM	0.393	1.195	5.150	11.65	459	0.709	0.606	0.717
5PUR	0.500	1.260	4.700	16.22	813	0.651	0.516	0.613
79PA	0.794	1.157	3.650	16.44	1308	0.608	0.462	0.580
12PUR	1.200	1.260	2.600	30.00	3614	0.457	0.400	0.491

OTHER STUDIES

Despite the fact that a serious tentative was made to examine the available literature, there are only few investigations available which in fact study the free settling in a quiescent fluid.

The research available before 1930 is well-reviewed by Schiller (7) and is reproduced in Fig. 4. There are the freely-falling spheres in laboratory experiments by Allen (1900), Schmidt (1920), Liebster (1927) and Lunnon (1928); there are the freely-falling spheres in outdoor conditions by Shakespeare (1914), Lunnon (1924) and Bacon and Reid (1924); there is the freely-rising balloon experiment by Hesselberg and Birkeland (1912) and there is the sphere's drag experiment in a windtunnel by Wieselsberger (1914). In addition it should be said that Schiller (7) was careful in choosing only data of high experimental quality. Eye observation shows that above R > 200, deviations though not always

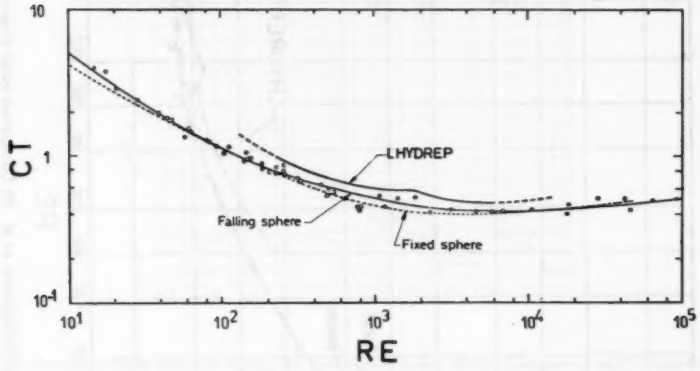

FIG. 4.—Data from Schiller (7) Compared with Present LHYDREP Data

systematic from the standard CTS = f(R) do occur; even a certain hump is evident.

In a study reported by Stringham, et al. (9) it is also evident that the "fixed sphere" data and the "falling sphere" data give different results. This may be seen in Fig. 5, where the present Laboratoire d'hydraulique, Ecole Polytechnique Fédérale (LHYDREP) data are plotted as well. Interestingly enough the hump appears to coincide with our experiments. Stringham's et al. (9) data were obtained with spheres of steel and plastic, which fell freely in different liquids such as water, water-glycerine mixtures and pure glycerine through a cylindrical tube, 40 cm in diam and 300 cm in height. These authors observed that notably the plastic spheres "exhibited small erratic horizontal movement." Nevertheless the authors assign the systematic deviations of their data from the "standard" curve to experimental errors.

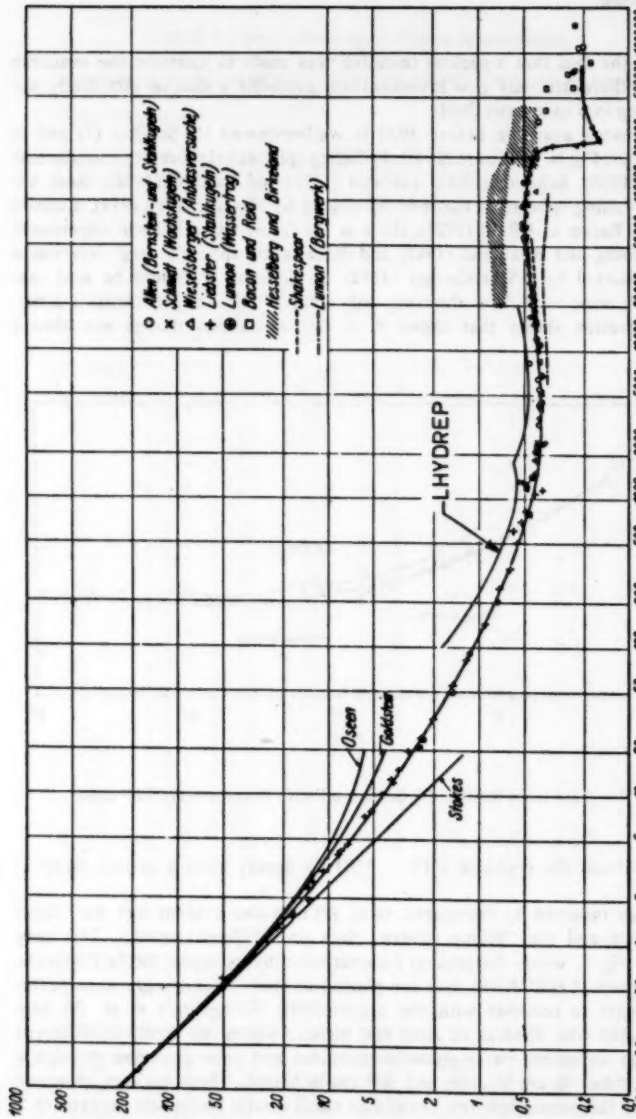

FIG. 5.—Data from Stringham, et al. (9) Compared with Present LHYDREP Data

ANALYSIS

The present writers submit to have no reason that their experimental setup and the data-taking procedure can be made responsible for such large deviations and account for experimental errors of this magnitude. As previously mentioned, deviations from the standard CTS = f(R) relationship are after all also reported by Schiller (7) and more recently by Stringham, et al. (9).

In the following the writers shall put forward some speculative ideas as to why the present data's CTR = f(R) show differencies if compared with "standard" CTS = f(R).

Firstly it appears that the standard CTS = f(R) curve was established mainly—if not exclusively—with data obtained on fixed spheres in wind tunnels; and this particularly in the region of R ≥ 800 [see Murray (6) p. 304]. Already Schiller (7) pointed to the fact that a windtunnel has always a certain degree of turbulence super-imposed upon the free-stream velocity, which could modify the drag coefficient. Secondly, it is important to note that in windtunnel experiments

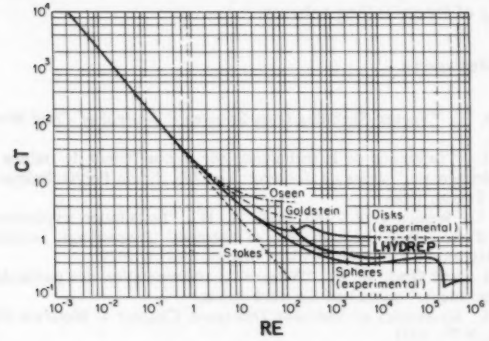

FIG. 6.—Data from Second Writer (5) for Spheres and Disks Compared with Present LHYDREP Data

the spheres are fixed in place. However, a freely-falling sphere will adjust its path according to R dependent vortex shedding at its rear, which in turn will lead to an oscillatory descent of the sphere. Theory of similarity would suggest that an adimensional frequency of oscillation—such as the Strouhal number S = nD/v_{ss}—should become an additional parameter. Unfortunately the measuring technique was not designed for observation of the entire path of the falling sphere and thus for evaluation of these frequencies. On the other hand, a good S = f(R) relationship for spheres is at the present not available [see Achenbach (1) and Taneda (10)].

From the foregoing it is reasonable to expect that spheres falling freely through a calm fluid render different results. Interestingly enough and thus supporting the writers' point the CT = f(R) relationship for disks reproduced in Fig. 6, was obtained for freely-falling disks and does show a pronounced hump. A falling disk wabbles, resulting in a pronounced Strouhal number effect. While there exist to the writers' knowledge no fixed-disk data in this hump region

($R \simeq 300$), Schiller (7) expressed convincingly that an absence of a hump would become evident.

Conclusions

The settling velocities of round and smooth spherical particles in calm water at $2 \times 10^2 < R < 6 \times 10^3$ were analyzed utilizing modern measuring techniques. If the present results are compared with the "standard" CTS = $f(R)$ curve, they fall on the average 20% higher as is to be seen in Fig. 3. However, the "standard" curve was established with the majority of data derived from fixed spheres tested in windtunnels. The experiments of Schiller (7) and of Stringham, et al. (9) show the same tendency as observed in the present data. To make a recommendation for a new drag-coefficient curve for freely falling spheres is premature in the light of the writers' limited experiments. To settle the existing discrepancy between "fixed" and "falling" spheres, it will be necessary that further research is done, possibly focusing on the effect of the Strouhal number S on the drag of freely falling spheres.

Appendix I.—References

1. Achenbach, E., "Vortex Shedding from Spheres," *Journal of Fluid Mechanics*, Vol. 62/2, 1974.
2. Boillat, J.-L., "Influence de la turbulence sur le coefficient de traînée des sphères, Etude expérimentale," *thèse de doctorat No. 388*, Ecole Polytechnique Fédérale de Lausanne, Suisse, 1980.
3. Boillat, J. L., Weske, J. R., and Graf, W. H., "Installation expérimentale pour la simulation d'une turbulence homogène et isotrope," *Proceedings*, International Association of Hydraulic Research, XVIII Congrès, Vol. 3, 1979.
4. Boillat, J.-L., and Graf, W. H., "Vitesse de sédimentation des particules sphériques en milieu turbulent," submitted for publication.
5. Graf, W. H., *Hydraulics of Sediment Transport*, Chapter 4, McGraw-Hill Book Co.; New York, N.Y., 1971.
6. Murray, H. "Die experimentellen Tatsachen des Widerstandes ohne Auftrieb," *Handbuch der Experimental-physik*, Vol. IV/2; Akad. Verlagsges., Leipzig, Germany, 1932.
7. Schiller, L., "Fallversuche mit Kugeln und Scheiben," *Handbuch der Experimentalphysik*, Vol. IV/2; Akad. Verlagsges., Leipzig, Germany, 1932.
8. Schlichting, H., *Boundary Layer Theory*, McGraw-Hill Book Co., Inc., New York, N.Y., 1968.
9. Stringham, G. H., Simons, D. B., and Guy, H. P., "The Behavior of Large Particles Falling in Quiescent Liquids," *Professional Paper 562-C*, United States Geological Survey, 1969.
10. Taneda, S., "Visual observations of the flow past a sphere at Reynolds numbers between 10^4 and 10^6," *Journal of Fluid Mechanics*, Vol. 85/1, 1978.

Appendix II.—Notation

The following symbols are used in this paper:

CT = general drag coefficient;
CTR = reference drag coefficient;
CTS = standard drag coefficient;

D = diameter of spherical particle;
R = $v_{ss} D/\nu$ = Reynolds number;
S = $n D/v_{ss}$ = Strouhal number;
v_{ss} = spherical particle's settling velocity;
ν = kinematic viscosity;
ρ = density of water; and
ρ_s = density of spherical particle.

LENGTH OF FLOW SEPARATION OVER DUNES

By Peter Engel[1]

INTRODUCTION

Open-channel flow over a mobile granular bed is a complex process because of the interrelationship between the fluid and the bed. When the flow is tranquil (Froude number <1), the water may deform the bed into ripples or dunes depending on the flow conditions and the grain size of the bed material. As the flow passes over each bed form, separation occurs at the crest creating a wake or eddy which extends some distance downstream to the point of reattachment on the back of the next bed form. Within these separation zones, reverse circulations exist. Knowledge of the length of the flow separation is useful in solving a variety of hydraulic problems. Crickmore (2) and the writer and Lau (3) developed equations to compute bed-load discharge from bed-profile records of migrating dunes, in which the position of the point of reattachment was an important consideration. Vanoni and Hwang (16) developed a relationship for the friction factor in which the projection of the upstream face of the bed forms exposed to the flow must be known. Chang (1) also derived a friction factor equation, valid for ripples, which required the length of the eddy zone behind the bed-form crests as one of the variables. Pillai (11) presented a correction factor for the average flow depth over a bed composed of sand waves, the magnitude of which varied with the steepness of the bed forms. It is most probable that this depth adjustment is related to the length of the flow separation, thereby defining the average depth of the water mass which is moving downstream. The writer and Lau (4) and Vittal et al. (17) found that it is not correct to assume that the friction factor due to the sand-grain roughness on the back of a dune is the same as that due to a plane bed of similar grain size. This is probably also due to the fact that the length of the bed form exposed to the flow varies with the dune steepness, and must therefore also be related to the length of the flow separation.

In this paper, an investigation of the length of the flow separation behind

[1]Research Engr., Environmental Hydr. Sect., Hydr. Div., National Water Research Inst., Canada Centre for Inland Waters, P.O. Box 5050, Burlington, Ontario, Canada, L7R 4A6.

Note.—Discussion open until March 1, 1982. To extend the closing date one month, a written request must be filed with the Manager of Technical and Professional Publications, ASCE. Manuscript was submitted for review for possible publication on November 26, 1980. This paper is part of the Journal of the Hydraulics Division, Proceedings of the American Society of Civil Engineers, ©ASCE, Vol. 107, No. HY10, October, 1981. ISSN 0044-796X/81/0010-1133/$01.00.

dunes is made. Consideration is given to the effects of the dune geometry, sand-grain roughness, and the variables defining the flow conditions.

Literature Review

A review of the literature showed that attempts have been made to obtain the length of the flow separation for different types of bed topographies. Raudkivi (13,14), in studying flow over ripples, found that in the lee of a ripple there is a much stronger agitation of the sand surface at five ripple heights–eight ripple heights downstream from the crest. Walker (18) measured the separation length behind a rearward facing rectangular step and found it to be slightly greater than about five times the step height. Tani (15), using a similar step, found the separation length to be about six times the step height. Measurements by Etheridge and Kemp (6), also over a rearward facing step, showed that the ratio of the separation length to step height varied between 5 and 7. Chang (1) measured the length of the separation zone behind a single cast iron angle placed on a plane bed in a rectangular flume, and repeated his tests for three different sizes of angles and three different flow conditions. He found that the ratio of the separation length to the height of the angle varied with the flow velocity from 5–8. However, it is not likely that flows over a single cast iron angle can be taken as being representative of flows over sand waves. Knoroz (10), in developing an equation for the friction factor for dune beds, determined that the length of the separation zone is ten times the dune height. Examination of data by Jonys (7,8) indicated that for his dunes, the length of the separation zone is on the average about 4.2 times the dune height. Most recently, Karahan and Peterson (9) found that for one particular dune shape, the ratio of separation length to dune height was constant and equal to 5.3. They used a new technique which utilizes the streaming birefringence of dilute colloidal suspensions of birefringent materials.

The results from the literature indicate that the length of the separation zone behind dunes may vary from five times–ten times the dune height. Unfortunately, the information is too limited to determine a general relationship between the separation length, bed-form shape, sand-grain roughness, and flow conditions. The results from measurements over dunes and ripples and rearward facing steps appear to be similar. However, it is doubtful that this similarity can be taken to be general, especially when the sand waves have steep upstream faces. In view of the limited information on the flow separation length, a set of experiments was conducted in an attempt to obtain a comprehensive relationship between the length of flow separation over dunes and the pertinent independent variables.

Dimensional Analysis

In order to have good control of the variables defining the dune height and length, it is convenient to use a rigid bed composed of artifical dunes. Under these conditions, considering two-dimensional flow in a straight uniform channel, the flow separation length can be expressed with reference to Fig. 1(*a*) by a set of independent variables

$$L = f_1(\Delta, \Lambda, \phi, D_{50}, h, U, \rho, \mu, g) \quad \ldots\ldots\ldots\ldots\ldots\ldots\ldots\ldots\ldots\ldots (1)$$

in which L = length of flow separation; Λ = length of the bed forms; Δ = height of the bed forms; ϕ = angle of inclination of downstream face of the dunes; D_{50} = median grain-size diameter; h = average depth of flow; U = average flow velocity; ρ = density of the fluid; μ = viscosity of the fluid; and g = acceleration due to gravity. Eq. 1 can be written in dimensionless form as

$$\frac{L}{\Delta} = f_2\left(\frac{\Delta}{\Lambda}, \phi, \frac{D_{50}}{\Delta}, \frac{h}{\Delta}, \frac{Uh\rho}{\mu}, \frac{U}{\sqrt{gh}}\right), \quad \text{for } \Delta > 0 \ldots\ldots\ldots\ldots (2)$$

Measurements by Etheridge and Kemp (6) have shown that flow in the separation zone is quite insensitive to the flow in the corner region at the foot of a reverse rectangular step. This suggests that quite crude modeling of the dunes in this region between the crest and downstream toe is justifiable. Therefore, since the angle ϕ does not normally vary a great deal, it is not a significant parameter in Eq. 2 and can be omitted from further consideration.

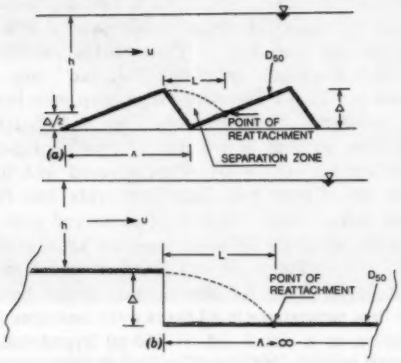

FIG. 1.—(*a*) Definition Sketch for Dunes; (*b*) Definition Sketch for Reverse Steps

In the dune regime, values of the Reynolds number are large enough so that the effect of viscosity is also not significant and the Reynolds number given as $Uh\rho/\mu$ can be deleted. The relationship being sought is then

$$\frac{L}{\Delta} = f_3\left(\frac{\Delta}{\Lambda}, \frac{D_{50}}{\Delta}, \frac{h}{\Delta}, \frac{U}{\sqrt{gh}}\right), \quad \text{for } \Delta > 0 \ldots\ldots\ldots\ldots\ldots\ldots (3)$$

Experiments were conducted to investigate the variations of L/Δ with the independent variables in Eq. 3.

Experimental Equipment and Procedure

Experiments were conducted in a tilting flume rectangular in cross section, 20 m long and 1 m wide. Discharges were measured at the downstream end using a weir box. The flow leaving the flume was split into three parts of

equal width and only the flow from the central portion was measured in the weir box. By working only with the nearly two-dimensional flow in the center portion of the flume, the effect of the side walls was practically eliminated. The flows were always uniform with Froude numbers not exceeding 0.5.

The dune roughness was obtained by using artificial bed forms fabricated from plywood and covered with sand. Four different bed-form shapes, Δ/Λ, each with different sand roughnesses, D_{50}, as well as the smooth bed forms, $D_{50} = 0$, were used. All bed forms had a height of 3 cm with a downstream toe angle of $\Phi = 30°$, and were placed over the full length of the flume. The sand was fixed to the bed forms by first covering these with "Mactac," self-adhesive vinyl covering. Then a thin layer of varnish was brushed on, and the sand was sprinkled on top so that the "Mactac" was completely covered (11). After drying overnight, the excess sand was washed off and a uniform layer of sand was left on the dunes. To change over to another sand roughness, the "Mactac" was stripped off and the process repeated. Each bed form was tested with one or more sand sizes before a new one was placed in the flume. In all, three different sand sizes were used having median diameters of 0.62 mm, 1.20 mm, and 2.60 mm. Therefore, each sand size was approximately twice as large as the one preceding it. Tests on the smooth bed forms were conducted using the smooth surface of the "Mactac" only. A special set of tests was conducted in which a rearward facing step with horizontal upstream and downstream boundaries was used, as shown in Fig. 1(*b*). The height of the step was the same as that of the dunes. This configuration was tested with a smooth surface (i.e. $D_{50} \approx 0$), when covered with a sand of 1.2-mm median diam. This set of tests was done to provide data for comparing the length of separation zones behind the crest of dunes and such a reversed step.

After examining the methods of measuring the separation length used by Chang (1), Etheridge and Kemp (6) and Karahan and Pederson (9), it was decided that a simple flow visualization method would be adequate for the present study. The flow separations in all cases were measured using a Potassium Permanganate solution as a visual aid. A 100-ml hypodermic syringe with a needle 45 cm long and 1-mm inside diam was attached to a traversing mechanism on a movable carriage which traveled on the rails on top of the flume walls. This permitted movement of the syringe in both the vertical and horizontal direction. The tip of the hypodermic needle was ground off at an angle of 30° with the vertical. This made it possible to place the needle so that the dye was always injected horizontally at right angles to the main flow, and ensured that no momentum in the streamwise direction was imparted to the dye. Once a given flow was set up, the syringe was filled with the dye and positioned on the center line of the flow, and then lowered so that the needle was about 1 mm or less above the dune surface.

The location of the point of flow reattachment was obtained by the following two steps. In both steps, dyes were injected into the flow in small short pulses, and were observed to note their direction of movement. In the first step, the syringe was always positioned well downstream of the anticipated separation zone, so that there was a clear and distinct movement of dye pulses downstream [Fig. 2(*a*)]. The syringe was then moved in small increments to new positions upstream, and in each case, the behavior of the dye pulses was carefully noted. The progressive upstream positioning continued until it was observed that some

of the dye tended to travel upstream. This point was defined as the downstream edge of the region in which the point of flow reattachment occurs. The concept of a region was adopted since, due to the turbulent fluctuations (6), it would not be possible to define a precise point, but rather an average. In the second step of the procedure, the syringe was placed at the toe of the bed form in the separation zone being considered. At this point, the dye pulses clearly moved upstream and up the steep face of the dune. The syringe was then placed at different positions, each being about 3 mm–4 mm further downstream than the previous one, and the movement of the dye observed [see Fig. 2(*b*)]. This was continued until once again a portion of the dye pulse was entrained in the downstream flow. This point was taken to be the upstream edge of the region for the point of flow reattachment. All positional measurements were related to the crest of the dune upstream of the separation zone and thus, the probable average location of the point of flow reattachment was simply

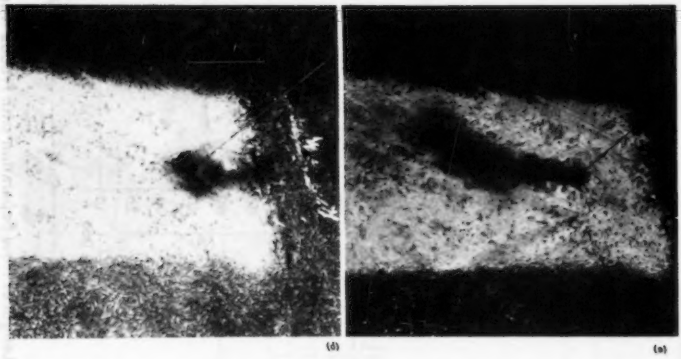

FIG. 2.—(*a*) Dye Downstream of Reattachment Point; (*b*) Dye Upstream of Reattachment Point

the average of the measured pairs. Several pairs of such measurements were made for a given flow condition to ensure a reasonably reliable position for the point of reattachment. The variation between values of the length of flow separation for the different pairs of measurement was less than 15%. These results are encouraging when compared with the results of Etheridge and Kemp (6). In all, data for 291 runs were obtained (4), in which dune length, flow depth, sand size, and the discharge were the basic variables that were varied.

Data Analysis

Separation Length behind Dunes.—Values of L/Δ were plotted versus the Froude number, $F = U/\sqrt{gh}$, for each dune shape, Δ/Λ, using h/Δ as a parameter for each given value of D_{50}/Δ. Due to the large amount of data, only the plots for $\Delta/\Lambda = 0.02$ and 0.07 are shown as Figs. 3 and 4. The computed values of L/Δ, F, D_{50}/Δ, and h/Δ are given in Ref. 5. In all cases,

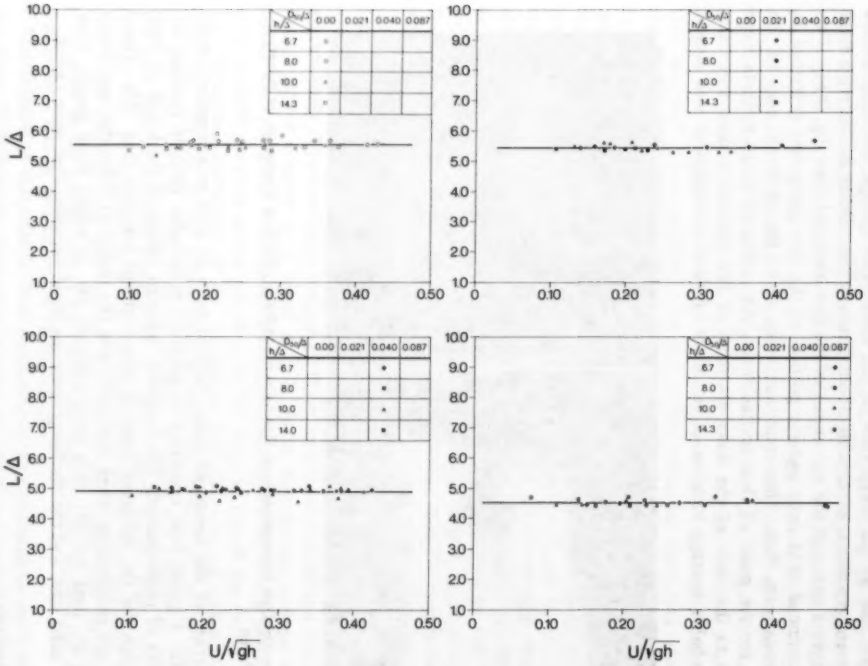

FIG. 3.—Variation of Dimensionless Length of Flow Separation with Froude Number When $\Delta/\Lambda = 0.02$

it was clear that for the flow conditions tested, L/Δ is virtually independent of the Froude number, and is, at best, only weakly dependent on h/Δ. Therefore, since F and h/Δ are shown to be insignificant, they can now be omitted from further consideration. The data analysis is then reduced to searching for the relationship

$$\frac{L}{\Delta} = f_4\left(\frac{\Delta}{\Lambda}, \frac{D_{50}}{\Delta}\right), \quad \text{for} \quad \Delta > 0 \quad \ldots\ldots\ldots\ldots\ldots\ldots\ldots\ldots\ldots\ldots (4)$$

Average values of L/Δ were obtained by fitting smooth straight lines through data on the plots of L/Δ versus $F = U/\sqrt{gh}$ for all values of Δ/Λ and D_{50}/Δ tested. Typical examples of this are also given in Figs. 3 and 4. The values of L/Δ thus obtained, together with the corresponding values of Δ/Λ and D_{50}/Δ, are given in Table 1. The values of L/Δ were then plotted as a function

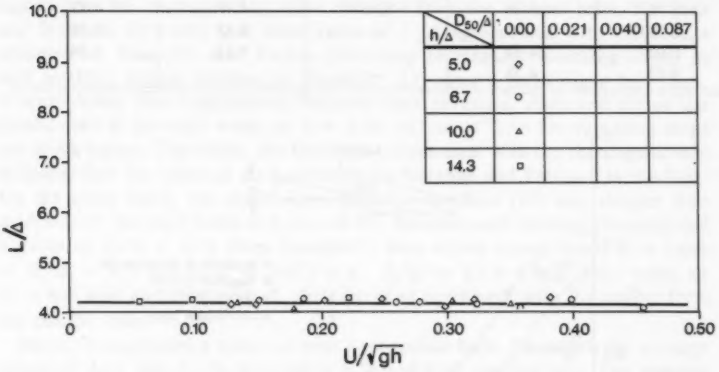

FIG. 4.—Variation of Dimensionless Length of Flow Separation with Froude Number When $\Delta/\Lambda = 0.07$

of Δ/Λ using D_{50}/Δ as a parameter in Fig. 5. The relationship in Eq. 4 is shown as a family of diverging nonlinear curves with one curve for each value of D_{50}/Δ. For each curve, values of L/Δ decrease as Δ/Λ increases from $\Delta/\Lambda = 0.02$–0.07. The rate of change of L/Δ with Δ/Λ appears to be greatest when $\Delta/\Lambda \simeq 0.02$, decreases progressively as Δ/Λ increases, and becomes very small when $\Delta/\Lambda = 0.06$. The curves also show that for small values of Δ/Λ, the effect of change in grain size is more significant than for larger values of Δ/Λ, and when $\Delta/\Lambda = 0.06$ the effect of D_{50}/Δ becomes virtually insignificant.

It should be noted at this point that the test conditions were idealized in many respects in order to provide a wide enough range of data to assess the effect of the important independent variables. In reality, values of Δ/Λ in the dune regime will probably not exceed 0.06 (19), and values of D_{50}/Δ will be between 0 and 0.080 with the lower values being representative of river conditions,

while the values tending toward $D_{50}/\Delta = 0.080$ can be expected to occur in laboratory flumes.

Separation Length behind Reverse Step.—The data for the reverse step were treated in the same way as those for the dunes and the conditions tested; the ratio L/Δ was again independent of $U/\sqrt{gh}$ and h/Δ. When examining the reverse step, it is useful to regard it in terms of the dune shape parameter Δ/Λ. In that case, the reverse step may be defined as a dune of infinite length

TABLE 1.—Average Values of L/Δ

Δ/Λ (1)	D_{50}/Δ 0.00 (2)	0.021 (3)	0.040 (4)	0.087 (5)
0.00	6.10	—	5.76	—
0.02	5.55	5.45	4.92	4.53
0.033	4.79	—	4.53	4.33
0.05	4.34	—	4.31	4.24
0.07	4.23	—	—	—

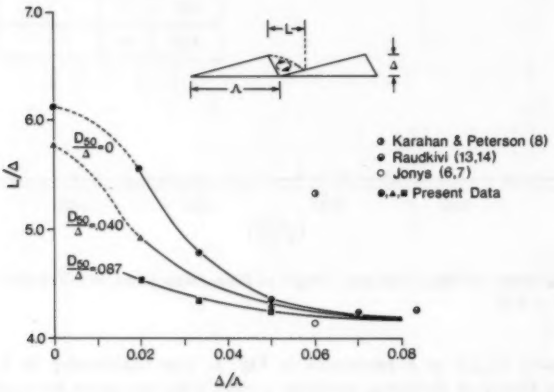

FIG. 5.—Variation of Dimensionless Length of Flow Separation

(i.e., $\Lambda \to \infty$), and for this case $\Delta/\Lambda \approx 0$. As a result, Eq. 4 can be written for this special case as

$$\frac{L}{\Delta} = f_5\left(\frac{D_{50}}{\Delta}\right), \quad \text{for} \quad \Delta > 0 \ldots\ldots\ldots\ldots\ldots\ldots\ldots\ldots\ldots\ldots (5)$$

Eq. 5 shows that for the reverse step, L/Δ is a function only of the surface roughness of the step, a result which has not been reported in the literature. This may partly explain the difference in reported values of L/Δ for such steps.

Values of L/Δ were plotted for $\Delta/\Lambda = 0$, and the two cases of $D_{50}/\Delta = 0$ and $D_{50}/\Delta = 0.040$ in Fig. 5. The values of L/Δ for each case are higher than the values for dunes for the same values of D_{50}/Δ, but the trend of decreasing L/Δ with increasing D_{50}/Δ is still maintained. The curves for values of $D_{50}/\Delta = 0$ and $D_{50}/\Delta = 0.040$ were smoothly connected to the points of L/Δ for the corresponding values of D_{50}/Δ at $\Delta/\Lambda = 0$ (see dashed segments in Fig. 5). The curves from $\Delta/\Lambda = 0$–0.07 are interpreted to mean that the vertical step is nothing but the limiting case for the dunes, and that values of L/Δ for dunes ($\Delta/\Lambda > 0$) can never be greater or equal to values of L/Δ obtained for a reverse step for a given value of D_{50}/Δ. Therefore, any comparison of L/Δ between dunes and reversing steps is incorrect, and errors incurred increase as Δ/Λ increases.

Comparison of Results with Data from Other Sources.—Karahan and Peterson (9) obtained a value of $L/\Delta = 5.3$ for their dune shape of $\Delta/\Lambda = 0.06$. This value was plotted on Fig. 5 which shows that their value of L/Δ is considerably higher than the corresponding value obtained from the present tests. Karahan and Peterson (9) stated that their value of L/Δ agreed well with the results obtained by Tani (15) and Walker (18) using rectangular reversing steps, as well as those results obtained by Raudkivi (13) using a fixed ripple bed form. It was shown that comparisons between such reversing steps and dunes are invalid and in the case when $\Delta/\Lambda = 0.06$, values of L/Δ for reversing steps are much higher. Therefore, the favorable comparison with the rectangular step indicates that the value of L/Δ obtained by Karahan and Peterson is too high. On the other hand, the ripple form used by Raudkivi (13) was steeper than $\Delta/\Lambda = 0.06$, having a value of $\Delta/\Lambda = 0.075$. Karahan and Peterson (9) computed a value of $L/\Lambda = 0.32$ from Raudkivi's data which would result in a value of $L/\Delta = 4.3$ for $\Delta/\Lambda = 0.075$ (i.e., $L/\Delta = L/\Lambda \cdot \Lambda/\Delta$). This value of L/Δ was also plotted on Fig. 5, showing good agreement with the curves from the present tests.

Jonys (7) conducted a series of tests over mobile beds, for which the average values of Δ/Λ and D_{50}/Δ were about 0.06 and 0.06, respectively. The position of flow reattachment could be obtained from Jonys (8) and the value of L/Δ was computed to be 4.2. This value of L/Δ was plotted on Fig. 5 at $\Delta/\Lambda = 0.06$. Considering that $D_{50}/\Delta \approx 0.06$, the point should plot between the curves for $D_{50}/\Delta = 0.040$ and 0.087. However, considering the variance in mobile boundary measurements, the agreement of L/Δ from Jonys (7,8) with that from the present tests is quite good.

Conclusions

The length of the flow separation on the lee side of dunes of different steepness, surface roughness, as well as for a reverse rectangular step was measured and the following conclusions were reached.

1. The length of the flow separation behind dunes is independent of the Froude number and virtually independent of the flow depth for Froude numbers less than 0.5 and values of h/Δ greater than about 5.
2. The length of the flow separation behind dunes is dependent on the sand-grain roughness on the dunes when the dunes are flat. When dunes are steep (i.e.,

$\Delta/\Lambda > 0.05$), the sand-grain roughness effect is virtually negligible. In fact, the separation length for steep dunes is approximately equal to four times the height.

3. The reverse rectangular step may be considered to be a special case of dunes with infinite wave length (i.e., $\Delta/\Lambda = 0$). The largest attainable flow separation occurs for this case. It is therefore not correct to compare flow separation lengths behind dunes (i.e., $\Delta/\Lambda > 0$) directly with those behind a reverse step.

4. The length of flow separation behind dunes for a given surface roughness increases significantly for values of $\Delta/\Lambda < 0.05$ as Δ/Λ decreases. This variation is most significant for values of $D_{50}/\Delta \approx 0$. As D_{50}/Δ increases, the rate of change in length of flow separation becomes less as Δ/Λ decreases.

5. The length of flow separation behind a rectangular reverse step is a function of surface roughness only for the range of flows tested.

6. Fig. 5 can be used to obtain estimates of the length of flow separation for most situations with dunes.

Acknowledgments

The writer is grateful to Y. Lam Lau for his critical review of the manuscript and his helpful comments in preparing this paper. All measurements and photographs were made by J. Dalton, assisted by D. Doede. The writer is grateful for their dedication to this project.

Appendix I.—References

1. Chang, F. F. M., "Ripple Concentration and Friction Factor," *Journal of the Hydraulics Division*, ASCE, Vol. 96, No. HY2, Proc. Paper 7067, Feb., 1970, pp. 417–430.
2. Crickmore, M. J., "Effect of Flume Width on Bed-Form Characteristics," *Journal of the Hydraulics Division*, ASCE, Vol. 96, No. HY2, Proc. Paper 7077, Feb., 1970, pp. 473–496.
3. Engel, P., and Lau, Y. L., "Computation of Bed Load using Bathymetric Data," *Journal of the Hydraulics Division*, ASCE, Vol. 106, No. HY3, Proc. Paper 15255, Mar., 1980, pp. 369–380.
4. Engel, P., and Lau, Y. L., "Friction Factor for Two-Dimensional Dune Roughness," *Journal of Hydraulic Research*, International Association for Hydraulic Research, Vol. 18, No. 3, 1980.
5. Engel, P., "Bed-Load Discharge Coefficient for Migrating Dunes," *Hydraulics Division Technical Report*, National Water Research Institute, Canada Centre for Inland Waters, Burlington, Ontario, Canada, Apr., 1980.
6. Etheridge, D. U., and Kemp, P. H., "Velocity Measurements Downstream of Rearward Facing Steps with Reference to Bed Instability," *Journal of Hydraulic Research*, International Association for Hydraulic Research, Vol. 17, No. 2, 1979.
7. Jonys, C. D., "An Experimental Study of Bed-Form Mechanics," thesis presented to the University of Alberta, at Edmonton, Alberta, Canada, in 1973, in partial fulfillment of the requirements for the degree of Doctor of Philosophy.
8. Jonys, C. K., "Pressure and Shear Stress Distribution on Alluvial Bed Forms," *Hydraulics Division Technical Report*, National Water Research Institute, Canada Centre for Inland Waters, Burlington, Ontario, Canada, 1974.
9. Karahan, M. E., and Peterson, A. W., "Visualization of Separation over Sand Waves," *Journal of the Hydraulics Division*, ASCE, Vol. 106, No. HY8, Proc. Paper 15652, Aug., 1980, pp. 1345–1352.
10. Knoroz, U. S., "The Effect of Channel Macro Roughness on its Hydraulic Resistance," Ozversticia Usesoiuznogo Nanchno-Ossledvovatel'k-kogo, Instituta, *Gidrotekkiuki*,

Vol. 62, pp. 75–96 (translated by I. Mitten, United States Geological Survey).
11. Lau, Y. L., and Krishnappan, B. G., "Transverse Dispersion in Rectangular Channels," *Journal of the Hydraulics Division*, ASCE, Vol. 103, No. HY10, Proc. Paper 13294, Oct., 1977, pp. 1173–1189.
12. Pillai, C. R. S., "Effective Depth in Channels having Bed Undulations," *Journal of the Hydraulics Division*, ASCE, Vol. 105, No. HY1, Proc. Paper 14336, Jan., 1979, pp. 67–81.
13. Raudkivi, A. J., "Study of Sediment Ripple Formation," *Journal of the Hydraulics Division*, ASCE, Vol. 89, No. HY6, Proc. Paper 3692, Nov., 1963, pp. 15–33.
14. Raudkivi, A. J., *Loose Boundary Hydraulics*, second ed., Pergamon Press, Inc., Elmsford, N.Y., 1976.
15. Tani, L., "Experimental Investigation of Flow Separation over a Step," *Symposium Freiburg/BR*, International Union of Theoretical and Applied Mechanics, Boundary Layer Research, Aug. 26–29, 1957.
16. Vanoni, V. A., and Hwang, L. S., "Relation Between Bed Forms and Friction in Streams," *Journal of the Hydraulics Division*, ASCE, Vol. 93, No. HY3, Proc. Paper 5242, May, 1967, pp. 121–144.
17. Vittal, N., Raju, K. G., and Garde, R. J., "Resistance of Two-Dimensional Triangular Roughnesses," *Journal of Hydraulic Research*, International Association for Hydraulic Research, Vol. 15, No. 1, 1977.
18. Walker, G. R., "A Study of Two-Dimensional Flow of Turbulent Field Past a Step," thesis presented to the University of Auckland at Auckland, New Zealand, in 1961, in partial fulfillment of the requirements for the degree of Master of Engineering.
19. Yalin, M. S., *Mechanics of Sediment Transport*, second ed., Pergamon Press, Inc., New York, N.Y., 1977.

Appendix II.—Notation

The following symbols are used in this paper:

D_{50} = median grain-size diameter;
f = denotes function;
F = Froude number = $U/\sqrt{gh}$;
g = acceleration due to gravity;
h = average depth of flow;
L = length of flow separation;
R = Reynolds number = $Uh\rho/\mu$;
U = average velocity of flow;
Δ = height of dunes;
Λ = length of dunes;
μ = viscosity of fluid;
ρ = density of fluid; and
ϕ = angle of inclination of downstream face of dunes.

RELIABILITY OF ALGORITHMS FOR PIPE NETWORK ANALYSIS

By Don J. Wood,[1] M. ASCE and A. G. Rayes,[2] A. M. ASCE

INTRODUCTION

Steady-state analysis of pressure and flow in piping systems is a problem of great importance in engineering. The basic hydraulics equations describing the phenomena are nonlinear algebraic equations which cannot be solved directly. These equations have been expressed in two principal fashions. They have been written in terms of the unknown flowrates in the pipes herein referred to as loop equations. Alternately, they have been expressed in terms of unknown heads at junctions throughout the pipe system (node equations). Several algorithms have been proposed for solving these equations and these techniques are in wide use today.

In this paper the principal algorithms are presented for applications to piping systems of general configuration and systems which contains pumps and other common hydraulic components. The reliability of these algorithms are examined by solving a large number of actual pipe network problems with each algorithm and comparing the results.

There is a considerable amount of published material dealing with pipe network analysis, all of which cannot be reviewed here. However, some principal contributions of historical interest will be cited. Hardy Cross authored the original and classic paper (4). In that article, which considered only closed loop networks with no pumps, a method for solving the loop equations based on adjusting flowrates to individually balance each of the energy equations is described. This method is very widely used today and is often referred to as the Hardy Cross method. Although it is not as widely used, Hardy Cross described a second method for solving the node equations by adjusting the head at each node so that the continuity equation is balanced. A number of subsequent papers have appeared which further describe these methods or computer programs utilizing these methods (2,5,8,11,15).

Because the adjustments are computed independent from each other, convergence problems using the methods described by Hardy Cross were frequently

[1]Prof., Dept. of Civ. Engrg., Univ. of Kentucky, Lexington, Ky. 40506.
[2]Engr., Metito International, Wimbledon, England.

Note.—Discussion open until March 1, 1982. To extend the closing date one month, a written request must be filed with the Manager of Technical and Professional Publications, ASCE. Manuscript was submitted for review for possible publication on January 7, 1981. This paper is part of the Journal of the Hydraulics Division, Proceedings of the American Society of Civil Engineers, ©ASCE, Vol. 107, No. HY10, October, 1981. ISSN 0044-796X/81/0010-1145/$01.00.

noted and procedures developed to improve convergence. Martin and Peters (14) and Epp and Fowler (6) described a procedure to simultaneously compute the flow adjustments for closed loop systems. This procedure had much improved convergence characteristics and forms the basis for more general applications (9,11).

Both the methods just described for solving the loop equations require an initial balanced set of flowrates and the convergence depends to a degree on how close this initial set of flowrates is to the correct solution. A third method, developed by this writer, solves the entire set of hydraulics equations simultaneously after linearizing the nonlinear terms in the energy equation. This procedure was first described for closed loop systems (18) and has subsequently been modified for more general applications (7,17). A similar approach has been developed for the node equations where all the node equations are linearized and solved simultaneously, and this method is described for closed loop systems by Shamir and Howard (16). Additional references to this method have been published (1,12).

The five methods just covered are described in the next section for general applications. No restrictions on network geometry are required and pumps may be included anywhere in the network. Certain special components such as check valves and pressure regulating valves are not considered since these components require special treatment which depend on the algorithm employed. Each of these methods require iterative computations where the solution is improved until a specified convergence criterion is met. If a sufficiently stringent convergence criterion is met, the solutions normally will be essentially identical for all five methods. In some cases, however, it is not possible with certain of the algorithms to meet a specified convergence criterion regardless of the number of trials completed. In other cases a seemingly stringent convergence criterion may be met but the solution is still in considerable error. Convergence difficulties such as these have been previously noted and reported.

In the original paper by Hardy Cross (4) he noted that "convergence was slow and not very satisfactory" when employing the head adjustment method he developed. This was attributed to using initial head estimates which were not very good. Of the two methods described by Hardy Cross, the method of adjusting flows became the most widely taught and used method. Convergence problems using this method were also recognized, however, and several suggestions were made for improving convergence. Investigators have advocated the use of an over-relaxation factor to multiply the flow adjustment factor (1,18). Hoag and Weinberg suggested using a selective procedure for choosing loops as a means of accelerating convergence (10). It appears that these and other procedures suggested for improving convergence of this method will improve it only in certain situations and will not assure convergence.

Convergence problems are largely unreported for the improved methods developed for solving the loop equations. However, additional convergence problems have been reported for methods based on the node equations since Hardy Cross first alluded to such problems in his original paper. Dillingham (5) stated that when the method of adjusting heads at individual nodes is applied to a large network it may not converge or may converge very slowly. He described some procedures for improving convergence. Robinson and Rossum (15) who developed a computer program based on this method state that, "convergence

is slow when a network contains short lengths of large diameter mains and convergence is not assured if there are dead end mains." They further state that "convergence may not occur if check valves are present." The method of simultaneously adjusting heads normally converges much more rapidly which lead Lemieux to state that convergence was assured (12). However, it appears that this assessment is optimistic and problems have been noted with this method. Oscillations have been noted by Shamir and Howard (16) who also report that there is a possibility that a solution can not be obtained. Liu also stated "for poor initial input the method (simultaneous node adjustment) may diverge from the true solution or converge slowly" (12). Collins and Kennington presented some data which documented convergence problems for a large network using this method (3).

The reliability of the algorithm employed for pipe network analysis is of great importance. Failure to obtain a solution is an inconvenience and the failure to recognize a poor solution may be even a greater problem because this may lead to poor design or management of water distribution systems. The purpose of this study is to document reliability problems which may occur using the various popular algorithms.

Algorithms for Pipe Network Analysis

The commonly used algorithms for pipe network analysis are described in this section. Detailed presentations can be founded in the references cited for each method. A brief description of pipe network geometry and the basic hydraulic equations are included so the algorithms can be presented using a common basis.

Pipe Network Geometry.—Basic geometry considerations for a pipe network are summarized as follows. A pipe network is comprised of a number of pipe sections which are constant diameter sections which can contain pumps and fittings such as bends and valves. The end points of the pipe sections are nodes which are identified as either junction nodes or fixed grade nodes. A junction node is a point where two or more pipe sections join and is also a point where flow can enter or leave the system. A fixed grade node is a point where a constant head is maintained such as a connection to a storage tank or reservoir or to a constant pressure region. In addition primary loops can be identified in a pipe network and these include all closed pipe circuits within the network which have no additional closed pipe circuits within them. When junction nodes, fixed grade nodes, and primary loops are identified the following relationship holds:

$$p = j + l + f - 1 \quad \text{(1)}$$

in which p = number of pipes; j = number of junction nodes; l = number of primary loops; and f = number of fixed grade nodes.

Basic Equations.—Pipe network equations for steady-state analysis have been commonly expressed in two ways. Equations which express mass continuity and energy conservation in terms of the discharge in each pipe section have been referred to as loop equations and this terminology will be followed here. A second formulation which expresses mass continuity in terms of heads at junction nodes produces a set of equations referred to as node equations.

Loop Equations.—Eq. 1 offers a basis for formulating a set of hydraulic equations to describe a pipe system. In terms of the unknown discharge in each pipe, a number of mass continuity and energy conservation equations can be written equaling the number of pipes in the system. For each junction node a continuity relationship equating the flow into the junction (Q_{in}) to the flow out (Q_{out}) is written as:

$$\Sigma Q_{in} - \Sigma Q_{out} = Q_e \ (j \text{ equations}) \quad \ldots \quad (2)$$

Here Q_e represents the external inflow or demand at the junction node. For each primary loop the energy conservation equation can be written for pipe sections in the loop as follows:

$$\Sigma h_L = \Sigma E_P \ (l \text{ equations}) \quad \ldots \quad (3)$$

in which h_L = energy loss in each pipe section including minor losses; and E_P = energy put into the liquid by pumps. If there are f fixed grade nodes, $f - 1$ independent energy conservation equations can be written for paths of pipe sections between any two fixed grade nodes as follows:

$$\Delta E = \Sigma h_L - \Sigma E_P \ (f - 1 \text{ equations}) \quad \ldots \quad (4)$$

in which ΔE = the head difference between the fixed grade nodes. The terms in the energy equations can be expressed as function of flowrate. Thus, the continuity equations (Eq. 2) and the energy equations (Eqs. 3 and 4) form the set of p simultaneous equations in terms of unknown flowrates which are termed the loop equations. Since these are nonlinear algebraic relationships, no direct solution is possible. Three algorithms for solving the loop equations are presented in this paper.

Node Equations.—The analysis is carried out in terms of an unknown total head, H, at each junction node in the piping system. The basic relationship used is the continuity relationship (Eq. 2). The flowrate in a pipe section connecting nodes labeled a and b is expressed in terms of the head at junction node a, H_a, the head at the other end of the pipe section, H_b, and the loss coefficient for the pipe, K_{ab}. This is

$$Q_{ab} = \left| \frac{H_a - H_b}{K_{ab}} \right|^{1/n} \quad \ldots \quad (5)$$

This expression assumes that the pipe section contains no pumps and a head loss relationship is used of the form

$$h_L = KQ^n \quad \ldots \quad (6)$$

in which the term K = the loss coefficient for the pipe section and is a function of pipe parameters and flow conditions and depends on the head loss expression used and may include minor loss terms. The exponent n also depends on the head loss expression used. Combining Eqs. 2 and 5 gives:

$$\sum_{b=1}^{N} \pm \left[\frac{H_a - H_b}{K_{ab}} \right]^{1/n} = Q_e \ (j \text{ equations}) \quad \ldots \quad (7)$$

This expresses continuity at junction node a, in which N pipes connect, in terms of the head at a, H_a, and the heads at adjacent nodes, H_b. The sign

of the term in the summation depends on whether the flow is into or out of junction node a. A total of j equations are written in this manner.

The basic set of equations can be expanded to incorporate pumps. For each pump, junction nodes are identified at the suction and discharge sides of the pump. Two additional equations can be written as terms of the two additional unknown heads at the suction and discharge sides of the pump and the adjacent heads. One equation expresses flow continuity in the suction and discharge lines (using Eq. 5) and a second equation relates the head change across the pump to the flow in either the discharge or suction line.

For a pipe network of j junction nodes and n_p pumps a set of $j + 2n_p$ equations are obtained. These represent the full set of pipe network node equations which are expressed in terms of the unknown heads at junction nodes and pump suction and discharge heads at all pumps in the pipe system. Like the loop equations, these are nonlinear algebraic equations and no direct solution is possible.

Algorithms for Solution of Loop Equations.—Three methods for the solution of the loop equations have been developed and are in significant use today. Each use gradient methods (Newton extrapolation) to eliminate nonlinear terms from the energy equations.

Single Path Adjustment (PATH) Method.—This method of solution was described by Hardy Cross (4) and is the oldest and most widely used technique. The original method was, however, limited to closed loop systems and included only line losses. The procedure has since been generalized. The method of solution is summarized as follows.

1. Determine an initial set of flowrates which satisfy continuity at each junction node.
2. Compute a flow adjustment factor for the path of pipes for each energy equation which tends to satisfy the energy equation written for that path. The application of this correction factor will not disturb the continuity balance.
3. Using improved solutions for each trial repeat step 2 until the average correction factor is within a specified limit.

The flow adjustment factor for a path is computed from the energy equation for that path and is intended to correct the flowrates so that the energy equation is satisfied. However, a correction for a particular path will disturb the energy relationship for all the other paths which have common pipes. A trial with this method requires a flow adjustment to all paths in the pipe network (l loops and $f - 1$ paths between fixed grade nodes).

Simultaneous Path Adjustment (S-PATH) Method.—In order to improve convergence characteristics a method of solution was devised which simultaneously adjusts the flowrate in each path of pipes representing an energy equation (6). This method can be summarized as follows.

1. Determine an initial set of flowrates which satisfy continuity at each junction mode.
2. Simultaneously compute a flow adjustment factor for each path which tends to satisfy the energy equations without disturbing the continuity balance.

3. Using the improved solutions repeat step 2 until the average flow adjustment factor is within a specified limit.

The simultaneous determination of the path flow adjustment factors requires the simultaneous solution of $l + f - 1$ equations. Each equation accounts for the unbalance in the energy equation due to incorrect values of flowrate and includes the contribution for a particular path as well as contributions from all other paths which have pipes common to both paths.

A set of $l + f - 1$ simultaneous linear equations are formed in terms of flow adjustment factors. These linear equations can be solved using standard procedures and the solution provides an improved set of balanced flowrates which can be used for another trial. Trials are repeated until a specified accuracy is attained.

Linear (LINEAR) Method.—This method is based on a simultaneous solution of the basic hydraulics equations for the pipe system and has been reported for closed loop systems (18) and general systems (17). Since the energy equations for the paths are nonlinear, these equations are first linearized in terms of an approximate flowrate, Q_i, in each pipe.

The $l + f - 1$ linearized energy equations combine with the j continuity equations (Eqs. 2) to form a set of p simultaneous linear equations in terms of the flowrate in each pipe.

The technique used to solve equations follows. Based on an arbitrary initial value for the flow in each line the linearized equations are solved using routine matrix procedures for solving linear equations. This set of flowrates is used to linearize the energy equations and a second solution is obtained. The procedure is repeated until the change in flowrates obtained in successive trials is insignificant.

Algorithms for Solution of Node Equations.—Two methods for solving the node equations are widely used and these are described here.

Single Node Adjustment (NODE) Method.—This method was also described in the paper written by Hardy Cross (4). However, the method has never been as widely used as the single path adjustment method. It is, nevertheless, in significant use today. The method is summarized as follows.

1. Assume a reasonable head for each junction node in the system. This assumed head does not have to satisfy any conditions. However, the better the initial assumption the fewer the required trials.
2. Compute a head adjustment factor for each junction node which tends to satisfy flow continuity at that junction.
3. Repeat step 2 until the average correction factor for heads is within a specified accuracy or some other specified convergence criterion is satisfied.

The head adjustment factor is the change in head at a particular node which will result in satisfying continuity (Eq. 2) considering the heads at the adjacent nodes as fixed. Again a gradient approximation is used to compute the required head change. A single trial for this method requires the adjustment of the head for each junction node within the pipe system. The trials continue until the specified convergence criterion is met.

Simultaneous Node Adjustment (S-NODE) Method.—This method is based

on a simultaneous solution of the basic pipe network node equations and requires a linearization of these equations in terms of approximate values of the head (16). This produces a set of $j + 2n_p$ simultaneous linear equations (in which n_p is the number of pumps). These equations are solved as follows: Starting with any assumed set of values for the junction node heads these linear equations are solved simultaneously for an improved set of junction node heads. These heads are then used to linearize the set of node equations and the procedure repeated until subsequent calculations satisfy a stated convergence or accuracy criterion.

Data Base for Study

A comprehensive comparison of the algorithms was possible because an extensive data base was available. These data were provided mostly by consulting engineers and water distribution engineers and represents actual or proposed distribution systems from all over the United States. In some cases these data were sent to the writer because analysis difficulties were encountered. These systems include very high or low resistance lines and pumps operating on steep curves. In general, however, the data is representative of the type of systems which are routinely analyzed. The data utilized includes 30 systems with under 100 pipes and 21 systems with over 100 pipes (up to 509 pipes). The data for a system can include changes which result in the analysis of additional situations with relatively minor changes in system characteristics incorporated into the data. A total of 60 situations were analyzed for systems of under 100 pipes and 31 situations for systems of over 100 pipes.

The data includes pumps described in two ways. Pumps operating at constant power and pumps operating on a curve passed directly through three points of operating data (head vs discharge) were considered. Components such as check valves and pressure regulating valves were not included since special procedures are required to handle these components. The Hazen Williams equation for head loss was employed in most situations. However, a few comparisons were made using the Darcy Weisbach equation. The data included a roughness term appropriate for the head loss expression employed.

Computer Programs for Comparisons

Computer programs were developed for each of the five algorithms studies. These programs were designed to solve the basic loop and node equations using the procedures previously described. Identical input data was used for all algorithms. The programs included algorithms to formulate the equations (determine pipes connecting junctions, forming loops, and connecting fixed grade nodes) from the connecting node data for the pipes. The programs also generated the necessary initial conditions. This required a balanced initial flowrate for the single and simultaneous path methods. An algorithm was developed that was designed to generate an arbitrary but reasonable initial balanced flowrate for these two methods. For the linear method an initial flowrate is needed but was not required to satisfy continuity. For this method an initial flowrate based on a constant flow velocity in an arbitrary direction was assigned. For the single and simultaneous node adjustment methods some initial values for

head are required to initiate the solution, and an algorithm was developed to provide arbitrary but reasonable initial values. It can be presumed, however, that calculations were often initiated with values of flowrate or head which are significantly different from the correct results.

Convergence Criterion.—For each method, the trials are continued until the specified convergence criterion was met and the same convergence criterion was applied for each method. Since updated flowrates are easily computed for each method the change in flowrate between successive trials was used to check convergence. The specific convergence criterion employed is referred to herein as the relative accuracy and is

$$\frac{\Sigma(Q - Q_i)}{\Sigma Q} \leq 0.005 \quad (8)$$

Here Q = the flowrate obtained for a trial; and Q_i = the initial flowrate used which was computed from the previous trial. This criterion roughly states that when the average change in flowrates between successive trials is less than 0.5% the calculations cease. This convergence criterion is more stringent than ones normally applied in practice. It does not, however, assure that the flowrates are within 0.5% of the correct values. Numerous other criterion can be applied to determine the acceptability of a solution and others have suggested and employed. Additional description of convergence criterion will be presented later.

Accuracy of Solutions.—Each of the methods for analyzing pipe networks yield approximate solutions. A solution is accurate when all the basic equations are satisfied to a high degree of accuracy. The mass continuity equations are exactly satisfied for the three methods based on the loop equations. Each of these methods are then designed to satisfy the energy equations through an iterative procedure and the unbalanced heads for the energy equations is evidence of solution accuracy. If these are satisfied to a high degree of accuracy then the solution is essentially exact. In this paper an exact solution of the loop equations will be assumed to be one where the average unbalanced head for the energy equations is less than 0.01 ft (0.00328 m). For the methods based on the node equation iterations are carried out to satisfy mass continuity at junction nodes and the unbalance in continuity is the most significant indication of the solution accuracy.

Comparison of Solutions

All five methods were compared to an exact solution for systems of under 100 pipes. This involved a total of 60 comparisons and the results for each comparison were tabulated and compared as depicted in Table 1. These are the results for the 14-pipe system which is depicted in Fig. 1. The exact solution was obtained in every case by carrying out the linear method one additional trial after the relative accuracy of 0.005 was reached. This table summarizes information which is essential in evaluating the effectiveness of each algorithm. The average flowrate and head range for this solution is output. Next the flowrates and heads at junction nodes are compared to exact solutions and average and maximum differences given for each method. The percent average and percent

TABLE 1.—Comparisons of Flowrate and Grades for 14 Pipe System (1 m = 3.2 ft, 1 m^3/s = 1,000 L/s = 35.3 ft^3/s)

Pipe number (1)	Exact flows (2)	Linear (3)	Difference (4)	SPATH (5)	Difference (6)	PATH (7)	Difference (8)	SNODE (9)	Difference (10)	NODE (11)	Difference (12)
				(*a*) Flowrates (in liters per second)							
1	273.35	273.35	0.0	273.36	0.01	273.31	0.04	273.36	0.01	272.60	0.75
2	149.21	149.21	0.0	149.21	0.0	149.25	0.04	149.22	0.01	149.16	0.05
3	36.21	36.21	0.0	36.21	0.0	36.25	0.04	36.22	0.01	36.72	0.51
4	1.66	1.66	0.0	1.66	0.0	1.71	0.05	−4.04	5.70	−6.87	8.53
5	−55.34	−55.34	0.0	−55.34	0.0	−55.29	0.05	−55.25	0.09	−56.40	1.06
6	95.23	95.23	0.0	95.23	0.0	95.07	0.16	95.18	0.05	95.68	0.45
7	−139.21	−139.21	0.0	−139.21	0.0	−139.24	0.03	−139.24	0.03	−141.01	1.80
8	−110.29	−110.29	0.0	−110.29	0.0	−110.26	0.03	−110.28	0.01	−110.54	0.25
9	258.24	258.24	0.0	258.24	0.0	258.23	0.01	258.24	0.0	258.44	0.20
10	124.15	124.15	0.0	124.15	0.0	124.06	0.09	124.14	0.01	124.09	0.06
11	60.76	60.76	0.0	60.76	0.0	60.79	0.03	60.72	0.04	67.61	6.85
12	−17.11	−17.12	0.01	−17.11	0.0	−17.22	0.11	−17.08	0.03	−15.78	1.33
13	531.59	531.59	0.0	531.59	0.0	531.54	0.05	531.59	0.0	530.85	0.74
14	90.95	90.95	0.0	90.95	0.0	90.97	0.02	90.95	0.0	92.30	1.35
Average differences			0.00		0.00		0.05		0.43		1.71
Percent average differences			0.00		0.00		0.04		0.31		1.23
Maximum differences			0.01		0.01		0.16		5.70		8.53
Percent maximum differences			0.01		0.01		0.12		4.11		6.15
Junction	Exact heads										
				(*b*) Heads (in meters)							
1	61.49	61.49	0.0	61.49	0.0	61.51	0.02	61.49	0.0	61.73	0.24
2	40.58	40.58	0.0	40.57	0.01	40.61	0.03	40.58	0.0	40.84	0.26
3	31.86	31.86	0.0	31.86	0.0	31.66	0.0	31.86	0.0	32.06	0.20
4	31.33	31.33	0.0	31.33	0.0	31.33	0.0	31.33	0.0	31.47	0.14
5	31.33	31.33	0.0	31.33	0.0	31.33	0.0	31.34	0.01	31.45	0.12
6	36.44	36.44	0.0	36.44	0.0	36.44	0.0	36.44	0.0	36.64	0.20
7	32.41	32.41	0.0	32.41	0.0	32.40	0.01	32.42	0.01	32.53	0.12
8	41.42	41.42	0.0	41.42	0.0	41.42	0.0	41.42	0.0	41.58	0.16
Averages differences			0.0		0.00		0.01		0.00		0.18
Maximum differences			0.0		0.01		0.03		0.01		0.26
Average diff/head range-in percent			0.0		0.00		0.02		0.01		0.60
Maximum diff/head range-in percent			0.0		0.03		0.10		0.03		0.86

Note: The average flowrate = 138.81; the head range = 30.16.

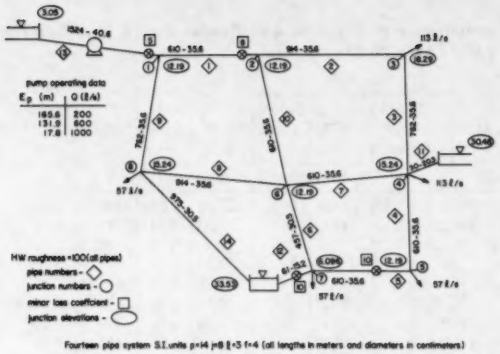

FIG. 1.—Example System (1 m = 1,000 mm = 3.28 ft, 1,000 L/s = 35.3 f^3/s)

maximum differences are based on the average flowrate and head range and these values are more useful for relative comparisons. Following this, additional data is given in Table 2 which further relates to the accuracy of these solutions. The unbalanced heads for each of the six equations for this example are summarized for the four solutions (including the exact one) obtained using the loop equations. Maximum and average values are also given. For the two solutions based on the node equations the unbalanced flows at the eight junction nodes are summarized along with maximum and average values. Finally the number of trials required and the accuracy attained for each of the six solutions is summarized. All the solutions for this example are quite good which is indicated by the good comparisons with the exact solution and also the small unbalanced heads and unbalanced flows obtained. The worst solution was attained with the single node adjustment method for which the average error in flowrate was only 1.23% and in grade was only 0.6%.

Similar comparisons were made using a relative accuracy of 0.005 for 60 situations and the results are summarized in Table 3. Since attainment of the convergence criterion is not assured some liberal upper limits on the number of trials allowed were imposed and these are noted. Calculations were terminated when the accuracy of 0.005 was attained or the limit on the number of trials was reached.

The solutions were considered to compare favorably with the exact solution if the average percent deviation based on average flowrate and the head range from the correct solution for flowrates and heads did not exceed 10% and the maximum percent deviations did not exceed 30%. A failure was considered to have occurred if the specified relative accuracy is reached and those conditions are not met or the maximum number of trials are run without attaining the specified accuracy. The number of failures for each method are included in Table 3.

Analysis and Additional Results

The LINEAR method proved to be very reliable. It converged in every situation

TABLE 2.—Checks on Accuracy and Convergence—14 Pipe System

(*a*) Unbalanced heads (in meters)

Exact	Linear	SPATH	PATH
0.0	0.0	0.0	0.02
0.0	0.0	0.0	−0.01
0.0	0.0	0.0	−0.05
0.0	0.0	0.0	0.05
0.0	0.0	0.0	−0.08
0.0	0.0	0.0	0.03
	Maximums		
0.0	0.0	0.0	−0.08
	Averages		
0.0	0.0	0.0	0.04

Unbalanced flows (in liters per second)

SNODE	NODE
0.0	1.42
0.0	3.02
0.0	2.94
−5.78	11.40
5.79	8.55
0.0	3.71
−0.01	1.94
0.0	1.40
Maximums	
5.79	11.40
Percent maximum unbalanced flows	
4.17	6.21
Averages	
1.45	4.30
Percent average unbalanced flows	
1.04	3.10

Number of trials

Exact	Linear	SPATH	PATH	SNODE	NODE
7	6	9	9	8	9

Accuracy

Exact	Linear	SPATH	PATH	SNODE	NODE
0.000010	0.000967	0.000280	0.002503	0.002408	0.003465

to the correct solution and for all practical purposes the solution reached using a relative accuracy of 0.005 was exact. The number of trials required does not depend on the size of the system and averaged around six for the 60 comparisons.

The S-PATH method also has excellent convergence characteristics and only one failure occurred. For this case a constant power pump was presented which operated on a very steep head-discharge curve. This was a low horsepower pump operating at a very low discharge. The steep gradient caused convergence problems for all but the LINEAR method. This convergence problem probably would not occur for the S-PATH method if the pump operated on a flatter head-discharge curve. Additional trials will not result in the attainment of an acceptable solution.

The larger systems of greater than 100 pipes were analyzed using the LINEAR and S-PATH methods and all attained a good solution in a reasonable number of trials. For the 31 situations analyzed the LINEAR method required an average of 6.4 trials and 5.4 sec and the S-PATH method required an average of 8.5 trials and 6.9 sec. This shows that both methods obtain accurate results with few trials and use comparable computer times.

TABLE 3.—Summary of Reliability Studies

	Accuracy = .005			Accuracy = .0005			
Method (1)	Trials allowed (2)	Accuracy attained (3)	Number failures (4)	Trials allowed (5)	Number runs (6)	Accuracy attained (7)	Number failures (8)
Linear	20	60	0				
S-PATH	30	59	1				
PATH	200	60	8	400	8	8	3
S-NODE	40	53	18				
NODE	200	53	51	400	15	15	2

The three other methods studied exhibited significant convergence problems, and the frequency of problems increased as larger systems were analyzed. Since adequate documentation of convergence problems were obtained for these methods using systems of less than 100 pipes, results for the larger systems were not compared for the PATH, NODE, and S-NODE methods. A number of these larger systems were analyzed with these methods and a significant number of convergence problems were encountered. However, excessive computer times would be required to completely document these results so the comparisons for these methods were limited to the smaller systems.

The eight failures obtained for the PATH method all reached the specified accuracy. In addition, for six of the pipe systems the solutions attained a relatively low average unbalanced head of 0.37 ft (0.11 m) for the energy equations. Yet significant errors exist in these solutions. These eight cases were rerun with relative accuracy of 0.0005 specified, and with additional trials, all attained this. The results are summarized in Table 3. Five of the cases improved to an acceptable degree. Two of the three failures are characterized by large unbalanced heads. However, the one additional failure was documented for

a system which by all indications reached a very good solution. The average unbalanced head was only 0.06 ft (0.02 m), yet some flowrates were in great error. This was especially evident for flow into and out of storage tanks and these results are presented in Table 5. Since this prediction is of significant engineering importance the results from the PATH method are unacceptable. This failure occurs in spite of the very high degree of relative accuracy attained and the low value of unbalanced head reached. The reason for this failure appears to be that some lines with very high and very low head losses are included in the same energy equations. This is not a highly unusual in water distribution systems and yet the PATH method encounters difficulty with this situation.

When the S-NODE method is successful a highly accurate solution is obtained in relatively few trials. However, a significant number of failures were recorded in Table 3 for this method. The patterns of failures is the most varied of the methods investigated. Six of the 18 failures noted attained an extremely accurate calculation of the heads. In these cases the calculation of most flowrates were also accurate. However, a few exhibit large errors. This occurs when lines which carry significant flows at very low head losses are present. This situation is not uncommon in many water distribution systems and small errors in head calculations can result in a few highly inaccurate calculations of flowrate. A second type of failure is one where oscillations occur and the specified accuracy is not attained regardless of the number of trials carried out. Table 4 summarizes results where many additional trials were carried out for the S-NODE method with five failures recorded after 400 trials. Failures of this type have been noted for this method, and previously published references to this type of

TABLE 4.—Summary of Results—Additional Trials

Method (1)	Accuracy = .005			
	Trials allowed (2)	Number runs (3)	Accuracy attained (4)	Number failures (5)
S-NODE	400	9	4	6
NODE	1000	5	1	5

TABLE 5.—Results for Tank Flows—79 Pipe System—Flows in gallons per minute ($1\ m^3/s = 35.3\ ft^3/sec$, $1\ ft^3/sec = 448.9\ gal/min$)

Correct solution (1)		Solution from PATH method (2)	
Accuracy		.005	.0005
Number of trials		43	163
Flow from source	812.2 IN	811.6 IN	813.5 IN
Tank A	175.7 IN	626.9 OUT	385.5 OUT
Tank B	91.5 IN	897.4 IN	632.5 IN
Tank C	399.2 IN	419.9 IN	405.0 IN
Tank D	871.3 IN	848.1 IN	884.1 IN

convergence difficulty were cited (3,13,16). For two systems, failures of this type occurred for several situations at the same time that a very accurate solution was obtained for other situations. For one system a convergence failure occurred for the first situation. For the second situation where a single additional inflow representing a new storage tank was added and an excellent solution was obtained in four trials which satisfied the required relative accuracy and had an average error in flowrate of only 0.18%. A third situation where this inflow was reduced by half was analyzed starting with very good values of heads (those just obtained) and yet a convergence failure occurred with a few extremely poor results. A similar situation occurred with another system where a very accurate solution was obtained for the second of three situations while the other two failed. In this case the third situation introduced a pump which significantly affects the system. These results document the very sensitive behavior of the algorithm. Failures for the S-NODE method are evidenced by relatively high values for unbalanced flows at junctions, and this is probably the most reliable indicator for this method.

Based on the criterion for a successful solution the NODE method was the least reliable of the methods studied. Although the specified accuracy was reached in most cases, the solution failed to meet the required standards. It is not summarized in Table 3 but the solutions which failed often reached a very low value for the average head change between trials. For example, one system which failed for three situations reached an average head change of 0.03 ft (0.01 m) along with a relative accuracy of less than 0.005, and yet the solutions contained large errors in flowrate. In many of the situations reported as failures average head changes of less than 0.1 ft (0.03 m) were attained. For these failures low resistance lines carrying significant flows are the principal cause of inaccuracies. It appears that neither the relative flowrate accuracy or the average head change for successive trials is a reliable indicator of an acceptable solution for this method. The relative average and maximum unbalanced flowrates at the junction nodes are more reliable indications.

For the NODE method some selected systems which reached the specified accuracy of 0.005 in a reasonable number of trials were run at an accuracy of 0.0005, and for all but one system (two situations) a good solution was attained. These results are summarized in Table 3. It appears that most of the solutions which failed at a relative accuracy of 0.005 but reached that accuracy in a reasonable number of trials could be improved to provide an acceptable result if a more stringent convergence criterion is met. Convergence may be slow, however, and it may be difficult to provide assurance that the solution is a good one. In the cases where the relative accuracy of 0.005 was not met in the allowable limit of trials (200), additional trials did not tend to improve the solution even if a more stringent relative accuracy could be met. Table 4 summarizes a few situations where up to 1,000 trials were carried out with very poor results. This implies that the NODE method is not capable of solving these systems regardless of the number of trials carried out. It appears that the most significant factor adversely affecting convergence of the NODE method is the presence of low resistance lines.

Conclusions

Significant convergence problems were documented for the PATH, NODE,

and S-NODE methods. These methods are widely used and the results of this study indicate that great care must be exercised when employing these methods. The single adjustment methods (PATH and NODE), which are usually employed if a hand solution or a small computer is used, must be carried out to much greater accuracy than normally called for to increase the probability that a good solution is attained. Attainment of a relative accuracy of 0.0005 with these methods greatly reduced the chances of failure. Stringent convergence requirements for unbalanced heads for the PATH method and unbalanced flows for the NODE method also may be employed to improve reliability. However, the attainment of a stringent convergence criterion does not assure that the solution is accurate and a significant number of situations were documented for both methods where substantial and serious errors occurred after meeting stringent convergence criterion. A few situations were documented where the specified accuracies could not be attained and the solutions were not acceptable. It is concluded that if a specified stringent convergence criterion cannot be met using single adjustment techniques, the solution is not reliable.

Failures for the S-NODE method were characterized by the inability to meet a reasonable convergence criterion, and if this occurs in a limited number of trials (40 in this study) additional trials are usually of no benefit. The failure rate was quite high with this method and the use of results obtained using this method is not recommended unless a good accuracy is attained in a reasonable number of trials. The best indication of an acceptable solution appears to be the average relative unbalanced flow at the junction nodes. The indications are that this value should be less than 2%.

Each of the three methods which experienced significant convergence problems requires a set of flowrates or heads to initiate the solution and the chance of failure can be reduced if initial values are employed which are closer to the correct values. However, there appears to be no reliable means of consistently determining better initial values. In addition, starting with an excellent set of initial conditions does not assure convergence as evidenced by failures for the S-NODE method for situations starting with solutions for similar situations. In some cases where line losses vary greatly or pumps operate on steep curves the correct solution cannot be attained unless the initial values are very close to the correct ones and this clearly is not possible. Many of the reliability problems documented using algorithms based on the node equations (NODE and S-NODE methods) are due to the inability of these methods to handle low resistance lines. For these lines small errors in head calculations may produce very large errors in flowrate calculations. The inability to handle this situation is inherent for algorithms based on node equations. This is due to the fact that solution algorithms for these equations do not incorporate an exact continuity balance.

It is possible that convergence can be improved and failure rates decreased for the PATH, NODE, and S-NODE methods by introducing considerations such as those which have been previously suggested. In this study the algorithms for pipe network analysis were applied in a basic manner. No attention was given to the various techniques for improving convergence. It does appear that many of the proposed techniques are deficient. In any case the technique should be thoroughly tested if the reliability is to be established.

Both the S-PATH and LINEAR methods provide excellent convergence.

Flowrates and heads are computed in a few trials with great accuracy and the attainment of a relative flowrate accuracy of 0.005 is adequate to assure this. There is, however, no absolute assurance of convergence. Many piping systems incorporate features which increase convergence difficulties. Since gradient methods are used to handle nonlinear terms, convergence problems are always a possibility, particularly if ill conditioned data such as a very wide range of pipe line resistance or poor pump descriptions are employed. However, this study indicates that the occurrence of convergence problems using these methods is unlikely. It is concluded that, if possible, either the S-PATH or LINEAR method should be employed for pipe network analysis and that convergence is virtually assured if reasonable data is employed.

Acknowledgments

This work was supported by a grant from the Kentucky Water Resources Research Institute under project A-076-KY and a grant from the Office of Water Research and Technology, United States Department of Interior, under project B-060-KY.

Appendix I.—References

1. Barlow, J. F., and Markland, E., "Computer Analysis of Pipe Networks," *Proceedings I. C. E.*, Vol. 43, June, 1969, pp. 249–259.
2. Chenoweth, H., and Crawford, C., "Pipe Network Analysis," *Journal, American Waterworks Waterworks Association*, Jan., 1974.
3. Collins, M. A., and Kennington, J. L., discussion of "Extended Period Simulation of Water Systems—Part B," by H. S. Rao, L. C. Markel, and D. W. Brue, Jr., *Journal of the Hydraulics Division*, ASCE, Vol. 103, No. HY12, Proc. Paper 13378, Dec., 1977, pp. 1496–1500.
4. Cross, H., "Analysis of Flow in Networks of Conduits or Conductors," *Bulletin No. 286*, University of Illinois Engr. Expr. Station, Urbana, Ill., 1936.
5. Dillingham, J. H., "Computer Analysis of Water Distribution Systems," Parts 1–5, *Water and Sewage Works*, Jan.–May, 1967.
6. Epp, R., and Fowler, A. G., "Efficient Code for Steady-State Flows in Networks," *Journal of the Hydraulics Division*, ASCE, Vol. 96, No. HY1, Proc. Paper 7002, Jan., 1970, pp. 43–56.
7. Fietz, T. R., "Steady Flow in Small Pipe Networks Using Linear Theory," *Water Research Laboratory Report No. 130*, University of New South Wales, Sydney, Australia, Jan., 1973.
8. Fietz, T. R., "Steady Flow in Pipe Networks by the Simple Loop Method," *Water Research Laboratory Report No. 128*, University of New South Wales, Sydney, Australia, Oct., 1972.
9. Heafley, A. H., and Lawson, J. D., "Analysis of Water Distribution Networks," *Proceedings of the Fifth Manitoba Conference on Numerical Mathematics*, University of Manitoba, Oct., 1975.
10. Hoag, L. N., and Weinberg, G., "Pipeline Network Analysis by Electronic Digital Computer," *Journal of the American Water Works Association*, Vol. 49, 1957, pp. 517–524.
11. Jeppson, R. W., "Analysis of Flow in Pipe Networks," *Ann Arbor Science*, Ann Arbor, Mich., 1977.
12. Lemieux, P. F., "Efficient Algorithm for Distribution Networks," *Journal of the Hydraulics Division*, ASCE, Vol. 98, No. HY11, Proc. Paper 9336, Nov., 1972, pp. 1911–1920.
13. Liu, K. T. H., "The Numerical Analysis of Water Supply Networks by Digital Computer," *Proceeding*, 13th Congress of the International Association for Hydraulic

Research, Vol. 1, Subject A, Sept., 1969, pp. 35–42.
14. Martin, D. W., and Peters, G., "The Application of Newton's Method to Network Analysis by Digital Computer," *Journal of the Institute of Water Engineers*, Vol. 17, 1963, pp. 115–129.
15. Robinson, P. M., and Rossum, J. R., "Program Documentation for Hydraulic Network Analysis Computer Program," *California Water Service Company*, June, 1975.
16. Shamir, U., and Howard, C. D. D., "Water Distribution Systems Analysis," *Journal of the Hydraulics Division*, ASCE, Vol. 94, No. HY1, Proc. Paper 5758, Jan., 1968, pp. 219–234.
17. Wood, D. J., "Users Manual—A Computer Program for the Analysis of Pressure and Flow in Pipe Distribution Systems," Office of Engineering Continuing Education, University of Kentucky, Lexington, Ky., 1974 (Revised 1975, 1977, and 1979).
18. Wood, D. J., and Charles, C. O. A., "Hydraulic Network Analysis Using Linear Theory," *Journal of the Hydraulics Division*, ASCE, Vol. 98, No. HY7, Proc. Paper 9031, July, 1972, pp. 1157–1170.

Appendix II.—Notation

The following symbols are used in this paper:

E_p = pump energy;
f = number of fixed grade nodes;
H = head at system node;
h_L = energy loss in pipe;
j = number of junction nodes;
K = loss coefficient for pipe;
l = number of loops in pipe system;
n = exponent for head loss expression;
N = number of pipes joining junction node;
n_p = number of pumps in pipe system;
p = number of pipes in pipe system;
Q = flowrate in pipe;
Q_e = flow leaving system at junction node;
Q_i = approximate or initial flow in pipe;
Q_{in} = net flow into junction node;
Q_{out} = net flow leaving junction node; and
ΔE = head difference for energy equation connecting fixed grade nodes.

Subscripts

a, b = junction nodes in pipe system.

BOUNDARY CALCULATIONS OF SLUICE AND SPILLWAY FLOWS

By Alexander H-D. Cheng,[1] James A. Liggett,[2] M. ASCE, and Philip L-F. Liu,[3] A. M. ASCE

INTRODUCTION

Some classical hydraulics problems reappear regularly in the literature as more efficient or accurate (or both) solutions are discovered. Because of their inherent difficulty, gravity driven (as opposed to purely pressure driven) free-surface flows have never been solved as accurately and efficiently as is necessary for some design and measurement purposes. The difficulties, as pointed out by von Karman (21), arise not only from the nonlinear character of the boundary condition, but also from the fact that the boundary is not known *a priori*.

One of the major achievements of classical hydrodynamics is the use of conformal transformation in solving a simplified version of the problem. If gravity is absent and the fixed part of the boundary is formed by plane surfaces, the orthodox treatment of G. Kirchhoff, H. Helmholtz, Lord Rayleigh, and others is able to linearize the boundary condition. However, if the fixed part of the boundary is curved or the gravity effect is not neglected, one is again confronted with a nonlinear problem. The mathematical difficulty is so far insurmountable if both effects are to be fully considered. It seems clear that under such conditions one must resort to numerical methods for the solution.

Serious numerical solutions to free-surface flow began with Southwell and Vaisey (18), which involved a heroic effort using finite differences with hand calculation. Other finite difference solutions include those by McNown, *et al.* (16), and Cassidy (3). Finite element solution began with McCorquodale and Li (15) for sluice gates. Many other papers appear in the literature including those by Larock (12), Isaacs (11), Ikegawa and Washizu (9), Chan, *et al.* (4), Taylor, *et al.* (19), Betts (2), Diersch, *et al.* (6), and Varoglu and Finn (20).

[1]Grad. Student, School of Civ. and Environmental Engrg., Cornell Univ., Hollister Hall, Ithaca, N.Y. 14853.

[2]Prof., School of Civ. and Environmental Engrg., Cornell Univ., Hollister Hall, Ithaca, N.Y. 14853.

[3]Assoc. Prof., School of Civ. and Environmental Engrg., Cornell Univ., Hollister Hall, Ithaca, N.Y. 14853.

Note.—Discussion open until March 1, 1982. To extend the closing date one month, a written request must be filed with the Manager of Technical and Professional Publications, ASCE. Manuscript was submitted for review for possible publication on September 26, 1980. This paper is part of the Journal of the Hydraulics Division, Proceedings of the American Society of Civil Engineers, ©ASCE, Vol. 107, No. HY10, October, 1981. ISSN 0044-796X/81/0010-1163/$01.00.

Since flows of this nature are characterized by highly curved boundaries, either a fine mesh or the use of higher order interpolation functions is usually required for a numerical approximation. In addition, due to the intrinsic nonlinearity of the problems, a formidable number of iterations seems to be unavoidable in the solution procedure. Thus, the efficiency of the solution method is important and can become a major factor in the selection of a numerical method.

For many problems in porous media flow, especially those involved in the determination of unknown location of a free surface where a nonlinear kinematic boundary condition is present, the Boundary Integral Equation Method (BIEM) has proved to be a superior numerical technique (13). Direct application of the current methodology to transient water wave problems poses greater numerical difficulty in terms of instability due to the additional nonlinearity from a dynamic free surface condition and the fact that there is no natural damping. For many hydraulic problems in open-channel flow, particularly those associated with flow measuring devices, one is concerned only with the steady-state properties, such as the steady-state free surface profile and the head-discharge relationship. In such cases it seems unnecessary to solve the transient problem. Instead, a scheme based on a perturbation principle is employed in this investigation to provide rapid convergence of the solution to problems of sluice gates and spillways. The BIEM, at least as now applied, is not the final answer to these classical problems. It does, however, represent a further step toward their solution and the replacement of physical models with numerical calculations.

Formulation and Basic Procedure

In the sluice gate and spillway problems only the steady state is considered. The governing equation is Laplace's equation

$$\nabla^2\psi = 0 \quad \text{(1)}$$

in which ∇^2 = the Laplacian operator; and ψ = the stream function. Both the fixed boundaries and the free surface are streamlines, therefore ψ is taken to be a constant, i.e.

$\psi = 0$ on the lower boundary;

$\psi = Q$ on the free surface and on the sluice gate . . . . (2)

in which Q = the flow rate per unit width. On the free surface the dynamic boundary condition requires

$$\frac{v^2}{2g} + y = B, \quad p = 0 \quad \text{(3)}$$

in which v = velocity; g = the acceleration of gravity; y = the free surface elevation measured from an arbitrary datum; B = a constant; and p = pressure. Since

$$v = \frac{\partial\psi}{\partial n} \quad \text{(4)}$$

in which n = the unit normal from the free surface; Eq. 3 becomes

$$\frac{1}{2g}\left(\frac{\partial \psi}{\partial n}\right)^2 + y = B \quad \text{on the free surface} \quad \ldots\ldots\ldots\ldots\ldots\ldots (5)$$

Either the flow rate, Q, or the Bernoulli constant, B, are known; the other is required as part of the solution.

Both the sluice gate and spillway flows extend to $\pm\infty$. For the purposes of the numerical solution the inflow and outflow streams are cut at right angles to the primary velocity. On the cut portions the boundary condition

$$\frac{\partial \psi}{\partial n} = 0 \quad \ldots\ldots\ldots\ldots\ldots\ldots\ldots\ldots\ldots\ldots\ldots\ldots\ldots\ldots (6)$$

is applied which means that there is no velocity normal to the main flow. This condition, although approximate, is applied sufficiently far from the sluice gate or the spillway crest that it is highly accurate and any small error does not affect the interesting part of the flow.

A description of the use of the BIEM using Eq. 1 with boundary conditions of the Dirichlet type (Eq. 2) and the Neumann type (Eq. 6) is found in Liggett (13). The addition of the free-surface boundary condition (Eq. 5) forms an additional complication. This factor is treated in much the same way as it has been for most of the finite difference and finite element solutions. That is, for problems with a known flow rate, Q, the position of the free-surface boundary is assumed and the problem solved from Eqs. 1, 2, and 6. The "constant," B, of Eq. 3 is then calculated on the free surface. If B is the same for all free-surface points, the problem is solved. Otherwise, the assumed free surface is adjusted, iteratively, in order that B becomes constant at all points. The method of adjusting the free surface is problem dependent: for the sluice gate the adjustment technique can be made efficient; on the spillway a more sophisticated technique must be used.

A similar procedure can be developed for problems with a given Bernoulli constant, B. The problem is solved first by assuming the location of free surface and applying the free-surface condition, Eq. 5. The flow rate, Q or ψ, of Eq. 2 is part of the solution. If Q is a constant for all free-surface points, the problem is solved; otherwise, an iteration scheme must be used to adjust the free-surface elevation.

Sluice Gate

Solution Procedure.—The geometry of a vertical sluice gate is shown in Fig. 1. If the flow rate is known, the iterative scheme for adjusting the free-surface location can be described as follows. Introducing $\bar{v}$ as the average velocity at a vertical cross section, the flow rate can be expressed as

$$Q = \bar{v}y \quad \ldots\ldots\ldots\ldots\ldots\ldots\ldots\ldots\ldots\ldots\ldots\ldots\ldots\ldots\ldots\ldots (7)$$

For the purpose of the free surface adjustment, it is assumed that $\bar{v}$ is the free-surface velocity, v. (Although this assumption is poor in the neighborhood of the stagnation point, S, of Fig. 1, the pertinent term in the iteration equation is so small in that neighborhood that it does not spoil the convergence.) Then Eq. 3 can be written in terms of the depth

$$\frac{Q^2}{2gy^2} + y = B \quad (8)$$

A small perturbation on y produces

$$\frac{Q^2}{2gy^2}\left(1 - 2\frac{\Delta y}{y}\right) + y + \Delta y = B + \Delta B \quad (9)$$

in which terms in $(\Delta y/y)^2$ and higher order have been neglected. Subtracting Eq. 8 from Eq. 9 and solving for Δy produces

$$\Delta y = \frac{\Delta B}{1 - \dfrac{Q^2}{gy^3}} \quad (10)$$

The Q^2/gy^3 is a type of Froude number which is less than unity upstream

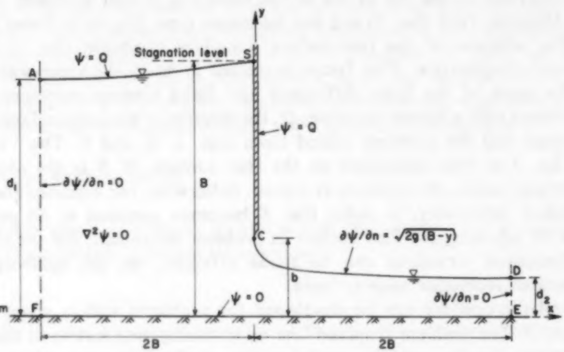

FIG. 1.—Definition Sketch of Vertical Sluice Gate

of the gate and greater than unity on the downstream side.

The solution procedure is:

1. The position of the free surface is estimated and nodes are distributed on the boundary, including the free surface.
2. The BIEM is used to solve for $v = \partial\psi/\partial n$ at each free-surface point.
3. Using Eq. 3, the Bernoulli constant, B_i, is computed for every free-surface point, i, including the tip of the sluice gate, point C (Fig. 1). Since point C cannot be adjusted, i.e., $y = b$ is fixed, yet Eq. 3 applies at C, it is assumed, temporarily, that B_c^k (where the superscript indicates the iteration number) is the correct value of B everywhere for the flow.
4. Using Eq. 10 the i-th node on the free surface is displaced an amount Δy_i in which $\Delta B_i = B_c^k - B_i^k$.
5. When $|\Delta B^k| < \epsilon$, in which ϵ is some small number, the iteration process is considered to have converged; otherwise, steps 2–4 are repeated.

Iteration is necessary because of the linearization of Eq. 8 and because the process assumes that moving one free-surface point does not change the Bernoulli constant at other points. Such an assumption is incorrect since all points are interdependent.

A similar method is used to solve for the flow rate given a Bernoulli constant. The flow problem is solved by replacing the kinematic free-surface condition, Eq. 2, with the dynamic free-surface condition, Eq. 5. The solution yields different values of the stream function at each of the free-surface nodes. A temporarily "correct" flow rate, Q^{k+1}, is needed for performing the free-surface adjustment. As in the previous calculation point C is used and in this case the stream function at point C, ψ_c^k, can be a good estimation of the correct value; however, a better rate of convergence is achieved by taking

$$Q^{k+1} = \psi_c^k + \alpha \left(\psi_c^k - \frac{1}{n_D - n_C} \sum_{i=n_C+1}^{n_D} \psi_i^k \right) \quad \ldots\ldots\ldots\ldots\ldots\ldots \quad (11)$$

in which n_D and n_C = node numbers of points C and D; and α, a weighting factor which can be used to accelerate the rate of convergence, must be determined empirically. (Eq. 11 can also be written in terms of the Bernoulli constant to improve the prediction of B^{k+1} for the case that the flow rate is given and the Bernoulli constant is sought.)

The free-surface adjustment scheme, which corresponds to Eq. 10, for the current case is found by rewriting Eq. 8 as

$$\frac{(\psi_i^k + \Delta Q_i)^2}{2g(y_i^k + \Delta y_i)^2} + y_i^k + \Delta y_i = B \quad \ldots\ldots\ldots\ldots\ldots\ldots\ldots\ldots \quad (12)$$

in which $\Delta y_i = y_i^{k+1} - y_i^k, \quad \Delta Q_i = Q^{k+1} - \psi_i^k \quad \ldots\ldots\ldots\ldots\ldots \quad (13)$

Linearizing and solving for Δy_i produces

$$\Delta y_i = -\frac{\psi_i^k}{g(y_i^k)^2} \left[\frac{\Delta Q_i}{1 - \dfrac{(\psi_i^k)^2}{g(y_i^k)^3}} \right] \quad \ldots\ldots\ldots\ldots\ldots\ldots\ldots\ldots \quad (14)$$

For large gate openings, however, the Froude number for portions of the downstream profile is not much larger than unity. In those cases the Δy_i of Eq. 14 tends to be too large. A more conservative, yet stable, scheme is used whenever the foregoing is observed

$$\Delta y_i = \frac{\Delta Q_i}{\psi_i^k} y_i^k \quad \ldots\ldots\ldots\ldots\ldots\ldots\ldots\ldots\ldots\ldots\ldots\ldots \quad (15)$$

Thus, Eq. 14 or Eq. 15 leads to a new location of the free surface in the same way as Eq. 10. The remainder of the procedure is similar except that accuracy checks are done on the flow rate instead of the Bernoulli constant.

Though the aforementioned methods give a reasonable rate of convergence, it is found that the stream function and the free-surface velocity (when obtained as a result of the calculation) are sensitive to the free-surface location in the subcritical and the supercritical flow regions, respectively. The assumption of a small perturbation, as used to derive Eqs. 10, 14, and 15, may fail if the

initial guess of the free-surface location is too far from the true solution. The process is improved by applying each method only to the region where it is most efficient. This method, which calls for a mixed boundary condition on the free surface, is presented in the following.

Eq. 2 is applied to the upstream free surface to give a Dirichlet type boundary condition and Eq. 5 to the downstream for a Neumann condition. Since only one of the two quantities, Q and B, as required in both Eq. 2 and Eq. 5, is known for a given problem, the other is replaced by a temporarily "correct" value, Q^{k+1} or B^{k+1}, determined from the aforementioned equations. The free-

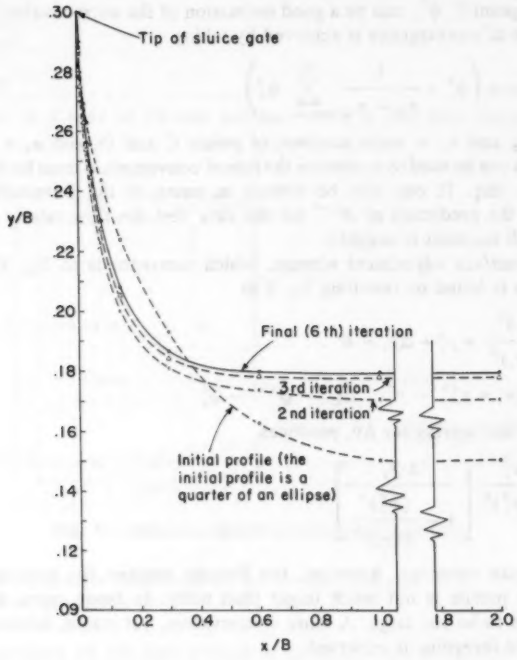

FIG. 2.—Convergence of Downstream Profile for Vertical Sluice Gate

surface adjustment schemes, Eq. 10 upstream of the gate and Eq. 14 or 15 downstream of the gate, are used to find the new free-surface location. Both types of sluice gate problems, those with known flow rate and those with known Bernoulli constant, can be treated by this method. A rapid rate of convergence is always observed, even with an initial guess which differs greatly from the true solution.

All the previously mentioned solution procedures require an initial guess of either the flow rate or the Bernoulli constant. Although equations similar to Eq. 11 can be used to give a temporarily "correct" value for each of the

subsequent iterations, an alternate procedure is necessary for the initial iteration. An empirical equation will suffice but another starting technique has been used in the calculations presented herein. For the case of known Bernoulli constant, the boundary conditions for the first iteration are modified as follows: $\partial\psi/\partial n$ computed from Eq. 5 is specified on both free surfaces, AS and CD. On the sluice gate, SC, $\partial\psi/\partial n$ is prescribed using an arbitrary interpolation formula, e.g., linear or quadratic, between the two known values at S and C. Thus a well-posed problem is defined which does not require an arbitrary guess of an initial trial value of Q. The problem with given flow rate can be treated similarly.

Sluice Gate Solution.—To compare the accuracy and efficiency of the BIEM solution with a most recent FEM solution (11), the following problem is solved.

TABLE 1.—Downstream Profile of Vertical Sluice Gate with $b/B = 0.3$

x, in feet (1)	y, in feet FEM[a] (2)	y, in feet BIEM[b] (3)	ψ, in square feet per second FEM[a] (4)	ψ, in square feet per second BIEM[b] (5)
0.000000	0.300	0.300	1.300	1.303
0.004006	0.289	0.288	1.302	1.304
0.010974	0.278	0.277	1.304	1.304
0.021181	0.267	0.265	1.305	1.304
0.031193	0.258	0.256	1.305	1.303
0.044680	0.248	0.246	1.306	1.303
0.074332	0.231	0.230	1.307	1.303
0.139618	0.209	0.208	1.307	1.303
0.300813	0.187	0.186	1.305	1.303
0.603109	0.180	0.180	1.304	1.303
1.000000	0.179	0.179	1.304	1.303
2.000000	0.179	0.179	1.304	1.302

[a]Isaacs (11).

[b]Solution of the 6th iteration.

Note: $B = 1$ ft; Q (Isaacs) = 1.304 cfs/ft; and Q (BIEM) = 1.303 cfs/ft; Q is the arithmetic mean of column (4) or (5).

The sluice gate geometry is given as shown in Fig. 1 with $B = 1$ (arbitrary length unit) and $b = 0.3$. The initial trial upstream free-surface profile is flat ($y = 1$) and the downstream profile is fit by a quarter of an ellipse with an arbitrary downstream depth of $y = 0.5b$ (Fig. 2). The optimum value of α, as defined in Eq. 11, for each problem can be found on a trial-and-error basis. For all cases of sluice gate flows solved in this paper, $\alpha = 0$ is found generally satisfactory, though values ranging from 0–2 tend to speed the rate of convergence.

The flow boundary is discretized into 39 linear isoparametric elements. The problem has also been solved using cubic spline elements as described by Liggett and Salmon (14). Since the results using the different elements do not differ, only those using linear elements are presented herein.

The transition of the downstream profile is plotted in Fig. 2. Starting with

a rather arbitrary profile, convergence is practically achieved at the 3rd iteration (i.e., free surface is adjusted only twice). Though not shown, the upstream profile converges to the solution even more quickly.

The computation is carried to the 6th iteration where the error, $\epsilon = \max(\Delta\psi_i^k / Q^{k+1})$, is within $\pm 0.1\%$. The results for the downstream profile are given

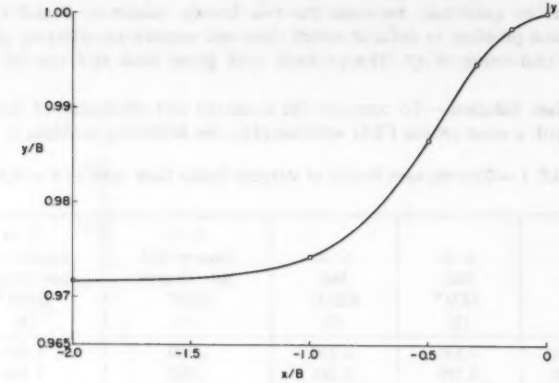

FIG. 3.—Upstream Free-Surface Profile for Sluice Gate

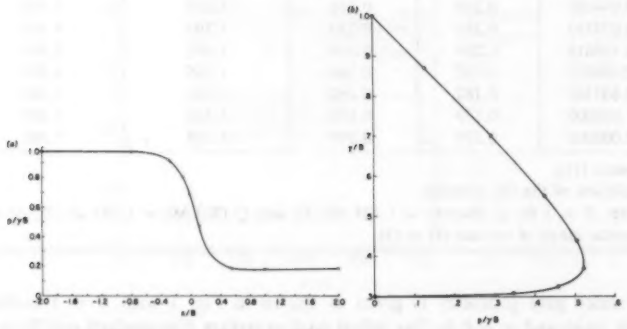

FIG. 4.—(*a*) Pressure Distribution along Channel Bottom for Sluice Gate; (*b*) Pressure Distribution along Sluice Gate

in Table 1. Also listed in Table 1 are results from Isaacs' (11) FEM solution. The FEM solution is obtained using approx 150 elements, some of which are curved cubic triangular elements (10), and 30–40 iterations. A similar finite element solution by Diersch, *et al.* (6) used 120–125 quadrilateral elements, corresponding to a maximum of 1,061 degrees-of-freedom, and 17–25 iterations. As demonstrated here, the efficiency of the BIEM solution in terms of the number of iterations,

number of elements, and computation time is clearly superior to the FEM for comparable accuracy. The outstanding accuracy for such low order elements may be attributed to the fact that all numerical approximation is confined to the boundary and the integration is exact. The upstream free-surface profile

TABLE 2.—Downstream Profile of Radial Sluice Gate

x, in feet (1)	y, in feet FEM[a] (2)	y, in feet BIEM[b] (3)	ψ, in square feet per second FEM[a] (4)	ψ, in square feet per second BIEM[b] (5)
0.39981	3.28	3.28	41.98	41.92
0.42409	3.20	3.23	41.68	41.90
0.46759	3.15	3.17	41.79	41.91
0.57881	3.03	3.04	41.89	41.91
0.90283	2.80	2.79	41.98	41.92
1.22311	2.63	2.62	42.01	41.92
1.54893	2.51	2.50	42.02	41.92
2.04077	2.37	2.36	42.03	41.93
3.51683	2.17	2.16	42.03	41.93
4.98725	2.09	2.08	42.03	41.92
8.03810	2.06	2.05	42.04	41.92
15.42010	2.06	2.05	42.04	41.92

[a]Isaacs (11).
[b]Solution of the 8th iteration.
Note: B = 8.556 ft; Q (Isaacs) = 41.96 cfs/ft; and Q (BIEM) = 41.92 cfs/ft; Q is the arithmetic mean of column (4) or (5).

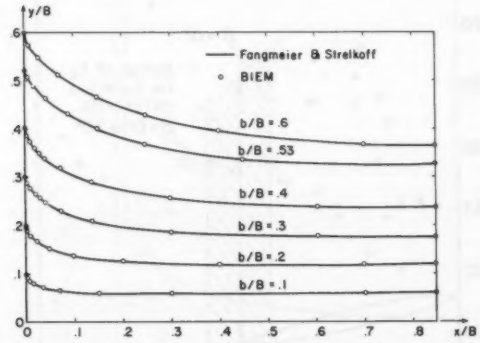

FIG. 5.—Downstream Free-Surface Profiles for Various Gate Opening Ratios

and the pressure distribution along the sluice gate and the bottom are plotted in Figs. 3 and 4, respectively.

A radial sluice gate flow problem, solved by Isaacs (11), is also presented herein. The detailed geometry is found in Isaacs' paper. Thirty-nine linear

segments were used to approximate the flow boundary. The resulting downstream profile of the 8th iteration ($\epsilon = \pm 0.05\%$) is compared with that from Isaacs' FEM solution in Table 2. The use of linear elements to represent a highly curved geometry is indeed adequate.

Vertical sluice gate flows with various gate opening ratios can also be solved. The downstream profiles for those with b/B ratios, 0.1, 0.2, 0.3, 0.4, 0.53, and 0.6 are sketched in Fig. 5. Also shown for comparison are analytical solutions by Fangmeier and Strelkoff (7). The agreement between the BIEM and analytical solutions is excellent.

The contraction coefficient for a sluice gate is

$$C_c = \frac{d_2}{b} \quad \text{(16)}$$

in which d_2, as shown in Fig. 1, = the downstream uniform flow depth. The contraction coefficient as a function of the gate opening ratio is plotted in Fig. 6 along with the analytical solution by Fangmeier and Strelkoff (7), numerical solutions by Southwell and Vaisey (18), and Isaacs (11), and experimental results

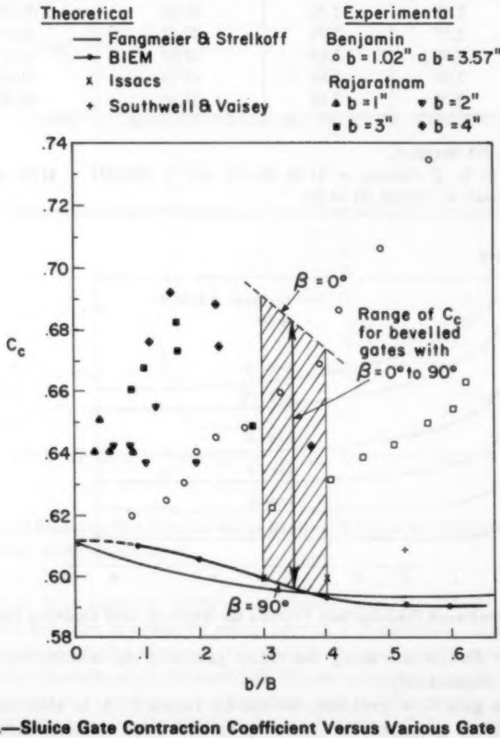

FIG. 6.—Sluice Gate Contraction Coefficient Versus Various Gate Opening Ratios

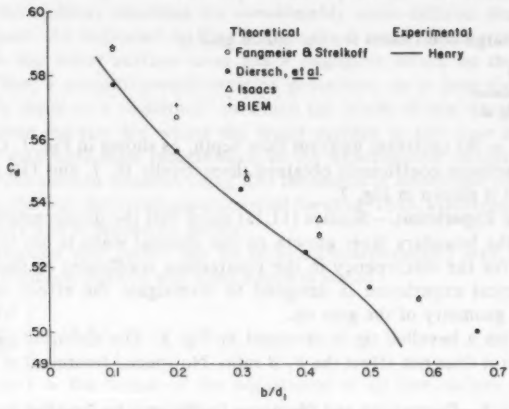

FIG. 7.—Sluice Gate Discharge Coefficient Versus Various Gate Opening Ratios

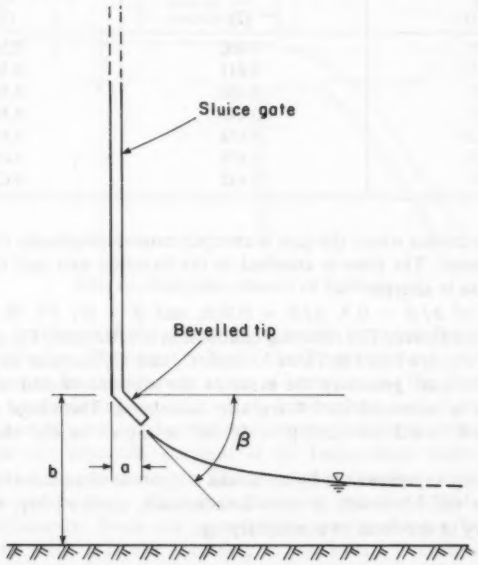

FIG. 8.—Bevelled Tip which is used to Represent Sluice Gate with Partially Rounded or Damaged Exit

by Benjamin (1) and Rajaratnam (17). The experimental coefficients are larger than the theoretical ones. A possible explanation is explored in the following paragraphs.

The discharge coefficient for the sluice gate is

$$C_d = \frac{Q}{b\sqrt{2g\,d_1}} \qquad (17)$$

in which d_1 = the upstream uniform flow depth, as shown in Fig. 1. Comparison between discharge coefficients obtained theoretically (6, 7, and 11), and experimentally (8) is shown in Fig. 7.

Numerical Experiment.—Studies (11,12) show that the displacement thickness caused by the boundary layer growth on the channel walls is not large enough to account for the discrepancy in the contraction coefficient as shown in Fig. 6. A numerical experiment is designed to investigate the effect of a change in the local geometry of the gate tip.

A gate with a bevelled tip is sketched in Fig. 8. The distorted part is made small so that it does not affect the b/B ratio. No special treatment of singularity is given to the corner where the gate is abruptly turned; physically this represents a rounded corner. The flow is attached to the bevelled part and thus the angle of flow release is altered.

TABLE 3.—Contraction and Discharge Coefficients for Bevelled Gates

β (1)	C_c (2)	C_d (3)
90°	0.600	0.550
65°	0.611	0.561
45°	0.630	0.576
30°	0.641	0.587
14.5°	0.652	0.597
5°	0.678	0.618
0°	0.692	0.630

The cases of b/B = 0.3, a/B = 0.003, and β = 0°, 5°, 14.5°, 30°, 45°, 65°, and 90° are solved. The resulting contraction coefficients, C_c, and discharge coefficients, C_d, are listed in Table 3. Both C_c and C_d increase as β decreases. The cases with gate geometry the same as the aforementioned while the gate opening ratio is increased to 0.4 are also calculated. The range of variability of C_c for b/B = 0.3–0.4, and β = 0°–90° is shown as the shaded area in Fig. 6.

The foregoing experiment is by no means a rigorous simulation of the physics near the gate tip. However, it does demonstrate, qualitatively, the effect of local geometry in the form of a nonsharp tip.

Spillway

Solution Procedure.—A typical spillway problem is shown in Fig. 9. Like the sluice gate, the problem can be viewed as solving for the Bernoulli constant

knowing the flow rate or vice-versa. Although the problem has been done both ways, the majority of the solutions are of the former type.

Overall, the spillway solutions are considerably more difficult than those of the sluice gate. As indicated in Fig. 9, there is a zone of uncertainty where a change in the water surface level has a negligible effect on the Bernoulli constant. Thus, a straightforward iteration procedure, as is done for the sluice gate, usually leads to a "solution" in which the result of one iteration differs negligibly from the last but where the water surface in and near the zone of uncertainty may bear little resemblence to the experimental results. The final calculated free-surface position using this technique is dependent on the initial guess and on the way the iterations are carried forward. Thus, a different procedure was necessary and is presented herein.

The assumption that points can be adjusted independently was abandoned. A Newton-Raphson method was used which is stated

$$\{\Delta y\} = \left[\frac{dB}{dy}\right]^{-1} \{\Delta B\} \quad \ldots\ldots\ldots\ldots\ldots\ldots\ldots\ldots\ldots\ldots \quad (18)$$

in which $\{\Delta y\}$ = the vector of the adjustment of all free-surface nodes; and

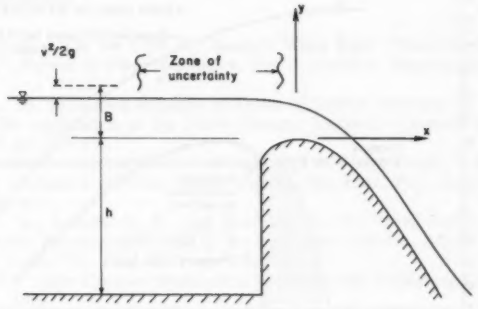

FIG. 9.—Definition Sketch of Spillway

$\{\Delta B\}$ = the departure of the Bernoulli constant for each free-surface node from its target value. The target value of the Bernoulli constant for iteration, $k + 1$, is taken to be the average value of iteration, k. The matrix $[dB/dy]$ is computed by displacing, in turn, each free-surface node a small distance Δy from its assumed value (or the results of the previous iteration) and computing the change in the Bernoulli constant at all free-surface nodes due to the displacement at that particular node. The calculation requires a complete solution for each free-surface node. Thus it is fortunate that the BIEM can do such calculation efficiently. Since the perturbation matrix changes little from one iteration to the next, it is not necessary to recalculate it each time. When it does have to be recomputed, it is necessary only to perturb and recompute those points in and near the zone of uncertainty.

Even when using the Newton-Raphson method the solution of the spillway problem with linear elements produces anomalous results in the zone of uncer-

tainty. Using cubic spline elements (14) leads to good solutions in which the error in Bernoulli constant can be made as small as desired at the nodes. However, the error between the nodes, as calculated from the interpolated velocity and position of the surface cannot be made arbitrarily small, although it is satisfactory.

The best procedure thus far discovered is to place a number of "pseudo-nodes" between the free-surface nodes. Either linear or cubic spline elements are used, with the elevation and velocity at the pseudo-nodes interpolated accordingly. Only the real nodes are perturbed yet $[dB/dy]$ is computed for all nodes. If there are N real free-surface nodes and M pseudo-nodes then $[dB/dy]$ becomes an $(N + M) \times N$ matrix. The error in Bernoulli constant is minimized at the larger number of nodes instead of only at the real nodes. Thus, Eqs. 18 are solved in the least square sense

$$\{\Delta y\} = \left(\left[\frac{dB}{dy}\right]^T \left[\frac{dB}{dy}\right]\right)^{-1} \left[\frac{dB}{dy}\right]^T \{\Delta B\} \quad \ldots\ldots\ldots\ldots\ldots\ldots \quad (19)$$

in which $\{\Delta B\}$ = a vector of the change in the Bernoulli constant for all nodes,

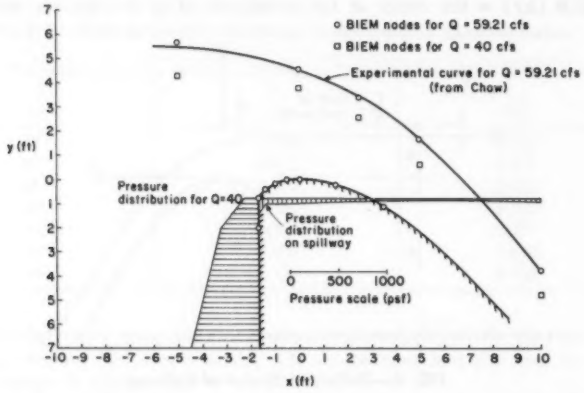

FIG. 10.—Surface Profiles for Spillway with $Q = 59.21$ cfs and $Q = 40$ cfs and Pressure Distribution on Spillway for $Q = 40$ cfs

both real and pseudo. The surface is adjusted only at the real nodes. As a practical matter some limits or damping, or both, is applied to the $\{\Delta y\}$ in order that the adjustments to the free surface are always reasonable. Of course, the departures of the Bernoulli constants cannot be made arbitrarily small since Eqs. 18 are never exactly satisfied. The solution is considered to have converged when the change in the surface position is sufficiently small.

Spillway Results.—Fig. 10 shows a standard WES spillway designed for 59.21 cfs/ft (5.5 $m^3/s/m$) of width. The height of the spillway is $h = 24.78$ ft (7.55 m). (Standard spillway designs are explained in Ref. 5.) The solid line is the experimental water surface. The BIEM results conform closely to the experimental curve. The computed discharge coefficient is $C = Q/B^{3/2} = 4.05$ whereas

Chow (5) gives 4.03. It is difficult to make the Bernoulli constant its target value on the last nodes of the spillway face since the velocity is high and a small velocity change makes a large difference. Of course Eq. 19 could be weighted in order to improve the accuracy in any region, but the result would be to shift the inaccuracy to some other area.

Fig. 10 also shows the surface profile for a flow of $Q = 40$ cfs/ft (3.72 $m^3/s/m$) over the same spillway. The computed discharge coefficient is 4.05 in this case. The figure shows the pressure on the spillway which is everywhere positive but at a low value for the node at $x = 3.5$ ft (1.07 m). The free-surface pressure was also computed. Although it should be identically zero (atmospheric), it had an average value of 2.6 psf (0.0012 atmosphere) with a maximum of 9.16 psf (0.0043 atmosphere). Thus, Eq. 3 has been satisfied to a close approximation.

Acknowledgment

The research reported herein is, in part, supported by the National Science Foundation (Grant Numbers PFR-7815358 and ENG 7902803).

Appendix I.—References

1. Benjamin, T. B., "On the Flow in Channels When Rigid Obstacles Are Placed in the Stream," *Journal of Fluid Mechanics*, Vol. 1, London, England, July, 1956, pp. 227–248.
2. Betts, P. L., "A Variational Principle in Terms of Stream Function for Free-Surface Flows and Its Application to the Finite Element Method," *Computers and Fluids*, Vol. 7, 1979, pp. 145–153.
3. Cassidy, J. J., "Irrotational Flow Over Spillways of Finite Height," *Journal of the Engineering Mechanics Division*, ASCE, Vol. 91, No. EM6, Proc. Paper 4591, Dec., 1965, pp. 155–173.
4. Chan, S. T. K., Larock, B. E., and Hermann, L. R., "Free-Surface Ideal Fluid Flows by Finite Elements," *Journal of the Hydraulics Division*, ASCE, Vol. 99, No. HY6, Proc. Paper 9787, June, 1973, pp. 959–974.
5. Chow, V. T., "*Open Channel Hydraulics*," McGraw-Hill Publishing Co., Inc., New York, N.Y., 1959.
6. Diersch, H. J., Schirmer, A., and Busch, K. F., "Analysis of Flows with Initially Unknown Discharge," *Journal of the Hydraulics Division*, ASCE, Vol. 103, No. HY3, Proc. Paper 12784, Mar., 1977, pp. 213–232.
7. Fangmeier, D. D., and Strelkoff, T. S., "Solution for Gravity Flow Under Sluice Gate," *Journal of the Engineering Mechanics Division*, ASCE, Vol. 94, No. EM1, Proc. Paper 5797, Feb., 1968, pp. 153–176.
8. Henry, H. R., discussion of "Diffusion of Submerged Jets," by M. L. Albertson, *et al.*, *Transactions*, ASCE, Vol. 115, 1950, pp. 687.
9. Ikegawa, M., and Washizu, K., "Finite Element Method Applied to Analysis of Flow Over a Spillway Crest," *International Journal for Numerical Methods in Engineering*, Vol. 6, 1973, pp. 179–189.
10. Isaacs, L. T., "A Curved Triangular Finite Element for Potential Flow Problems," *International Journal for Numerical Methods in Engineering*, Vol. 7, No. 3, 1973, pp. 337–344.
11. Isaacs, L. T., "Numerical Solution for Flow Under Sluice Gates," *Journal of the Hydraulics Division*, ASCE, Vol. 103, No. HY5, Proc. Paper 12923, May, 1977, pp. 473–481.
12. Larock, B. E., "Flow Over Gated Spillway Crests," *Developments in Mechanics*, Vol. 8, *Proc. of the 14th Midwestern Mechanics Conference*, C. W. Bert, ed., University of Oklahoma Press, Norman, Okla., 1975, pp. 437–451.

13. Liggett, J. A., "Location of Free Surface in Porous Media," *Journal of the Hydraulics Division*, ASCE, Vol. 103, No. HY4, Proc. Paper 12851, Apr., 1977, pp. 353–365.
14. Liggett, J. A., and Salmon, J. R., "Cubic Spline Boundary Elements," *International Journal for Numerical Methods in Engineering*, (In press).
15. McCorquodale, J. A., and Li, C. Y., "Finite Element Analysis of Sluice Gate Flow," *Engineering Journal*, Vol. 54, No. 3, Montreal, Canada, Mar., 1971, pp. 1–4.
16. McNown, J. S., Hsu, E.-Y., and Yih, C.-S., "Application of the Relaxation Technique in Fluid Mechanics," *Transactions*, ASCE, Vol. 120, 1955, pp. 650–686.
17. Rajaratnam, N., "Free Flow Immediately Below Sluice Gates," *Journal of the Hydraulics Division*, ASCE, Vol. 103, No. HY4, Proc. Paper 12867, Apr., 1977, pp. 345–351.
18. Southwell, R. V., and Vaisey, G., "Relaxation Methods Applied to Engineering Problems: XIII, Fluid Motions Characterized by Free Streamlines," *Philosophical Transactions, Royal Society of London, Series A*, Vol. 240, London, England, 1946, pp. 117–161.
19. Taylor, C., France, P. W., and Zienkiewicz, O. C., "Some Free Surface Transient Flow Problems of Seepage and Irrotational Flow," presented at the April, 1972, Conference on the Mathematics of Finite Elements and Applications, held at Brunel University.
20. Varoglu, E., and Finn, W. D. L., "Variable Domain Finite Element Analysis of Free Surface Gravity Flow," *Computers and Fluids*, Vol. 6, 1978, pp. 103–114.
21. von Karman, T., "The Engineer Grapples with Non-Linear Problems," *Bulletin of the Mathematics Society*, 46, 1940, pp. 615–683.

Appendix II.—Notation

The following symbols are used in this paper:

B = Bernoulli constant;
b = sluice gate opening;
C = discharge coefficient for spillway;
C_c = contraction coefficient for sluice gate;
C_d = discharge coefficient for sluice gate;
d_1 = upstream uniform flow depth;
d_2 = downstream uniform flow depth;
g = acceleration of gravity;
h = spillway height;
n = unit outward normal;
p = pressure;
Q = flow rate per unit width;
v = velocity;
y = free surface elevation;
α = weighting factor;
β = angle of bevelled sluice gate tip; and
ψ = stream function.

JET INJECTIONS FOR OPTIMUM MIXING IN PIPE FLOW

By Steven D. Fitzgerald,[1] A. M. ASCE and Edward R. Holley,[2] M. ASCE

INTRODUCTION

The mixing of a miscible substance with water flowing in a pipeline is often part of a chemical, or biological water treatment process, or both, and is also required in the dilution method of measuring discharge in a pipe. Conventional mixing devices such as batch mixers, fixed blades in a pipe line, pumps, orifices, valves, etc. are used in many operations. However, their use may require a disruption of the flow or cause a substantial head loss. Thus, for some situations, investigation of alternative mixing methods may be warranted. One viable alternative is to use the pipeline as a mixing chamber by injecting the substance into the pipe flow. The method is sometimes referred to as pipe-flow mixing, in-line mixing, or mixing-on-the-fly.

In situations in which enough pipe length is available and the speed with which mixing is accomplished is not important, the ambient turbulence in a pipe flow can ultimately provide complete mixing of miscible substances. Information is available on the distance required to achieve a certain degree of mixing in such situations (6,9). This paper is concerned with those situations in which more rapid mixing is required and, more specifically, with the use of jet injections to provide initial mixing, thereby hastening the mixing process. With the injection tube at the wall, a jet-injection system can be installed, maintained, and operated with minimal interruption of the flow. There are no concerns about structural problems or flow-induced vibrations of the injection tubes since there are no struts or tubes extending into the pipe. Also, the loss of total energy in the ambient flow due to the jet injection is usually negligible.

In this paper, the injected fluid or additive is called a tracer. The mixing distance is defined as the flow distance from the point of injection to the point where the variation in concentration over the cross section is some small, specified amount. "Optimum" refers to those conditions which result in the most rapid mixing for a given type of jet injection. "Source" or "source-type" injection

[1]Sr. Grad. Engr., Turner Collie & Braden Inc., Houston, Tex.
[2]Prof., Dept. of Civ. Engrg., The Univ. of Texas at Austin, Austin, Tex. 78712.

Note.—Discussion open until March 1, 1982. To extend the closing date one month, a written request must be filed with the Manager of Technical and Professional Publications, ASCE. Manuscript was submitted for review for possible publication on September 3, 1980. This paper is part of the Journal of the Hydraulics Division, Proceedings of the American Society of Civil Engineers, ©ASCE, Vol. 107, No. HY10, October, 1981. ISSN 0044-796X/81/0010-1179/$01.00.

refers to situations in which the injected fluid has no significant initial momentum or buoyancy.

The objectives for this study were to: (1) Experimentally investigate several jet injection systems to determine their mixing characteristics; (2) identify those injection systems providing the most rapid mixing, and determine the optimum operating conditions; and (3) investigate the effects which secondary currents have on the mixing.

This paper summarizes some of the background and experimental results. A more complete report is given elsewhere (6).

Background

Some Definitions.—A parameter which can be used to characterize the uniformity of a concentration distribution over a cross section is the coefficient of variation defined as

$$C_v = \left[\frac{1}{A_p}\int_{A_p}\left(\frac{c}{\bar{c}} - 1\right)^2 dA_p\right]^{1/2} \quad \ldots\ldots\ldots\ldots\ldots\ldots\ldots\ldots\ldots\ldots (1)$$

in which c = tracer concentration at a point in the cross section; $\bar{c}$ = cross-sectional average concentration; and A_p = area of the pipe. The variable C_v is largest near the point of injection where the concentration distribution is highly nonuniform and decreases with increasing flow distance as the concentration distribution becomes progressively more uniform. For large flow distances, empirical C_v values are nonzero and are a function of the random measurement errors associated with the experimental apparatus. For a given injection system and given flow, the mixing distance increases as the desired C_v decreases, i.e., as the requirement for the degree of uniformity increases. Both analytical and experimental evidence indicates that, for small C_v, the maximum concentration variation within a cross section, i.e., $|c - \bar{c}|_{max}$, is linearly related to C_v (9).

From dimensional analysis, the ultimate penetration, Y, of a nonbuoyant jet into the ambient crossflow can be written as

$$\frac{Y}{D_p} = f(M_r, Q_r, \mathsf{R}_j, \alpha) \quad \ldots\ldots\ldots\ldots\ldots\ldots\ldots\ldots\ldots\ldots (2)$$

in which M_r = the momentum flux ratio defined by

$$M_r = Q_r V_r = (V_r D_r)^2 \quad \ldots\ldots\ldots\ldots\ldots\ldots\ldots\ldots\ldots\ldots (3)$$

and Q_r = volume flux or discharge ratio = Q_j/Q_p; V_r = velocity ratio = V_j/V_p; D_r = diameter ratio = D_j/D_p; R_j = initial jet Reynolds number; α = initial angle of jet relative to the pipe wall; and subscripts j and p refer to the jet and the pipe, respectively. In Eq. 2 it is assumed that the turbulence characteristics of the pipe flow do not influence the jet penetration. Experimental results (1,7,10) indicate that the behavior of jets injected into pipes is not influenced by the volume flux ratio so that Q_r can be eliminated from Eq. 2. [Wright (11) considered the significance of the volume flux for jets in unbounded crossflows.] Further, if R_j is large enough so that kinematic similarity of the jets exists, then R_j is not a significant parameter and Eq. 2 can be written as

$$\frac{Y}{D_p} = f(M_r, \alpha) \quad \text{(4)}$$

Similarly, the initial mixing provided by jets is a function of M_r and α, plus the number and location of the jets around the pipe wall. Sources are the limiting case in which $M_r = 0$ so that there is zero penetration and zero initial mixing.

Ambient Mixing.—Ambient mixing in uniform pipe flow has been considered by the second writer and Ger (8) with a summary given in Refs. 6 and 9. It was shown that for given locations of passive sources, C_v is a function of a dimensionless longitudinal distance

$$Z = \frac{e_r z}{V_p R_p^2} \quad \text{(5)}$$

in which e_r = radial diffusion coefficient, R_p = pipe radius; and z = flow distance from injection point. Based on empirical values of the eddy viscosity, e_r can be estimated and Eq. 5 can be written as (8)

$$Z = \frac{0.048\sqrt{f}}{Sc_t}\frac{z}{D_p} \quad \text{(6)}$$

in which f = friction factor; and Sc_t = turbulent Schmidt number. The differential mass balance equation was solved analytically to investigate the diffusion of a conservative, neutrally buoyant substance released continuously from point sources in a steady, uniform, turbulent pipe flow (8). Except for source configurations which are symmetrical about the pipe center line, the asymptotic slope of log C_v versus Z is a function of a dimensionless parameter

$$\eta = \frac{e_\theta}{e_r} \quad \text{(7)}$$

in which e_θ = circumferential diffusion coefficient. Experimental results were used to evaluate η and e_θ, but the values depended on the value assumed for Sc_t. Using the concentration data collected by Filmer and Yevdjevich (5), Clayton et al. (3), and Ger and the second writer (7), η was found to be 1.8, assuming a turbulent Schmidt number of 1.0, or $\eta = 1.2$, assuming $Sc_t = 0.77$.

Fig. 1 is a plot of log C_v versus Z with $\eta = 1.8$ and $Sc_t = 1.0$ for a number of different point source locations represented by $\rho' = r/R_p$, in which r = radial coordinate measured from the pipe center line. Thus, $\rho' = 1$ represents a source at the pipe wall, and $\rho' = 0$ is at the center line. The asymptotic (large Z) slope for the $\rho' = 0$ curve also represents the asymptotic rate of mixing or slope of log C_v versus Z for any initial concentration distribution or any number of point sources provided that the initial distributions or sources are symmetrically arranged about the pipe center line. Similarly, the $\rho' = 1$ curve for large Z represents the asymptotic slope for all asymmetrical cases and for the slowest rate of ambient mixing. For brevity, these characteristic slopes will be called the "symmetrical" slope and the "asymmetrical" slope. For asymmetrical initial concentration distributions or point source distributions, the log C_v versus Z curve can have somewhat different shapes for small Z.

The curve can follow the center line source curve, but eventually it will break away to the "asymmetrical" slope. See, e.g., the curve for $\rho' = 0.2$ in Fig. 1. The point at which the curve changes from the "symmetrical" to the "asymmetrical" slope depends on the initial degree of asymmetry.

The "symmetrical" slope for $\rho' = 0$ is associated with perfect symmetry, but perfect symmetry can never be obtained in experiments. Thus, it might be expected that empirical curves for log C_v versus Z should eventually have the asymptotic slope for all asymmetrical conditions, but this is not necessarily the case for two reasons. First, Fig. 1 shows that the value of Z at which the curves for asymmetrical injections break away from the curve for $\rho' = 0$ depends on the value of ρ', or more generally, on how nearly symmetrical the initial or injection condition is. For $\rho' = 0.05$ and $Z < 0.4$ (or $C_v > 0.01$),

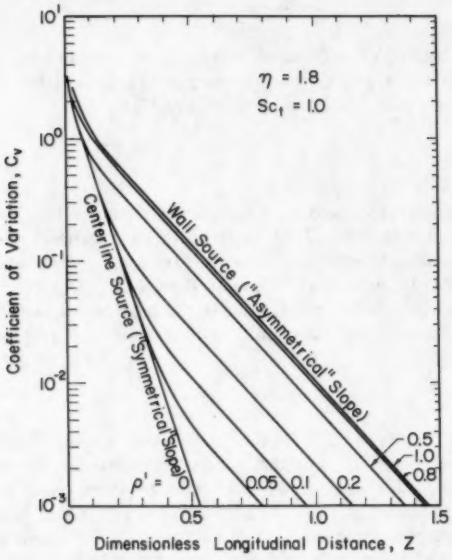

FIG. 1.—Calculated Coefficient of Variation for Point Sources

e.g., it probably would not be possible to distinguish empirically between sources corresponding to $\rho' = 0.05$ and $\rho' = 0$. Thus, a slightly asymmetrical injection could give results which followed the "symmetrical" slope. The second reason is that at some value of C_v, the empirical results begin to represent random measurement errors rather than degree of uniformity of the concentration distribution. Thus, it is normally not possible to measure extremely small values of C_v to determine if the log C_v versus Z curve has broken away from the "symmetrical" slope. Empirical curves for nearly symmetrical situations can therefore follow the "symmetrical" slope throughout the range of significant C_v values. Typical values of C_v below which measurement errors predominate

are 0.05 for fluorescent tracers (9), 0.02 for conductivity (6), and 0.003 for radioactive tracers (3,9).

Experimental and analytical studies dealing with ambient mixing have been summarized elsewhere (6,8,9).

Jet-Injection Experiments.—A turbulent jet injected with significant momentum across the ambient flow can create rapid initial mixing and can significantly reduce the mixing distance. Chilton and Genereaux (1) published one of the first reports addressing the use of different configurations of injection systems to promote rapid mixing. They used air flowing through a glass pipe and an air jet containing smoke as the tracer so visual evaluation could be made concerning the relative mixing for each injection system. They recognized from their qualitative measurements that a range of optimum momentum ratios existed for a given method of injection.

Some information on the relationship of jet penetration to M_r can be obtained from Wright's (11) work on jets in cross flows. His momentum length scale, ℓ_m, can be expressed as

$$\frac{\ell_m}{D_p} = M_r^{1/2} \quad \ldots\ldots\ldots\ldots\ldots\ldots\ldots\ldots\ldots\ldots\ldots\ldots\ldots\ldots\ldots\ldots (8)$$

Wright's Fig. 4, using y for the distance from the pipe wall, indicates that for the momentum-dominated far field, which is the region of interest for characterizing the penetration for most of the jet injections, the trajectory can be written as

$$\frac{y}{D_p} = 1.6\, M_r^{1/3} \left(\frac{z}{D_p}\right)^{1/3} \quad \ldots\ldots\ldots\ldots\ldots\ldots\ldots\ldots\ldots\ldots\ldots\ldots (9)$$

It is difficult to use Eq. 9 to obtain an absolute evaluation of the jet penetration because of uncertainties concerning the point of transition from initial mixing to ambient mixing. Nevertheless, it is possible to use Eq. 9 to obtain relative penetrations for different M_r values by assuming, e.g., that the transition can be represented by the same slope (dy/dz) of the trajectory for any two M_r values represented by the subscripts 1 and 2. Differentiation of Eq. 9 and appropriate manipulation shows that

$$\frac{\dfrac{y_1}{D_p}}{\dfrac{y_2}{D_p}} = \left(\frac{M_{r_1}}{M_{r_2}}\right)^{1/2} \quad \ldots\ldots\ldots\ldots\ldots\ldots\ldots\ldots\ldots\ldots\ldots\ldots\ldots\ldots (10)$$

so that the relative penetration of jets into the pipe should be proportional to the square root of M_r.

Ger and the second writer (7) experimentally found the optimum momentum ratio, M_r^*, to be approx 0.016 for a single cross-flow jet. This value is considered again later. Their experiments were conducted in the same 6-in. (152-mm) inside diam galvanized steel pipe used for this study. They showed that for $M_r = M_r^*$, the concentration distribution of the tracer was approximately symmetrical about the center line of the pipe after the jet was bent over by the ambient

flow. For $M_r < M_r^*$, the jet did not reach the center line, and for $M_r > M_r^*$, the jet overshot the center line. For M_r either greater than or less than M_r^*, the mixing distance increased compared to the situation in which $M_r = M_r^*$. Therefore, for a single jet-injection system to have the maximum effectiveness as a mixing device, it must promote rapid initial mixing and distribute the tracer symmetrically about the center line of the pipe to allow the diffusion processes to efficiently continue the mixing.

The curves in Fig. 1 are related only to ambient mixing since they were calculated for passive sources. The characteristic slopes are applicable for the downstream, ambient mixing part of the process even with initial jet mixing (8). Normally, the jet is dissipated rather rapidly so that the initial mixing region is rather short (only a few pipe diameters, at most, for small diameter jets).

Experiments and Results

Experiments were conducted in a 6-in. (152-mm) inside diam galvanized steel pipe under steady, fully-turbulent flow conditions. For most of the experiments, the pipe Reynolds number was between 30,000 and 40,000 and the friction factor

TABLE 1.—Location of Sampling Stations

Sampling station (1)	z/D_p (2)	Z^a (3)
1	7.00	0.053
2	17.00	0.129
3	27.00	0.205
4	37.00	0.281
5	47.00	0.357

[a]Eq. 5 or 6 with $Sc_t = 1.0$.

was approx 0.025. A nonbuoyant, sodium chloride tracer was injected at a steady rate into the flowing water through 1/8-in. (3.2-mm) inside diam brass tubes with the outlet flush with the pipe wall. The distribution of tracer concentration in the ambient flow was determined by conductivity measurements on two perpendicular diameters with a total of 13 points at sampling stations spaced 10 pipe diameters apart, as given in Table 1.

The two types of injection systems investigated were: (1) A single jet originating at the pipe wall with the angle of injection, α, varied from 90° (cross flow) relative to the ambient flow direction to 150° (almost counter flow); and (2) two jets which originated at the pipe wall, were at opposite ends of the vertical diameter, and had an angle of injection of 90°. After finding the optimum conditions for the jet injections, the effect which a particular secondary current had on the mixing distance was investigated by placing a fixed three-bladed outboard motor propeller upstream of the injection point.

Wall Source Experiments.—Previous experiments with a single wall source were repeated to check the experimental techniques. The data from this study were in good agreement with the data from the other studies (3,7) and with the analytical solution for a wall source (see Fig. 1 with $\rho' = 1.0$). It was

concluded that the experimental techniques were satisfactory, and that the 13 sampling points were sufficient to provide an accurate evaluation of C_v at each of the measurement cross sections.

Single Jet Injections.—The single jet-injection experiments consisted of an injection tube positioned at the top of the pipe with the outlet flush with the pipe wall and at angles of 90°, 120°, 135°, and 150° relative to the pipe flow. The fluctuations in the background salt concentration and the random errors in the measurements had a negligible effect on C_v for the highly nonuniform concentration distributions near the point of injection. However, the experimental inaccuracies became progressively more significant with increasing uniformity of the concentration distributions and with increasing flow distance. By comparing

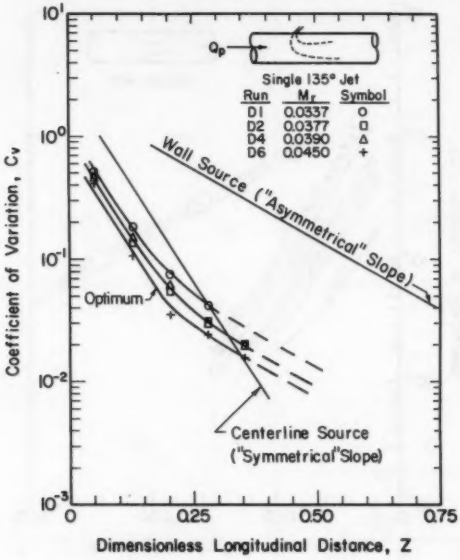

FIG. 2.—Coefficient of Variation for Single 135° Jet

the empirical log C_v versus Z curves to the general analytical behavior of log C_v versus Z curves (see Fig. 1), it was estimated that C_v values equal to or less than approx 0.02 represented random measurement errors rather than degree of uniformity of the concentration distribution. Thus, the values of C_v below 0.02 were not necessarily reliable and some of the points for $0.02 < C_v < 0.025$ may have been questionable.

For each α, M_r was varied to provide concentration data for estimating the optimum M_r^*. The method for selecting M_r^* is considered at the end of this section. Fig. 2 shows the empirical C_v values obtained for $\alpha = 135°$; similar variations of C_v with Z were found for each α. The individual C_v values have been published elsehwere (6). Fig. 3 shows the comparison of C_v values for

the optimum M_r^* for each α. For each M_r, the mixing distance, Z_m, was defined as the flow distance required for C_v to reach some specified value. For C_v equal to 0.02, Fig. 3 shows essentially no reduction in Z_m for $M_r = M_r^*$ as α was increased from 90°–135° and a reduction of only about 15% at α = 150°. The reason for this behavior is that transverse symmetry of the jet became progressively more difficult to maintain as α was increased. The asymmetry could be seen directly in the concentration distributions (6), and the results of the asymmetry can be seen in that the C_v values for the larger α values tend to curve away from a line with the "symmetrical" slope. For C_v = 0.1, there is a consistent decrease in Z_m with increasing α since this value of C_v is in the linear part of each curve with the "symmetrical" slope (see Fig. 3).

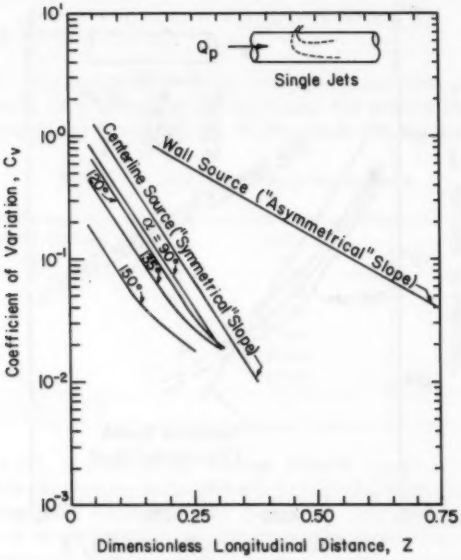

FIG. 3.—Coefficient of Variation for Optimum Momentum Ratios

The variable Z_m for α = 150° is more than 50% smaller than for α = 90°. However, the optimum momentum ratio for α = 150° is approximately six times greater than that for 90°. The variable Z_m for C_v = 0.02 is 66% less when a 90° jet is used instead of a wall source and 71% less when a 150° jet is used instead of a wall source.

Fig. 4 depicts the variation of Z_m with M_r for each α and for two values of C_v. For C_v = 0.10, Z_m is not very sensitive to small variations of M_r from M_r^*, as indicated by the relatively flat curves through the data points. The data indicate a greater sensitivity of Z_m to M_r for C_v = 0.02. The calculated value of Z_m for M_r = 0, i.e., a wall source, is shown in Fig. 4 for each α to demonstrate the reduction in Z_m which is achieved by using jet injections.

The dashed lines in Fig. 4 are very approximate, having been estimated from the information in Fig. 1, assuming that the jet penetration is proportional to the square root of M_r (Eq. 10) and that each jet can be represented by a virtual source at the ρ' corresponding to jet penetration.

The experimental program was designed and executed to conduct tests for a range of M_r values which would bracket M_r^* for each α. Unfortunately, as Figs. 2 and 4 indicate, not all of the sets of experiments actually provided this bracketing. This is an unfortunate condition which resulted from a re-analysis of the data after the project support had ended so that it was not possible

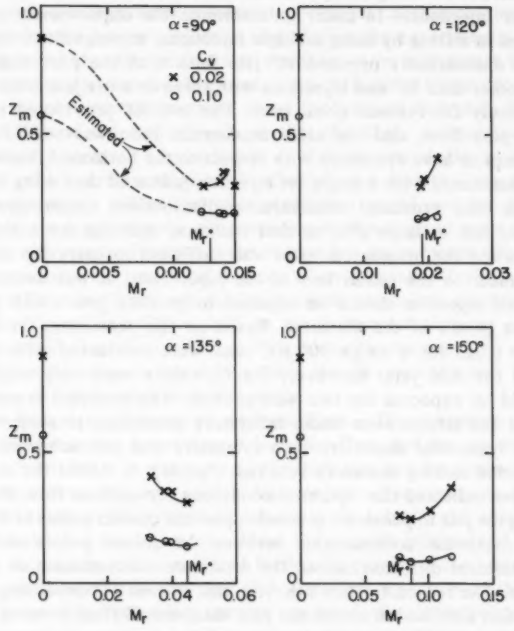

FIG. 4.—Mixing Distances for C_v = 0.02 and 0.10

to conduct additional tests. In some cases (primarily for α = 150°, Fig. 4) a clear definition of M_r^* could be obtained from the available log C_v versus Z graphs. However, the values of M_r^* for the other injection angles were selected both by studying the C_v graphs and by checking the concentration distributions at the downstream stations for symmetry with respect to the horizontal diameter since it was this symmetry which was indicative of optimum penetration of the jets. Due to the horseshoe or kidney-shaped concentration contours which develop for jets in cross flows (4), it was not uncommon for optimum conditions to have the maximum concentration near the center line at Station 1 and below the center line (e.g., at r/R_p = 0.1) for Stations 2 and 3. At Station 4, the

concentration distributions were nearly symmetrical about the horizontal diameter for optimum conditions. Symmetry about the vertical center line related to alinement of the jets. By thus studying the concentration distributions, all of which have been published elsewhere (6), it can be seen that $M_r = 0.0124$ for $\alpha = 90°$ gave underpenetration while $M_r \geq 0.0138$ gave overpenetration, so that the optimum conditions were bracketed. Since the results for $\alpha = 90°$ and 150° gave a good indication of the shapes of the concentration distributions for optimum conditions, it could be concluded from the concentration distributions for $\alpha = 120°$ and 135° that optimum conditions had been reached or very nearly approximated even though they were not bracketed.

Dual Jet Injections.—In order to determine the improvement which could be obtained in mixing by using multiple injections, experiments were conducted using two diametrically opposed 90° jets flush with the pipe wall. Angles of injection other than 90° and injections with three or more jets were not studied experimentally for reasons given later. The two 90° jets issued into uniform turbulent pipe flow, and the same momentum ratio was used for both jets in an attempt to have symmetry with respect to the horizontal diameter.

The experiments with a single jet injection indicated that using the optimum momentum ratio produced concentration distributions symmetrical about the pipe center line at large Z's, so that optimum injection for a single jet was obtained when the momentum ratio was sufficient to carry the center of the injected tracer to the center line of the pipe. Thus, it was assumed that M_r for the dual injection should be adjusted to produce jets which penetrate to the quarter points of the diameter. Based on this reasoning, on Eq. 10, and on $M_r^* = 0.013$ for a single 90° jet, runs were conducted with $M_r = 0.003$ and 0.004 for dual jets. However, the C_v values were only slightly smaller than would be expected for two wall sources. The apparent reason was that, in spite of the efforts even under laboratory conditions to achieve symmetry about the horizontal diameter, such symmetry was not achieved, and larger than expected mixing distances resulted. For $M_r^* > 0.006$, the concentration distributions indicated that optimum conditions for uniform flow were obtained by causing the jets to penetrate somewhat past the quarter points of the diameter. With the maximum concentration between the quarter points and the center line, the ambient diffusion caused the maximum concentration to move to the center line. The reason for this behavior can be seen by visualizing a two-peak concentration distribution across the pipe diameter. Diffusion moves mass from the two regions of high concentration to the three regions of low concentration. If the jets penetrate past the quarter points, diffusion from the large concentrations will "fill in" the distribution in the center of the pipe faster than at the walls since there is less to "fill in." Then diffusion will take place only toward the wall and the maximum concentration will be in the central portion of the pipe. Apparently, since it is not possible to obtain precise symmetry of the injection, the practical optimum is for penetration past the quarter points of the diameter. Thus, essentially the same concentration distributions and C_v values were obtained for the tests with M_r from 0.006 to 0.010, so that M_r^* is in this range. For this optimum dual injection, $Z_m = 0.28$ and 0.17 for $C_v = 0.02$ and 0.10, respectively. The corresponding values of Z_m for two passive wall sources 180° apart (9) would be 0.32 and 0.21, so that the use of the two jets gives only a 13% or a 19% reduction in Z_m (depending on the definition used) as compared

to two passive sources for uniform flow.

Effects of Jet Misalinement.—Fig. 1 shows C_v calculated from the analytical solution of the mass balance equation for single point sources. The results indicate that the mixing distance is more sensitive to a source's being off the center a short distance than to being moved inward from the pipe wall a short distance if a small C_v (e.g., 0.01 or 0.02) is used in defining Z_m. This analytical indication of the effect which a slight misplacement of a center line point source would have on the mixing distance for small C_v is an indication that the mixing distance for a jet with M_r near M_r^* would also be rather sensitive to the concentration distribution immediately downstream from the initial mixing zone and therefore to the transverse alinement of the jet. Sensitivity tests per se were not run for the jet-type injection, but during the experimental program, it became apparent that the mixing was sensitive to jet alinement. Even with the utmost attention given to the alinement, it was difficult to obtain concentration distributions which were symmetrical about the vertical diameter. With care, the jets could be alined well enough so that the slight asymmetry was not evident in the C_v versus Z graphs for $C_v > 0.03$ for the single jet injections. The distance which a concentration distribution can deviate from the center before the asymmetry effect becomes significant could not be determined accurately without measuring the concentration distributions in more detail than was done for this study. However, the results for an optimum 90° single jet in the present work were compared to those of an optimum 90° single jet which was slightly off center (7) and which, for optimum conditions, produced a peak concentration located at $r/D_p = 0.05$ on the horizontal diameter at $z/D_p = 4$. The optimum Z_m for $C_v = 0.03$ was 55% larger for the previous study than for the optimum injection in this study. Also, the previous M_r^* was 17% larger than the value of 0.013 obtained in this study.

Tests with Secondary Currents in Ambient Flow.—The symmetry which has been considered requires symmetry of both the flow and the injection. Since secondary currents exist in many pipes, the flow may not be symmetrical with respect to the center line and even a high degree of accuracy in alining the jets may not produce the symmetry necessary to achieve the same rates of mixing as measured in the laboratory. Thus, the possible influence of secondary currents on the mixing was considered further by placing a three-blade, fixed, outboard motor propeller in the pipe 13.5 diameters upstream of the point of injection. The resulting secondary current consisted of a single cell swirl which was approximately symmetrical with respect to the center line and which caused a full rotation of the flow in approx 8 diameters.

A single 90° jet injection ($M_r = 0.013$, Run $G1$) and dual 90° jet injections ($M_r = 0.010$, Run $G2$) were used to compare the mixing characteristics with and without the secondary current. The semilog graph of C_v versus z/D_p is presented in Fig. 5. Variable C_v was plotted versus z/D_p rather than Z because the propeller changed the structure of the pipe flow and thus probably changed e_r compared to the previous tests. Experiments were not conducted to determine e_r with the propeller in place.

A comparison (Fig. 5) of the single 90° jet with and without the secondary current shows that the swirling motion caused the log C_v versus z/D_p curve to break away from the "symmetrical" slope sooner than for the condition with no swirl. The concentration distributions showed that the swirl apparently

deflected the jet toward the side of the pipe and thereby caused an asymmetrical distribution. Thus, even though the propeller probably increased e_r, the asymmetry increased the mixing distance. On the other hand, a comparison of the C_v values for two 90° jets ($M_r = 0.010$) issuing into a flow with and without the secondary current (Fig. 5) indicated that the swirl decreased the mixing distance for this dual jet arrangement. There is too little data to obtain a definite explanation for this observed decrease in mixing distance, but the explanation might be as follows: With no secondary currents, the two jets approached each other and the two concentration distributions which resulted from the initial mixing merged together about the center line. With the single cell swirl in the flow, the top and bottom jets were deflected in opposite directions so that they did

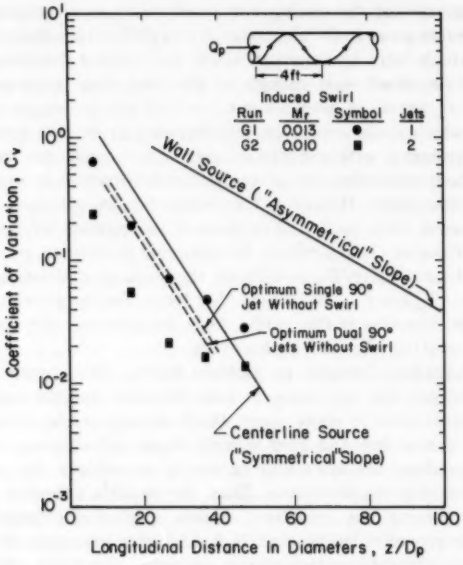

FIG. 5.—Coefficient of Variation with Secondary Current in Pipe Flow

not merge at the center and therefore produced a greater amount of initial mixing, i.e. a more "spread out" concentration distribution at the end of the initial mixing zone.

Other Multiple-Jet Injections

Uniform Flow.—The results from the dual 90° jets did not indicate a significant decrease in the mixing distance as compared to the single 90° jet for uniform flow. It was assumed that any decrease which could be obtained by using two jets with $\alpha > 90°$ instead of one jet would be on the same order of magnitude as the decrease for $\alpha = 90$. Therefore, dual jet injections for $\alpha > 90°$ did not seem justified for uniform flow conditions.

The second writer (9) has shown that for equally-spaced, passive wall sources there is only a small reduction in the calculated mixing distance, Z_m, when using three sources instead of two, and that there is no reduction in Z_m when using four or more wall sources instead of three. In view of these results, and in view of the fact that: (1) The optimum condition for two jets corresponded to the concentration distributions' merging at the center of the pipe; and (2) the optimum two-jet injection gave only a small reduction in Z_m compared to the optimum single jet, it appeared that there would probably be only marginal further reduction in Z_m by using three or more jets for uniform flow.

Flow with Secondary Currents.—Many natural pipe flows have secondary currents rather than being truly uniform. Because of the various types of secondary flows which can exist, it is difficult to generalize on possible interactions of jet injections and secondary currents. Nevertheless, some secondary currents destroy the symmetry required to achieve the rates of mixing which existed for the optimum conditions with uniform flow. Even though the use of three or four injections apparently would give only small reductions in Z_m, compared to one or two injections for uniform flow, Fig. 5 shows that the use of two injections provides a definite advantage compared to one injection in a particular flow with a secondary current. At least for some flows, it might be expected that the use of two or more injections would provide a sort of factor of safety against possible effects of secondary currents on Z_m. However, there is not enough data presently available to quantify this possible effect.

Applications

Pump Mixing.—Pump mixing deserves some mention even though this paper has not dealt with that subject, and even though there is apparently very little available data. Clayton (2) has shown that nearly complete mixing (less than 2% variation in concentration) was obtained in a mixed-flow pump with a 20-in. discharge line and with a flow of 8.2 cfs. The injection was made at the bell-mouth suction port, which was submerged in a sump.

The efficiency of pumps gives one indication that pumps should serve as rapid-mixing chambers. If a pump has an efficiency of 80%, then 80% of the energy input goes into the mean flow while 20% is lost, with a significant part of the loss being in the generation of turbulence which produces the mixing. Large turbines generally have higher efficiencies so that there is little turbulence and, therefore, little mixing generated by the blades of a large turbine.

If a pump is being considered for mixing, the considerations should include possible volitalization of the additive due to low pressures on the suction side of pump and any possible corrosion of metal parts, deterioration of seals, etc., due to the concentration of the additive in the pump.

Pipe Mixing.—If speed of mixing is not important and if sufficient pipe length is available, then a simple injection at or near the pipe wall may be all that is required. A distance corresponding to $Z_m \simeq 1.0$ will produce enough mixing to give $C_v = 0.01$ when a negligible density difference exists between the fluid in the pipe and the injected fluid. The corresponding maximum deviation from the average concentration would be less than 2% (9). For a friction factor of 0.02, Z_m of 1.0 corresponds to 147 pipe diameters with $Sc_t = 1.0$, or $f = 0.01$ gives 208 diameters for $Z_m = 1.0$. The use of two points sources, 180°

apart at the wall, would reduce Z_m from 1.0 to 0.37 for $C_v = 0.01$ (9). If there is insufficient pipe length to accomplish the mixing by ambient turbulence, or if more rapid mixing is required, then jet injections could be considered. When it is desirable to use a combination of initial mixing due to the injection and ambient mixing due to the pipe flow, the selection of the best injection system for promoting rapid mixing in a specific application requires consideration of at least six factors: (1) The required degree of uniformity or the required coefficient of variation for the additive; (2) the speed with which mixing needs to be accomplished; (3) the pipe length available for mixing; (4) the hydraulics of the pipe flow, i.e., the friction factor and secondary current pattern; (5) the accessibility of the injection region and possible problems installing and operating an injection system; and (6) the cost and availability of power for the injection.

In general, the required degree and speed of mixing will depend on the particular application. When using the method of dilution for measuring discharge in a pipe, e.g., it may be advantageous to measure the tracer at only one point in the pipe flow at a cross section where C_v is small, say less than 0.01. For other applications, larger C_v values may be acceptable.

The pipe length available for mixing should be determined. Some injection configurations may be excluded from consideration because the flow distance required to reach the specified C_v is longer than the available pipe length. For established, uniform flows with negligible secondary currents, the results from Figs. 3 and 5 may be used to estimate the distance required to obtain a certain degree of mixing for the optimum momentum ratios for injections with one and two jets. For two jets, e.g., with $M_r = 0.010$, $C_v = 0.10$ would be achieved at $Z = 0.17$ and $C_v = 0.01$ at $Z = 0.33$. For $f = 0.015$ with $Sc_t = 1.0$, $Z = 0.17$ corresponds to $z/D_p = 29$. Similarly, $Z = 0.33$ gives $z/D_p = 56$. For a 3-ft (0.91-m) diam pipe with a velocity of 5 fps (1.52 m/s) and with 1-in. (2.54-cm) diam injection tubes with $M_r = 0.010$, the injection velocity and discharge for each jet could be calculated from

$$M_r = \left(\frac{V_j D_j}{V_p D_p}\right)^2 = 0.010 \quad \ldots\ldots\ldots\ldots\ldots\ldots\ldots\ldots\ldots\ldots\ldots\ldots \quad (11)$$

$$V_j = \sqrt{0.010}\,\frac{V_p D_p}{D_j} = 18.0 \text{ fps } (5.5 \text{ m/s}) \quad \ldots\ldots\ldots\ldots\ldots\ldots\ldots\ldots \quad (12)$$

$$Q_j = A_j V_j = 0.10 \text{ cfs } (2.8\ l/s) \quad \ldots\ldots\ldots\ldots\ldots\ldots\ldots\ldots\ldots\ldots\ldots\ldots \quad (13)$$

Power requirements are considered later.

As mentioned previously, many flows have significant secondary currents which can destroy the symmetry that is necessary to achieve the optimum rates of mixing obtained for uniform flows. Some experimental results were obtained for a flow with a particular type of secondary current, but that current was a rather strong, single cell swirl and the results for that case are not necessarily indicative of the behavior in other situations. On the basis of present information, in order to achieve the most rapid possible mixing with jet injections, it would appear to be advisable to use two or more 90° jets equally spaced around the pipe periphery, with each jet having M_r of 0.006 to 0.010. The use of more than two jets provides a factor of safety against the unknown influences of

secondary currents which might exist in the flow. For pipe flows with natural secondary currents, there is a sparsity of data on the behavior of jet injections and more research is needed on this topic.

Power Requirement.—The power requirement, P_j, for supplying the kinetic energy to the jets can be written in dimensionless form as

$$\frac{P_j}{P_p} = \frac{N\gamma Q_j \dfrac{V_j^2}{2g}}{\gamma Q_p \dfrac{V_p^2}{2g}} = N M_r^{3/2} \frac{D_p}{D_j} \quad \ldots\ldots\ldots\ldots\ldots\ldots\ldots\ldots\ldots\ldots (14)$$

in which P_p = power in kinetic energy of pipe flow; Q = discharge; V = velocity; D = diameter; p = pipe; j = jet; and N = number of jets. The variable P_j decreases as D_j increases for a given pipe flow and given M_r. Eq. 14 represents only the power required for the velocity head of the jet. A major additional power requirement could come from the need to pump the jet against the internal pressure in high pressure lines. However, most of this additional power requirement can be eliminated by a closed system where the fluid for the jet injection is extracted from the pipe. Then a small-power, high-pressure pump could be used to inject a concentrated tracer (additive) into the closed system. The injection should be made in the by-pass line so that complete mixing occurs before the jet enters the main pipe. This mixing could be accomplished by injecting upstream of the pump or by providing sufficient length of the by-pass line. Friction losses and pump efficiency must also be included in a calculation of total power requirement.

Assume that two jets with 1-in. (25.4-mm) diam are to be used to obtain $M_r = 0.010$ in a 10-ft (3.05-m) diam pipe with a flow velocity of 5 fps (1.52 m/s). The value of P_j would be 1690 ft-lb/sec or 3.1 hp (2.3 kw) for the jets. Using D_j of 2 in. (50.8 mm) would reduce the required power by a factor of 2 for the same M_r (Eq. 14).

Conclusions

When injecting a miscible fluid into a flow in a pipe, the use of jet injections can speed the mixing relative to that which would take place just due to the ambient flow. The jets can be at the pipe wall and therefore do not require that any appurtenances or devices be placed inside the pipe.

In this study, laboratory experiments were conducted to investigate the effectiveness of jet-induced mixing in pipe flows. The coefficient of variation, C_v, of the concentration distribution was used as a measure of the degree of mixing at a given cross section. The dimensionless mixing distance, Z_m, was defined as the flow distance required to obtain a specified C_v. Increases in the effectiveness of the jet mixing produced decreases in Z_m and vice versa. For uniform pipe flow with a given number and orientation of jets, the ratio, M_r, of the jet momentum flux to the pipe-flow momentum flux is the parameter indicative of the mixing induced by the jets. For a single jet oriented at various angles to the ambient flow, the momentum ratios for optimum mixing and the corresponding mixing distances were determined. Increasing the angle of injection

from 90° (cross flow) to 150° (almost counterflow) decreased the optimum Z_m, but at the cost of a large increase in the momentum ratio and in the power requirement. Under many circumstances, it might not be practical to consider any angle of injection other than 90°.

Experiments were also conducted with two diametrically opposed 90° jets in uniform flow. Optimum mixing was obtained with the momentum ratio for each jet being on the order of one-half of the optimum momentum ratio for a single jet injection. Thus, even though the use of two jets in uniform flow did not produce a significant decrease in the mixing distance compared to a single jet, the two jets would require less total power than a single jet. Furthermore, limited experiments in a pipe flow with an induced secondary current indicated that the use of two or more jets for the injection would provide a factor of safety against the effects which unknown secondary currents could have on the jets and on the mixing process.

Acknowledgments

The work upon which this publication is based was supported in part by funds provided by the Office of Water Research and Technology, (Project A-091-111), United States Department of the Interior, Washington, D.C., as authorized by the Water Research and Development Act of 1978. Contents of this publication do not necessarily reflect the views and policies of the Office of Water Research and Technology, United States Department of the Interior, nor does mention of trade names or commercial products constitute their endorsement or recommendation for use by the United States Government. The research was conducted while the writers were affiliated with the Department of Civil Engineering of the University of Illinois at Urbana-Champaign. The project was administered through the University's Water Resources Center.

Appendix.—References

1. Chilton, T. H., and Genereaus, R. P., "The Mixing of Gases for Reaction," *Transactions*, American Institute of Chemical Engineers, Vol. 25, 1930, pp. 102–122.
2. Clayton, C. G., "The Use of a Pump to Reduce Mixing Length in the Dilution Method of Flow Measurement," *Report AERE-R 4623*, Wantage Research Laboratory, AERE, Wantage, Berkshire, England, 1964, 9 pp.
3. Clayton, C. G., Ball, A. M., and Spackman, R., "Dispersion and Mixing during Turbulent Flow of Water in a Circular Pipe," *Report AERE-R 5569*, Isotope Research Division, Wantage Research Laboratory, Wantage, Berkshire, England, 1968, 31 pp.
4. Fan, L. N., "Turbulent Buoyant Jets into Stratified or Flowing Ambient Fluids," W. M. Keck Laboratory of Hydraulics and Water Resources, California Institute of Technology, Pasadena, Calif., 1967, 196 p.
5. Filmer, R. W., and Yevdjevich, V. M., "The Use of Tracers in Making Accurate Discharge Measurements in Pipelines," *Report CER66RWF-VMY 38*, Colorado State University, Fort Collins, Colo., 1966, p. 90.
6. Fitzgerald, S. D., and Holley, E. R., "Jet Injections for Optimum Mixing in Pipe Flow," *Research Report No. 144*, Water Resources Center, University of Illinois at Urbana-Champaign, Urbana, Ill., Dec., 1979, 89 pp.
7. Ger, A. M., and Holley, E. R., "Turbulent Jets in Crossing Pipe Flow," *Hydraulic Engineering Series Report 30*, University of Illinois at Urbana-Champaign, Urbana, Ill., 1974, p. 198.
8. Holley, E. R., and Ger, A. M., "Circumferential Diffusion in Pipe Mixing," *Journal*

of the Hydraulics Division, ASCE, Vol. 104, No. HY4, Proc. Paper 13663, Apr., 1978, pp. 471–485.

9. Holley, E. R., "Dilution Method of Discharge Measurement in Pipes," *Special Publication 484, Proceedings*, Flow Measurement Symposium, National Bureau of Standards, Oct., 1977, pp. 395–421.
10. Morgan, W. D., Brinkworth, B. J., and Evans, G. V., "Upstream Penetration of an Enclosed Counterflowing Jet," *Industrial and Engineering Chemistry Fundamentals*, Vol. 15, No. 2, 1976, pp. 125–127.
11. Wright, S. J., "Mean Behavior of Buoyant Jets in a Crossflow," *Journal of the Hydraulics Division*, ASCE, Vol. 103, No. HY5, Proc. Paper 12944, May, 1977, pp. 499–513.

INTEGRAL EQUATION FORMULATION FOR GROUND-WATER FLOW

By Bruce Hunt[1] and Lewis T. Isaacs[2]

INTRODUCTION

Integral equation techniques provide one of the most accurate and efficient methods known for obtaining numerical solutions for certain types of harmonic boundary-value problems. One of the biggest reasons for this relatively great accuracy and efficiency is that the solution of the Laplace equation and its boundary conditions is reduced to the solution of a single integral equation in which the unknown is a function of one fewer variables than the unknown in the original boundary-value problem. For example, a two-dimensional problem is reduced to the solution of a one-dimensional integral equation. Thus, the resulting set of simultaneous equations that must be solved contains N unknowns, whereas the solution of the problem with either finite difference or finite element methods would require the solution of a set of simultaneous equations with approximately N^2 unknowns.

Linear, Fredholm integral equations are classified as equations of the first and second kind, respectively

$$\int_a^b \phi(\xi)\, K(x,\xi)\, d\xi = f(x),\ (a < x < b) \quad \ldots\ldots\ldots\ldots\ldots\ldots\ldots\ldots (1)$$

and

$$\phi(x) + \int_a^b \phi(\xi)\, K(x,\xi)\, d\xi = f(x),\ (a < x < b) \quad \ldots\ldots\ldots\ldots\ldots\ldots (2)$$

The functions, $f(x)$ and $K(x,\xi)$, in Eqs. 1 and 2 are known, and the unknown function, $\phi(x)$, occurs both outside and within the integral for a Fredholm integral equation of the second kind. Both types of integral equations are encountered in applied problems, but equations of the second kind are usually preferred whenever a choice is available. This is partly because the theory for equations of the second kind is relatively complete, and mathematicians have been able to apply the Fredholm theory to equations of the second kind

[1]Reader in Civ. Engrg., Univ. of Canterbury, Christchurch, 1 New Zealand.
[2]Sr. Lect. in Civ. Engrg., Univ. of Queensland, Brisbane, Australia.

Note.—Discussion open until March 1, 1982. To extend the closing date one month, a written request must be filed with the Manager of Technical and Professional Publications, ASCE. Manuscript was submitted for review for possible publication on November 13, 1980. This paper is part of the Journal of the Hydraulics Division, Proceedings of the American Society of Civil Engineers, ©ASCE, Vol. 107, No. HY10, October, 1981. ISSN 0044-796X/81/0010-1197/$01.00.

to prove existence theorems for solutions to the Dirichlet and Neumann problems [Kellogg (2), and Sternberg and Smith (10)]. Probably more important from an engineer's viewpoint, though, is the fact that equations of the second kind often provide more accurate and stable numerical solutions. This is because the numerical solution of Eqs. 1 and 2 always reduces to the solution of a set of simultaneous, algebraic equations, and the presence of $\phi(x)$ outside the integral in Eq. 2 strengthens the main diagonal of the coefficient matrix. The net result is that equations of the second kind often yield a set of simultaneous equations that is well conditioned, and decreasing the nodal spacing (which increases the number of nodes and equations) leads to a more accurate solution for $\phi(x)$. On the other hand, decreasing the nodal spacing in equations of the first kind often leads to a poorly conditioned set of equations with a resulting loss in accuracy in the solution for $\phi(x)$.

Techniques for the use of integral equations in irrotational flow problems have been investigated fairly intensively since the well-known work by Smith and Pierce (9) in 1958. On the other hand, integral equation methods have only been applied to ground-water problems since the work by Liggett (6) in 1977. This is largely a result of the fact that irrotational flow problems can be formulated either as Neumann or Dirichlet problems, both of which lead to Fredholm integral equations of the second kind. However, application of similar methods to the mixed boundary-value problems in ground-water flow often leads to a mixed system of integral equations of the first and second kinds. For example, Liggett (6) used the following equation in his work when (x, y) was a point on the boundary where the boundary tangent turned continuously

$$\phi(x,y) = \frac{1}{\pi} \oint \left(\phi \frac{\partial (\ln r)}{\partial n} - \ln r \frac{\partial \phi}{\partial n} \right) ds \quad \ldots\ldots\ldots\ldots\ldots\ldots (3)$$

In Eq. 3, ϕ = velocity potential; s = arc length along the boundary; r = distance between the "fixed" point, (x, y), and the integration point (ξ, η); and n = arc length in the direction of the outward normal. When (x, y) is a point on a boundary of specified, $\partial\phi/\partial n$, Eq. 3 becomes an integral equation of the second kind. However, an integral equation of the first kind is obtained when (x, y) becomes a point on a boundary of specified ϕ. The implication is that the resulting set of algebraic equations that are used to obtain an approximate, numerical solution of Eq. 3 may become ill-conditioned when nodal spacings become too close on boundaries of specified ϕ. In fact, Liggett (6) mentions that he has encountered an ill-conditioned matrix when nodes are spaced too closely near points where ϕ and $\partial\phi/\partial n$ change rapidly. Later work by Liggett and coworkers (3, 4, 5, 7, and 8) has extended the method to obtain steady and unsteady solutions for two-dimensional, axisymmetric, and three-dimensional flows with free surfaces.

The purpose of this work is to investigate an alternative integral equation formulation for the two-dimensional, mixed problems of ground-water flow. This formulation yields a simultaneous set of integral equations of the second kind which have boundary values of the velocity potential and the stream function as its unknowns. The formulation has advantages of simplicity and compactness, and it is hoped that the set of integral equations will yield a set of algebraic equations for its approximate solution that remains well-conditioned when boundary node spacings are decreased.

Formulation

Let $\phi(x,y)$ and $\psi(x,y)$ be the velocity potential and stream function for a ground-water flow problem. The exterior boundary of the flow region is denoted by Γ, and, since the aquifer is assumed to be homogeneous and isotropic, the problem is equivalent to finding a complex potential

$$w(z) = \phi(x,y) + i\psi(x,y) \quad \ldots\ldots\ldots\ldots\ldots\ldots\ldots\ldots\ldots\ldots (4)$$

in which $i = \sqrt{-1}$; $z = x + iy$; and $w(z)$ = a complex-valued function that is analytic within Γ. It is assumed that either ϕ or ψ are specified on the adjoining boundary segments that form Γ.

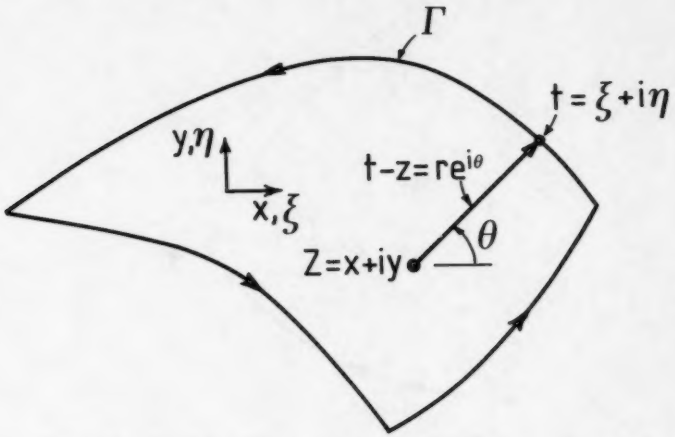

FIG. 1.—Definition Sketch for Solution of Harmonic Boundary-Value Problem within Boundary, Γ

The Cauchy integral theorem [Carrier, Krook and Pearson (1)] states that $w(z)$ can be calculated from the following contour integral

$$w(z) = \frac{1}{2\pi i} \oint_{\Gamma} \frac{w(t)}{t - z}\, dt \quad \ldots\ldots\ldots\ldots\ldots\ldots\ldots\ldots\ldots\ldots (5)$$

In Eq. 5, z = coordinate of a point within Γ, t = coordinate of a point on Γ and the contour integral is calculated around the closed boundary Γ by traversing Γ so that the flow region lies on the left. A definition sketch for this problem is shown in Fig. 1.

The integral equation is obtained from Eq. 5 by letting z approach a point on the boundary. Carrier, Krook, and Pearson (1) show that this can be done by placing z on the boundary and then deforming the boundary near z into a portion of a small circular arc that places z within the flow region, as shown in Fig. 2. The end result, after letting the radius of the circular arc approach zero, is

$$w(z) = \frac{(P)}{\Omega i} \oint_{\Gamma} \frac{w(t)}{t - z}\, dt, \quad (z \text{ on } \Gamma) \quad \ldots\ldots\ldots\ldots\ldots\ldots\ldots\ldots\ldots\ldots (6)$$

in which (P) denotes the Cauchy principal value of the integral; and Ω = interior angle between the boundary tangents at point, z. At points where the boundary tangent turns continuously, $\Omega = \pi$.

Eq. 6 can be rewritten as two real equations by setting $w = \phi + i\psi$ and by taking the logarithmic derivative of $t - z = r\, e^{i\theta}$, in which r = modulus;

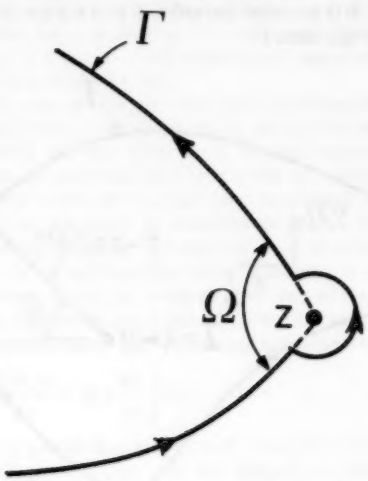

FIG. 2.—Calculation of $w(z)$ as z Approaches Point on Γ

and θ = argument of $t - z$. Then equating real and imaginary parts in Eq. 6 gives

$$\phi = \frac{(P)}{\Omega} \int_{\Gamma} \left(\psi \frac{dr}{r} + \phi\, d\theta \right) \quad \ldots\ldots\ldots\ldots\ldots\ldots\ldots\ldots\ldots\ldots (7)$$

$$\psi = \frac{(P)}{\Omega} \int_{\Gamma} \left(\psi\, d\theta - \phi \frac{dr}{r} \right) \quad \ldots\ldots\ldots\ldots\ldots\ldots\ldots\ldots\ldots\ldots (8)$$

Eq. 7 becomes an integral equation of the second kind when (x, y) is a point on a boundary of specified, ψ, and Eq. 8 becomes an equation of the second kind when (x, y) is a point on a boundary of specified ϕ. Thus, the solution of Eq. 6 for a mixed problem is equivalent to the simultaneous solution of two sets of real, integral equations of the second kind with ϕ and ψ as unknowns. Eq. 6, rather than Eqs. 7–8, will be used herein since the use of complex variables makes a considerable simplification in both the mathematics and computer coding.

INTEGRATIONS

The numerical solution of Eq. 6 proceeds by first dividing the boundary, Γ, into N segments. These segments should be shorter in regions where ϕ or ψ change rapidly and longer in regions of slowly varying ϕ or ψ. It is convenient to assume that $w(t)$ varies as a linear function of the complex variable, t, along each segment in a piecewise continuous manner. Thus, along the segment joining the nodes, t_j–t_{j+1}, $w(t)$ is approximated with

$$w(t) = \frac{t - t_j}{t_{j+1} - t_j} w_{j+1} + \frac{t_{j+1} - t}{t_{j+1} - t_j} w_j \quad \ldots \ldots \ldots \ldots \ldots \ldots \ldots \ldots \quad (9)$$

If $z \equiv t_i$; and $i \neq j$; or $i \neq j + 1$; then Eq. 9 can be inserted into Eq. 6 and integrated over one boundary element to obtain

$$\int_{t_j}^{t_{j+1}} \frac{w(t)}{t - t_i}\, dt = \left[1 + \left(\frac{t_i - t_j}{t_{j+1} - t_j}\right) \ln\left(\frac{t_{j+1} - t_i}{t_j - t_i}\right)\right] w_{j+1}$$

$$- \left[1 + \left(\frac{t_i - t_{j+1}}{t_{j+1} - t_j}\right) \ln\left(\frac{t_{j+1} - t_i}{t_j - t_i}\right)\right] w_j \quad \ldots \ldots \ldots \ldots \ldots \ldots \quad (10)$$

The logarithms in Eq. 10 are multiple-valued, and care must be taken to ensure

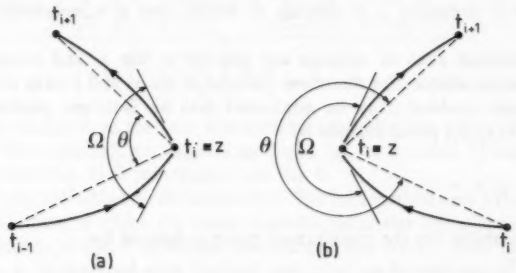

FIG. 3.—Boundary Geometry for Integration Along Elements Adjacent to Singular Node when: (*a*) $\Omega \leq \pi$; and (*b*) $\Omega \geq \pi$

that a correct branch is used for all calculations. Since the imaginary part of the logarithms is just the change in amplitude of $t - t_i$ as t varies from t_j–t_{j+1}, trouble can be avoided by choosing the argument or amplitude of all complex numbers to lie between $-\pi$ and π.

Eq. 10 cannot be used to compute the contribution that comes from integrating over the elements that lie on each side of the singular node at $z \equiv t_i$. In this case, calculation of the Cauchy principal value gives

$$(P) \int_{t_{i-1}}^{t_{i+1}} \frac{w(t)}{t - t_i}\, dt = w_{i+1} - w_{i-1} + \left[\ln\left|\frac{t_{i+1} - t_i}{t_{i-1} - t_i}\right| + i(\Omega - \theta)\right] w_i \quad \ldots \quad (11)$$

As shown in Fig. 3, Ω = angle between the boundary tangents at the point,

$z \equiv t_i$; θ = angle between straight lines joining the points, t_{i+1}–t_i; and t_{i-1}–t_i. The angle, θ, can be computed numerically in a computer by first calculating

$$\beta = \text{Argument}\left(\frac{t_{i+1} - t_i}{t_{i-1} - t_i}\right) \quad \ldots\ldots\ldots\ldots\ldots\ldots\ldots\ldots\ldots\ldots \quad (12)$$

in which $-\pi \leq \beta \leq \pi$. Then, if $\beta > 0$; $\theta = 2\pi - \beta$; and, if $\beta < 0$, $\theta = |\beta|$. The difference, $\Omega - \theta$, vanishes if the boundary elements on each side of the node, $z \equiv t_i$, are straight-line segments.

It is important to point out that Eqs. 10, 11, 12 hold for boundary elements that have any geometry. The fact that the integrals depend only upon quantities calculated at the endpoints of each element is a direct consequence of a theorem in complex variable theory that states that the value of a contour integral of an analytic function depends upon the beginning and ending point and not upon the path followed between these two points.

Anisotropic Seepage

The seepage head, h, is defined by

$$h = \frac{p}{\rho g} + y \quad \ldots\ldots\ldots\ldots\ldots\ldots\ldots\ldots\ldots\ldots\ldots\ldots\ldots\ldots \quad (13)$$

in which p = pressure; ρ = density of water; and g = acceleration due to gravity.

If the principal axes of seepage are parallel to the x- and y-axes and k_x, k_y are the permeabilities for directions parallel to the x- and y-axes respectively, an anisotropic problem may be converted into an isotropic problem on the transformed (x_t, y_t) plane defined by

$$x_t = \sqrt{\frac{k_y}{k_x}}\, x, \; y_t = y \quad \ldots\ldots\ldots\ldots\ldots\ldots\ldots\ldots\ldots\ldots\ldots\ldots \quad (14)$$

The permeability for the transformed plane is defined by

$$k_t = \sqrt{k_x k_y} \quad \ldots\ldots\ldots\ldots\ldots\ldots\ldots\ldots\ldots\ldots\ldots\ldots\ldots\ldots \quad (15)$$

The velocity potential function, ϕ, is defined by

$$\phi = -k_t h \quad \ldots\ldots\ldots\ldots\ldots\ldots\ldots\ldots\ldots\ldots\ldots\ldots\ldots\ldots\ldots \quad (16)$$

Velocity components are given by

$$u = -k_x \frac{\partial h}{\partial x}, \; v = -k_y \frac{\partial h}{\partial y} \quad \ldots\ldots\ldots\ldots\ldots\ldots\ldots\ldots\ldots\ldots\ldots \quad (17)$$

and the stream function is defined, in the normal manner

$$d\psi = \int u\, dy - \int v\, dx \quad \ldots\ldots\ldots\ldots\ldots\ldots\ldots\ldots\ldots\ldots\ldots\ldots \quad (18)$$

The preceding computational algorithm for isotropic seepage is used in the transformed plane to solve the anisotropic problem.

An advantage of the transformation used is that the solution method can be easily extended to multizone, anisotropic problems.

Multizone, Anisotropic Seepage

Sometimes the region of analysis consists of a number of zones such that k_x, k_y are constant within a zone but the values vary from one zone to the next. The anisotropic seepage within any one zone can be analyzed by the method given in the preceding section but the overall solution needs compatibility between adjacent zones.

At a point on a boundary between zones a and b, h has the same value and continuity must be preserved. Therefore

$$\frac{\phi_a}{k_{t_a}} = \frac{\phi_b}{k_{t_b}} \qquad (19)$$

and $\psi_a = \psi_b$ . . . . (20)

Computational Algorithm

The numerical solution of Eq. 6 is carried out by using N nodes to divide the boundary into discrete segments. Then use of Eq. 11 to calculate the contribution from the two elements adjacent to the singular node at $z \equiv t_i$ gives

$$w_i = \frac{w_{i+1} - w_{i-1} + \sum_{j=1}^{i-2} \int_{t_j}^{t_{j+1}} \frac{w(t)}{t - t_{t_i}} dt + \sum_{j=i+1}^{N} \int_{t_j}^{t_{j+1}} \frac{w(t)}{t - t_i} dt}{\ln \left| \frac{t_{i-1} - t_i}{t_{i+1} - t_i} \right| + i\theta} \qquad (21)$$

in which the integrals in the two summations are computed from Eq. 10; and $t_{N+1} \equiv t_1$. The angle, Ω, no longer appears in Eq. 21 because of cancellations that occur when Eq. 11 is substituted into Eq. 6.

Eq. 21 may be solved in two different ways. The first method uses a Gauss-Seidel iterative procedure in which the latest available estimates for w are substituted into the right side of Eq. 21 to obtain the next estimate for w_i. Then the previous estimate for ϕ_i is replaced with the real part of w_i on boundaries of specified, ψ, and the previous estimate for ψ_i is replaced with the imaginary part of w_i on boundaries of specified, ϕ. The values of ψ on each streamline boundary are set equal to the imaginary part of w calculated at the first node on that streamline for each cycle. The modulus of the difference between values of w calculated for two successive cycles at each node is summed for each cycle, and calculations are stopped when this sum ceases to change significantly from one cycle to the next.

The iterative procedure can be easily coded into a computer program which requires a minimum of core storage. It may be used for multizone problems if each zone is treated in turn. After the new estimates for w_i have been calculated for a zone, the values of w_i in adjacent zones along common boundaries are updated to satisfy Eqs. 19 and 20 before proceeding to the next zone. The fact that the iterative method converges in most cases indicates the good conditioning of the equations. However, problems occur with very high ratios of k_t for which the second method of solution is found to be satisfactory.

The second method requires the assembly of all equations for all zones and uses Gaussian elimination to obtain a direct solution. Eq. 21 may be rewritten

$$w_i + G(w_{i+1} - w_{i-1}) + \sum_{\substack{j=1 \\ j \neq i, i-1}}^{N} (A\, w_{j+1} - B\, w_j) = 0 \quad \ldots\ldots\ldots\ldots \quad (22)$$

in which $$G = g_1 + ig_2 = \frac{1}{\left(\ln \left| \frac{t_{i-1} - t_i}{t_{i+1} - t_i} \right| + i\theta\right)} \quad \ldots\ldots\ldots\ldots \quad (23)$$

$$A = a_1 + ia_2 = G\left[1 + \left(\frac{t_i - t_j}{t_{j+1} - t_j}\right) \ln \left(\frac{t_{j+1} - t_i}{t_j - t_i}\right)\right] \quad \ldots\ldots\ldots\ldots \quad (24)$$

and $$B = b_1 + ib_2 = G\left[1 + \left(\frac{t_i - t_{j+1}}{t_{j+1} - t_j}\right) \ln \left(\frac{t_{j+1} - t_i}{t_j - t_i}\right)\right] \quad \ldots\ldots\ldots \quad (25)$$

Eqs. 24 and 25 are derived from the result for the integration along a segment given by Eq. 10.

The complex equation, Eq. 22, may be split into two equations, one each for the real and imaginary parts. Multizone problems are formulated with h and ψ as the nodal variables instead of ϕ and ψ because ϕ may vary from zone to zone. The real equation is

$$-k_i h_i - g_1 k_i h_{i+1} - g_2 \psi_{i+1} + g_1 k_i h_{i-1} + g_2 \psi_{i-1}$$
$$- \sum_{\substack{j=1 \\ j \neq i, i-1}}^{N} (a_1 k_i h_{j+1} + a_2 \psi_{j+1} + b_1 k_i h_j + b_2 \psi_j) = 0 \quad \ldots\ldots\ldots\ldots \quad (26)$$

and the imaginary equation is

$$\psi_i - g_2 k_i h_{i+1} + g_1 \psi_{i+1} + g_2 k_i h_{i-1} - g_1 \psi_{i-1}$$
$$- \sum_{\substack{j=1 \\ j \neq i, i-1}}^{N} (a_2 k_i h_{j+1} - a_1 \psi_{j+1} - b_2 k_i h_j + b_1 \psi_j) = 0 \quad \ldots\ldots\ldots\ldots \quad (27)$$

When a node lies on a boundary common to two or more zones, the final equations for h and ψ at that node are obtained by combination of the separate equations from each zone.

The full set of equations for all zones may be written

$$[C]\{\alpha\} = 0 \quad \ldots\ldots\ldots\ldots\ldots\ldots\ldots\ldots\ldots\ldots\ldots\ldots \quad (28)$$

in which $[C]$ = a matrix composed of known coefficients; and $\{\alpha\}$ = a vector comprising the nodal value of h and ψ arranged so that $\alpha_{2m-1} = h_m$ and $\alpha_{2m} = \psi_m$.

Matrix $[C]$ is formed by accumulating the contributions from each segment and for all zones. The procedure can be implemented directly from Eqs. 26 and 27. The coefficients for the real equation for node, i, are stored in row $2i - 1$ of $[C]$ and the coefficients for the imaginary equation are stored in

row $2i$. The first five terms in Eqs. 26 and 27 are the contributions from the two segments adjacent to node, i, and the summations represent the contributions from all other segments around the zone boundary. The column position for each coefficient is determined from the location of the variable in $\{\alpha\}$, e.g., considering the term, $a_2\psi_{j+1}$, in Eq. 26, a_2 is added into location $[2i - 1, 2(j + 1)]$ in $[C]$. This method for the assembly of equations is analogous to the assembly of equation in the finite element method. In the analogy, each zone is treated as a separate element.

After assembly, the full set of equations is modified to take account of the boundary conditions. If h_i (or ψ_i) is known, the equation for h_i (or ψ_i) is replaced by an equation which specifies 1. h_i (or 1. ψ_i) = known value. If i is a point on a boundary where $\psi = q$ but q is unknown, one nodal value of ψ on that boundary, e.g., ψ_m, is chosen as the unknown and the equations for the remaining values of ψ_i are replaced by $1.\psi_i - 1.\psi_m = 0$.

Examples

The first example (see Fig. 4) is of flow beneath a dam with a sheet-pile, cutoff wall. The lower boundary has been chosen to coincide with a streamline

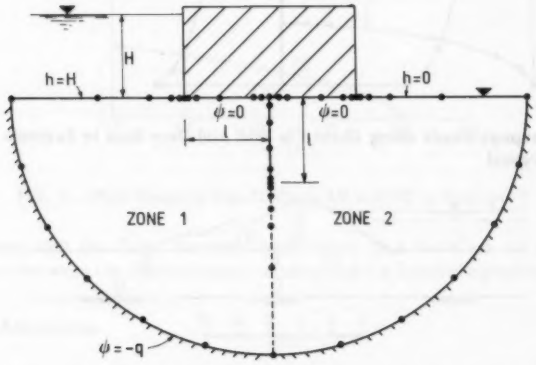

FIG. 4.—Example 1: Flow beneath Dam with Sheet-Pile, Cut-Off Wall

from the analytical solution for a semi-infinite region so that the results may be compared with analytical results. The cutoff wall is of zero thickness and, as a result, if only one zone were used for the analysis, numerical problems would arise in the calculation of coefficients when z is located at a node on the wall. These problems are avoided if the region is subdivided into two zones as shown in Fig. 4. Since $w(t)$ is assumed to be a linear function of t, a reduced spacing of nodes is employed near the singularities to improve the modelling.

The variation of h along the dam and cutoff wall is shown in Fig. 5, where the calculated and analytical values are compared. Lafe, Montes, Cheng, Liggett, and Liu (3) use a similar example to show how specialized quadrature formulae can be used to improve numerical accuracy near singularities, such as the one

encountered at the cutoff wall tip in this example. Undoubtedly, a similar approach would improve the accuracy of this solution. However, the agreement between exact and calculated solutions in Fig. 5 is close enough to suggest that an accuracy sufficient for most engineering purposes can be obtained with no special treatment other than closer node spacings near singularities. The calculated value of g/KH is 0.464 and has an error of 1% when compared with the analytical value of 0.459.

The second example is the analysis of seepage through the mine tailings dam shown in Fig. 6. The ratio of k_x/k_y is 4.0 in all three zones and the values for k_x were $k_{x_1}:k_{x_2}:k_{x_3} \equiv 1{:}4{:}30$.

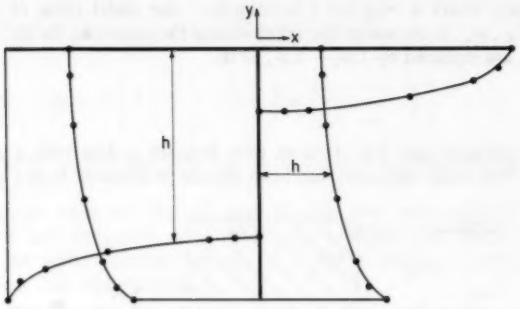

FIG. 5.—Seepage Heads along Sheet-Pile Wall and Dam Base in Example 1 · BIEM, —— Analytical

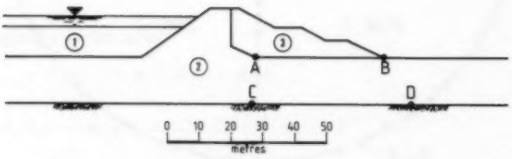

FIG. 6.—Example 2: Cross Section of Tailings Dam

An alternative solution is available as the dam had previously been analyzed using the finite element method. A 6 node triangular element was used in the finite element solution and the mesh comprised 172 elements and 399 nodes. A total of 37 nodes is used in the integral equation solution. Of these, 5 are located on the common boundary between zones 1 and 2 and 7 on the boundary between zones 2 and 3. The positions of the phreatic line from the two analyses are shown in Fig. 7. Since the purpose of the original analysis was the determination of pore pressures for a stability analysis, a comparison of the calculated pore pressures along AB and CD (see Figs. 6, 7) is presented in Fig. 8. The seepage discharge is also available from both analyses, and the values differ by 2%. This second example demonstrates the practicality of the method, and the

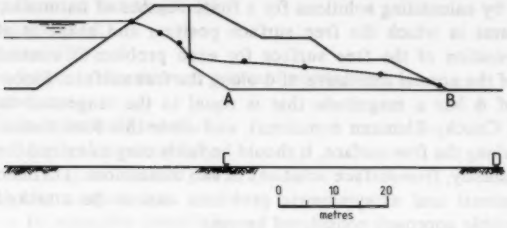

FIG. 7.—Location of Phreatic Line in Example 2 · BIEM, ——— FE

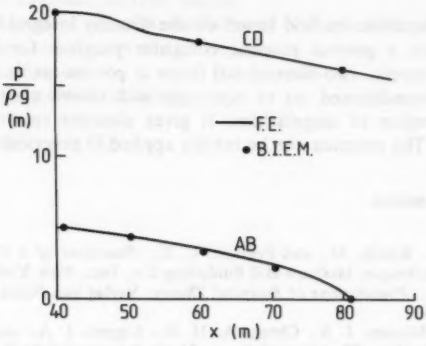

FIG. 8.—Pore Pressure Heads along AB and CD in Example 2

comparisons with the finite element results show that there are no significant differences between the finite element solution and the integral equation solution.

Practical Applications

A major objective of the study was the development of a computer program which could be easily used in practical applications. Since the method can model irregular boundary geometries and a number of different anisotropic zones, this objective has been achieved. The second example demonstrates one such application. Furthermore, the method has a significant practical advantage over the finite element method because of the big reduction in data preparation. This advantage is still important when values of the solution are required within the region of analysis because only the points where the solution is required need be specified. The value of w at any specified internal point can be evaluated from Eq. 5 with the integral taken around the boundary of the zone containing the point.

Unsteady, free-surface solutions have not yet been attempted with this formulation, but it seems reasonable to expect that they could be carried out in a straightforward way. This is because an unsteady-flow problem is solved

numerically by calculating solutions for a finite number of harmonic, boundary-value problems in which the free surface position and shape is altered with time. The position of the free surface for each problem is controlled by the magnitude of the normal derivative of ϕ along the free surface. Since the normal derivative of ϕ has a magnitude that is equal to the tangential derivative of ψ (from the Cauchy-Riemann equations), and since this formulation calculates values of ψ along the free surface, it should be fairly easy to extend the technique to obtain unsteady, free-surface solutions in two dimensions. On the other hand, three-dimensional and axisymmetric problems cannot be attacked with the complex-variable approach considered herein.

Conclusions

The integral equation method based on the Cauchy integral theorem can be easily coded into a general purpose computer program for the analysis of multizone, anisotropic, two-dimensional flows in porous media. This formation leads to a well-conditioned set of equations and allows nodes to be closely spaced in the region of singularities. It gives accurate results in the region of singularities. The program can be readily applied to practical problems.

Appendix I.—References

1. Carrier, G. F., Krook, M., and Pearson, C. E., *Functions of a Complex Variable: Theory and Technique*, McGraw-Hill Publishing Co., Inc., New York, N.Y., 1966.
2. Kellogg, O. D., *Foundations of Potential Theory*, Verlag von Julius Springer, Berlin, Germany, 1929.
3. Lafe, O. E., Montes, J. S., Cheng, A. H. D., Liggett, J. A., and Liu, P. L. F., "Singularities in Darcy Flow through Porous Media," *Journal of the Hydraulics Division*, ASCE, Vol. 106, No. HY6, Proc. Paper 15467, June, 1980, pp. 977–997.
4. Lennon, G. P., Liu, P. L. F., and Liggett, J. A., "Boundary Integral Equation Solution to Axisymmetric Potential Flows 1. Basic Formulation 2. Recharge and Well Problems in Porous Media," *Water Resources Research*, Vol. 15, No. 5, Washington, D.C., Oct., 1979, pp. 1102–1115.
5. Lennon, G. P., Liu, P. L. F., and Liggett, J. A., "Boundary Integral Solutions to Three-Dimensional Unconfined Darcy's Flow," *Water Resources Research*, Vol. 16, No. 4, Washington, D.C., Aug., 1980, pp. 651–658.
6. Liggett, J. A., "Location of Free Surface in Porous Media," *Journal of the Hydraulics Division*, ASCE, Vol. 103, No. HY4, Proc. Paper 12851, Apr., 1977, pp. 353–365.
7. Liggett, J. A., and Liu, P. L. F., "Unsteady Free Surface Flow through a Zoned Dam using Boundary Integration," *Proceedings of the Symposium on Application of Computer Methods in Engineering*, 1979, pp. 357–365.
8. Liu, P. L. F., and Liggett, J. A., "Boundary Solutions to Two Problems in Porous Media," *Journal of the Hydraulics Division*, ASCE, Vol. 105, No. HY3, Proc. Paper 14419, Mar., 1979, pp. 171–183.
9. Smith, A. M. O., and Pierce, J., "Exact Solution of the Neumann Problem. Calculations of Non-Circulatory Plane and Axially Symmetric Flow about or within Arbitrary Boundaries," *Douglas Aircraft Company Report ES26988*, 1958.
10. Sternberg, W. J., and Smith, T. L., *The Theory of Potential and Spherical Harmonics*, Toronto University Press, Toronto, Canada, 1946.

Appendix II.—Notation

The following symbols are used in this paper:

g = acceleration due to gravity;
h = seepage head;
k = permeability;
n = arc length in direction of outward normal;
p = pressure;
r = distance between z and t;
s = arc length along boundary;
t = point (ξ, η) on boundary, Γ;
u, v = velocity components;
w = $\phi + i\psi$, complex potential;
x, y = Cartesian coordinates;
z = $x + iy$;
Γ = exterior boundary of flow region;
θ = (1) argument of complex number; and (2) angle defined in Fig. 3;
ξ, η = Cartesian coordinates of t;
ρ = density of water;
ϕ = velocity potential function;
ψ = stream function; and
Ω = angle defined in Fig. 3.

EROSION RESISTANCE OF COHESIVE SOILS

By William E. Kelly,[1] M. ASCE and Ronald C. Gularte,[2] M. ASCE

INTRODUCTION

Erosion of cohesive soils has been studied extensively from the hydraulics point of view but less attention has been given so far to soil behavior. The importance of understanding the soil strength mechanisms controlling erosion resistance is recognized (27). Recent work has shown that rate process theory may be useful for understanding the erosion resistance of cohesive soils and emphasized the importance of physicochemical aspects such as pore and eroding fluid chemistry and mineralogy.

The purpose of this paper is to analyze results of research designed to test the applicability of both rate process and double layer theories to the erosion of cohesive soils. The analysis will show that critical shear stress for surface erosion of a cohesive soil exhibits the same dependency on the number of interparticle bonds per unit area as reported for soil strength at higher stress levels indicating that they are phenomenologically similar.

BACKGROUND

There is an extensive body of literature dealing with the erodibility of cohesive soils and only a brief review of aspects touching on this study will be included. To that end, only work dealing with weak, saturated cohesive soils will be reviewed.

The fact that a sediment exposed to fluid stressing is eroded is well known. The average fluid shear stress imposed on the soil surface can be related to the velocity of flow, and velocity and stress are often used interchangeably in erosion studies. Since, according to Partheniades and Paaswell (25), the major hydraulic parameter is the average fluid shear stress, it is logical that relations between the fluid shear stress that cause erosion and sediment shear strength would be sought. For weak soils, this approach has resulted in, at best, poor correlations, and Partheniades and Paaswell stated that there is no correlation. Moreover, they suggested that the so-called critical shear stress that initiates

[1]Prof., Dept. of Civ. Engrg., Univ. of Rhode Island, Kingston, R.I.
[2]Asst. Prof. of Naval Systems Engrg., U.S. Naval Academy, Annapolis, Md.

Note.—Discussion open until March 1, 1982. To extend the closing date one month, a written request must be filed with the Manager of Technical and Professional Publications, ASCE. Manuscript was submitted for review for possible publication on August 12, 1980. This paper is part of the Journal of the Hydraulics Division, Proceedings of the American Society of Civil Engineers, ©ASCE, Vol. 107, No. HY10, October, 1981. ISSN 0044-796X/81/0010-1211/$01.00.

erosion is constant and essentially independent of undrained shear strength. For cohesive soils, they concluded that surface erosion is controlled by the strength of individual interparticle bonds.

If interparticle bonds do actually control rates of erosion as Partheniades and Paaswell stated, then the concepts of soil deformation and strength based on interparticle bonds (14) may apply. Mitchell and his colleagues (12,13,14,15,17) have developed a comprehensive theory of soil strength starting from rate process theory. For rate process theory to apply the rate to be described must be temperature dependent. Several studies have shown that temperature does affect the rate of erosion of cohesive sediments (5,9,11,26). In fact, rate process theory has been used by Raudkivi and Hutchison (26), Christensen and Das (5), and Kelly, et al. (11), to explain the temperature dependency of measured erosion rates. Christensen and Das and Kelly, et al., recognized the similarity of erosion at constant stress to creep at constant stress and used the methodology developed by Mitchell, et al., to determine experimental activation energies and flow volumes.

Christensen and Das studied erosion rates by maintaining a constant flow of water through a brass tube lined with clay. They tested kaolinitic and illitic clays and mixtures of these clays and Ottawa sand. They reported that both the stress and temperature dependency of erosion rates were in agreement with rate process theory, although the experimental activation energies and flow volumes they determined were somewhat lower than those generally reported for soil creep (14). Paaswell (22) commented on the potential usefulness of an erosional model based on rate process theory, but cautioned that pipe flow may not be representative of field conditions.

Raudkivi and Hutchison (26) reported results of a flume study of kaolinite erosion in which the effects of salinity and temperature were both evaluated. Although there is considerable scatter in their data, they concluded that, at low salinities, temperature is important while at high salinity there is little or no effect of temperature on erosion rates. Generally, erosion rates increased with increasing temperature.

Reinterpretation of Raudkivi and Hutchison's results indicates experimental activation energies in the range of 5–10 Kcal/mole. These values are lower than those reported by Raudkivi and Hutchison, but as they experienced considerable scatter in their data alternate interpretations are possible. Their plots of erosion rate versus temperature are U-shaped, which implies negative activation energies. It should be noted that Raudkivi and Hutchison did not try to explain the mechanism of erosion resistance, but rather the observed temperature dependence of erosion rates.

Some attention must be given to the effect of temperature on the eroding water. Taylor and Vanoni (29) reported that an increase in temperature may increase the intensity of the high-intensity turbulence fluctuations at the bed which accomplish the dislodgement and transport of bed particles. Vanoni and Brooks (30) reported that sediment discharge decreases with increasing water temperature and that the concentration of suspended sediment decreases with increasing temperature. Abou-seida and Arafa (2) reported that an increase in water temperature reduced bed resistance as well as bed form resistance. Both the study by Vanoni and Brooks and that by Abou-seida and Arafa were for sands.

A decrease in bed shear stress with increased temperature follows from the effect of temperature on viscosity and its influence on the shear stress coefficient. An increase in water temperature of 10° K in the normal range of water temperatures results in approx a 25% reduction in viscosity. Since the shear coefficient is approximately proportional to the inverse of viscosity to the negative fifth power for turbulent flow, the result is about a 5% decrease in shear stress. Therefore, although changes in viscosity with temperature are significant, the change in shear stress is much less and would tend to decrease erosion rates for turbulent flow.

Physicochemical factors have also been shown to be important in erosion (3,4,23,24,25,28). For soil behavior, Mitchell indicates that the primary role of the physicochemical forces is probably to control the initial soil fabric following sedimentation and to modify the normal interparticle forces from what they would be due to the applied stresses. For surface erosion, it is reasonable to assume that physico-chemical forces are the primary interparticle forces since the applied stresses may be, essentially, zero.

Theoretical Development

The rate process theory proposed by Eyring (7) has been applied to a variety of particulate systems undergoing time-dependent flow or deformation. The theory does not provide an exact description of the deformation mechanism, since the basis of the theory is the assumption that atoms and molecules make up flow units which are continuously attempting to move but are constrained from movement by energy barriers separating equilibrium positions. The energy a flow unit must acquire to cross an energy barrier is assumed to come from thermal energy and applied directed potentials. A complete development of the theory can be found in Glasstone, et al. (8).

Applications of rate process theory to soil behavior are extensive and include work by Murayama and Shibata (18,19,20), Christensen and Wu (6), Mitchell (12,14), Andersland and Douglas (1), Wu, Resindez, and Neukirchner (31), Mitchell, Campanella, and Singh (15), Christensen and Das (5), Raudkivi and Hutchison (26), and Noble and Demirel (21).

To apply rate process theory to the erosion of a cohesive soil a deformation mechanism must be postulated. For the application of rate process theory to soil creep, Mitchell argues that the rate that flow units cross energy barriers is proportional to axial strain rate. For erosion of a soil with constant fabric it is reasonable to assume that the rate that flow units cross energy barriers in the direction of the applied stress would be proportional to the rate that particles leave the soil surface and hence the rate of erosion. This is essentially the approach taken by Christensen and Das and is the approach taken in this study.

Following Mitchell, and Andersland and Douglas, expressions for experimental activation energy (E)

$$E = \frac{RT_2T_1}{T_2 - T_1} \ln\left(\frac{\dot{\epsilon}_2 T_1}{\dot{\epsilon}_1 T_2}\right) \quad \ldots\ldots\ldots\ldots\ldots\ldots\ldots\ldots\ldots\ldots\ldots\ldots\ldots\ldots (1)$$

and experimental flow volume (V_f) can be written

$$V_f = \frac{2kT}{(\tau_2 - \tau_1)} \ln\left(\frac{\dot{\epsilon}_2}{\dot{\epsilon}_1}\right) \quad \ldots\ldots\ldots\ldots\ldots\ldots\ldots\ldots\ldots\ldots\ldots\ldots\ldots\ldots\ldots\ldots (2)$$

These expressions are completely analogous to those used in studies of soil creep, except that here the stress, τ, is the average bed shear stress and the rate is the erosion rate. In these expressions, R is the universal gas constant, k is Boltzman's constant, and T is absolute temperature. From these expressions it can be seen that it is the ratios of rates of erosion at different temperatures and stresses and not the absolute magnitudes that will be important in determining the rate process parameters.

Two approaches are possible for determining the rate process parameters. First, tests could be run on identical samples at different temperatures and stresses. This is generally impractical because of the difficulty of insuring identical samples. A second method is to increment temperatures or stresses and to compute experimental activation energies or flow volumes using equations (1) and (2). In this study, rather than compute rates immediately before and after an increment, the equilibrium rate at several stresses or temperatures is fitted in a least squares sense using equations (1) and (2) to obtain experimental activation energies and flow volumes.

Experimental Procedures

Apparatus.—Samples were tested in a water tunnel and designed and fabricated specifically for this research. The unit is shown in Fig. 1, and is approx 18 ft (5.5 m) long, 6.5 ft (2 m) wide and 4.9 ft (1.5 m) high. Water, 38 gal (145 L) is recirculated in an essentially oval path (in the horizontal plane) about 33 ft (10 m) long. Water is recirculated by a 9-in. (23-cm) diameter four-bladed, dynamically-controllable, ducted propeller. The propeller is driven (through a variable speed drive; 500–1,500 rpm) by a 10-hp electric motor. The tunnel is described in more detail by Gularte (10).

Average velocities from 0–90 cm/s can be produced in the tunnel's working section, shown enlarged in Fig. 2. The velocity in the working section can be controlled by either the pitch or speed of the propeller or by adjusting a valve. In the working section, which has a square 6-in × 6-in. (15.24-cm × 15.24-cm) cross section about 10 ft (3 m) long, the entire sample is visible from both sides through 2-in. (5-cm) thick transparent windows. The entire water tunnel is refrigerated and temperature in the tunnel can be maintained within ±0.2° K for extended periods of time or increased or decreased at a rate of 0.5° K/min.

Two types of test were run; in one, temperature was held constant and velocity varied while, in the other, velocity was held constant and temperature varied. The tests were run on remolded Grundite (illite clay) at four different salinities (ranging from approx 2.5–10 ppt NaCl) and five different water contents (ranging from 40–80%). In all cases, the eroding and interstitial fluids were maintained at the same salinity and at a pH of 8.5. The remolded samples, which weighed approximately 44 kg with 1.5 sq ft (0.14 m^2) exposed to fluid stressing, were placed in clear lucite trays and inserted into the working section of the water tunnel. Samples were secured to an instrumented shear plate. The instrumented

shear plate, described in detail by Gularte (10), provided a means of measuring the average horizontal shear force on the eroding surface, from which the average stress was computed.

The center line velocity in the working section was measured continuously with a ducted propeller-fiber optic current meter (10). The amount of material in suspension at any time was measured with a calibrated laser-photocell arrangement which may be seen in Fig. 2.

Sample Preparation.—To prepare a sample, sodium chloride was added to tap water to obtain water with a preselected salinity. Next, a dispersant (sodium metaphosphate) was added and pH adjusted to 8.5 by adding sodium hydroxide or hydrochloric acid as necessary. The addition of the dispersant and the basic

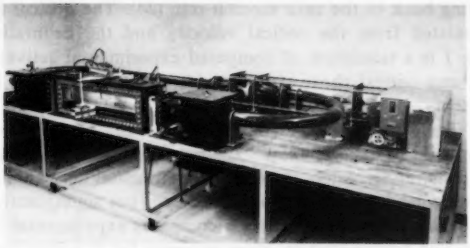

FIG. 1.—Refrigerated Recirculating Water Tunnel

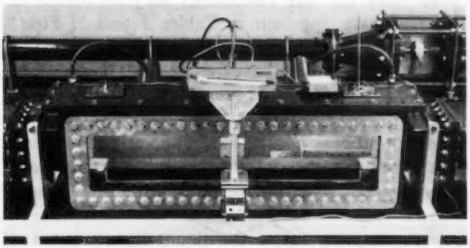

FIG. 2.—Working Section of Water Tunnel

pH was necessary to neutralize or eliminate edge effects which would complicate any explanation with double layer theory. Water at the preselected salinity was then added to the Grundite and mixed with a mechanical mixer to obtain samples for testing.

Prior to placing samples in the support tray, they were remolded in their storage containers. After placing in the tray and just before insertion into the tunnel, they were again remolded with a mechanical mixer. At this point, the sediment was considered to be completely remolded. Water contents (three) were taken and undrained shear strength measured by a fall cone device just before placing and again after removing samples from the tunnel. After testing

in the water tunnel, samples were stored in air-tight containers for rheological testing at a later date.

Results and Analyses

Results from a typical temperature increment test in the water tunnel are shown in Fig. 3. Experimental activation energies were determined by least squares regression analyses of the data from each run. A summary plot is shown in Fig. 4. Results from a typical velocity increment water tunnel test are shown in Fig. 5. Experimental flow volumes were determined from the slopes of semi-log plots of the rate of erosion versus bed shear stress, as shown in Fig. 6. Critical velocities were obtained by plotting erosion rates versus velocity and extrapolating back to the zero erosion rate (24). The critical erosion stress was then calculated from the critical velocity and the calibration curve for the tray. Table 1 is a tabulation of computed experimental activation energies, flow volumes, and critical shear stresses with the corresponding test salinities and water contents.

The data in Table 1 may be compared with results from earlier studies on soils. Table 2 compares experimental activation energies determined from creep and viscosity tests, and erosion tests; the experimental activation energies for erosion are somewhat lower than those for creep, but significantly higher than those for dilute clay suspensions. Table 3 compares experimental flow volumes from this study and earlier studies. Flow volumes for Raudkivi and Hutchison and Partheniades were computed from their data and those for Christensen and Das by dividing their values for bonds per unit area by their assumed bond spacing. The basis for this calculation may be found in Mitchell (14). Some significant trends are apparent in Tables 1 and 3. First, flow volumes from erosion studies are several orders of magnitude greater than those for soil creep and second, the tabulated experimental flow volumes for erosion vary with salinity.

An examination of the data in Table 1 indicates the effects of water content and salinity on the rate process parameters. The variation of experimental flow volume with salinity exhibits a well-defined trend with experimental flow volumes decreasing roughly one-half over the range of salinities tested. The effect of water content alone is less clear; experimental flow volumes appear to decrease with increasing water content below the liquid limit (approx 55%) and then increase with increasing water content above the liquid limit. Experimental activation energies exhibit no discernable trend with water content, but there appears to be a slight tendency for activation energies to increase with increasing salinity over the range tested.

If the number of interparticle bonds per unit area is inversely proportional to the experimental flow volume as proposed by Mitchell then these results may be interpreted to mean that the number of interparticle bonds per unit area increases with increasing salinity and, above the liquid limit, with decreasing water content. Mitchell also showed how changes in the number of interparticle bonds per unit area for a normally consolidated clay could be accounted for by changes in effective stress with increased effective stress meaning increased number of interparticle bonds. Here the decreasing experimental flow volumes with increasing salinity and decreasing water content can be interpreted as

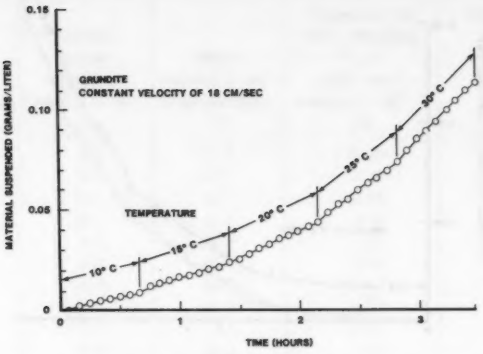

FIG. 3.—Variation of Suspended Sediment Concentration with Time and Temperature

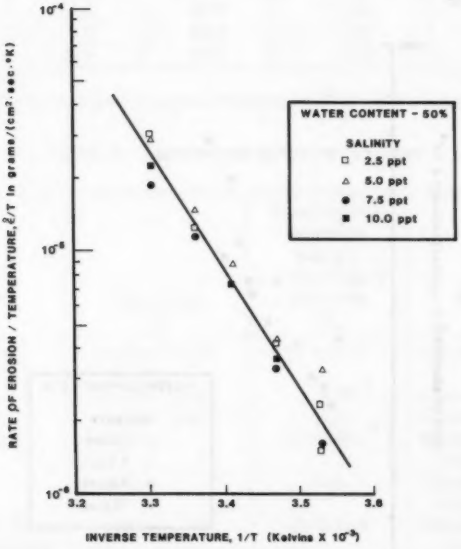

FIG. 4.—Variation of Erosion Rate with Inverse of Absolute Temperature (1 in. = 2.54 cm)

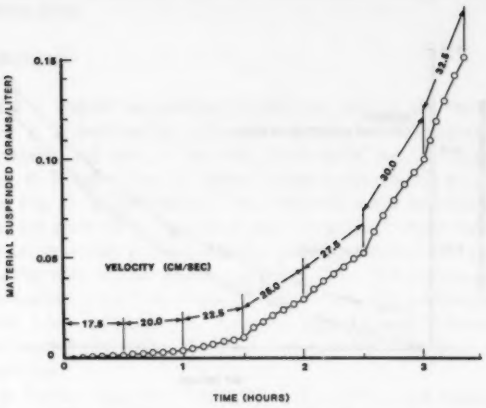

FIG. 5.—Variation of Suspended Sediment Concentration with Time and Velocity (1 in. = 2.54 cm)

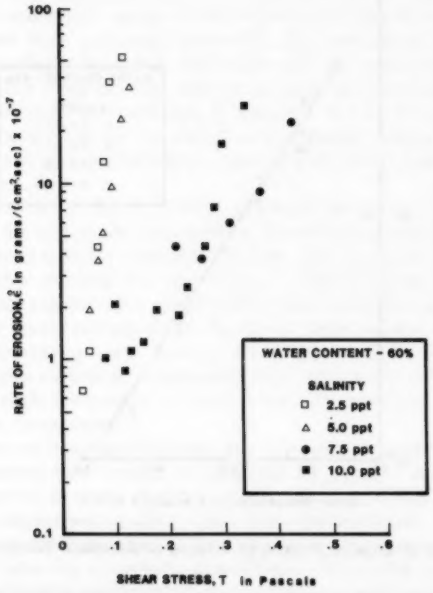

FIG. 6.—Variation of Erosion Rate with Hydraulic Shear Stress (1 psf = 47.9 Pa)

TABLE 1.—Experimental Data for Erosion of Grundite

Salinity NaCl, in parts per thousand (1)	Critical shear stress, in Pascals $\times 10^{-2}$ (2)	Water content, as a percentage (3)	Experimental flow volumes, V_f, in cubic centimeters $\times 10^{-13}$ (4)	Experimental activation energies, in kilocalories per mole (5)
2.5	6.6	51.2	5.00	25.16
5.0	9.7	52.5	1.19	19.58
7.5	15.7	51.5	0.59	21.18
10.0	26.7	53.2	0.48	19.76
2.5	6.6	64.4	5.13	25.40
5.0	8.4	61.6	3.04	22.25
7.5	20.0	64.2	0.67	19.82
10.0	27.7	60.9	0.93	31.69
2.5	5.5	74.1	10.25	14.34
5.0	8.4	70.3	1.73	17.21
7.5	12.6	67.8	1.93	13.88
10.0	—	73.9	2.61	21.83
2.5	2.7	84.1	9.09	24.35
5.0	3.6	83.7	5.04	29.44
7.5	7.8	84.3	1.45	31.78
10.0	13.3	83.7	1.69	29.52

[a]1 psf = 47.9 Pa.

TABLE 2.—Experimental Activation Energies

Material (1)	Type of test (2)	Experimental activation energy, in kilocalories per mole (3)	Reference (4)
Illite (remolded)	erosion—water tunnel	17.4–25.6	this study
Illite	erosion—pipe	15.4	Christensen & Das[a]
Kaolinite	erosion—pipe	16.3	Christensen & Das[a]
Illite (remolded)	creep	25.0–40.0	Mitchell, Singh and Campanella[b]
Illite (dried)	creep	37.0	Mitchell, Singh and Campanella[b]
San Francisco Bay mud (undisturbed)	creep	25.0–32.0	Mitchell, Singh and Campanella[b]
Sault St. Marie clay	viscosity	3.8	Andersland and Douglas[c]

[a]In Ref. 5.
[b]In Ref. 17.
[c]In Ref. 1.

indicating increasing effective stress. An increased net attractive force between clay particles with increasing salinity is consistent with double-layer theory (14). The weak dependence of flow volumes on water content is a reflection of the dominance of physicochemical effects at the soil water interface and the fact that only a relatively soft soil was tested.

Fig. 7 shows the variation of critical shear stress with water content. Lines are approximately parallel for the different salinities. The importance of salinity relative to water content is apparent. Fig. 8 is a plot of critical shear stress versus the number of interparticle bonds per unit area. The number of interparticle bonds per unit area have been computed by dividing the assumed bond spacing (2.8×10^{-8} cm) by the tabulated flow volumes (14). Also shown is the extension

TABLE 3.—Experimental Flow Volumes

Material (1)	Type of test (2)	Flow volume, in cubic centimeters (3)	Reference (4)
Illite (remolded)	erosion—water tunnel	$1.54–6.09 \times 10^{-13}$	this study
Illite	erosion—pipe	0.81×10^{-13}	Christensen and Das[a]
Kaolinite	erosion—pipe	0.49×10^{-13}	Christensen and Das[a]
San Francisco Bay mud	erosion—flume	0.13×10^{-13}	Partheniades[b]
Kaolinite	erosion—flume	0.13×10^{-13}	Raudkivi and Hutchison[c]
San Francisco Bay mud	creep	8.7×10^{-18}	Mitchell, et al.[d]
Illite (remolded)	creep	7.3×10^{-18}	Mitchell, et al.[d]
Illite (remolded)	creep	3.0×10^{-18}	Mitchell, et al.[d]
Sault St. Marie clay	creep	$0.6–4.2 \times 10^{-18}$	Andersland and Douglas[e]

[a] In Ref. 5.
[b] In Ref. 24.
[c] In Ref. 26.
[d] In Ref. 15.
[e] In Ref. 1.

of the line given by Mitchell and Matsui (16) relating shear strength and number of interparticle bonds per unit area. The limits of the data presented by Mitchell and Matsui are also shown approximately. It may be significant to note that data given by Mitchell and Matsui for consolidated soils tend to fall along the line or above it while data given for clay suspensions tend to fall along or below it.

The erosion results reported here follow the same trends reported for soils at higher stresses and clay pastes at high water contents. If the number of interparticle bonds per unit area is controlled by the effective stress, then the effective stress can be seen to be controlled in surface erosion by the interparticle electrical forces, which are described approximately by double-layer theory.

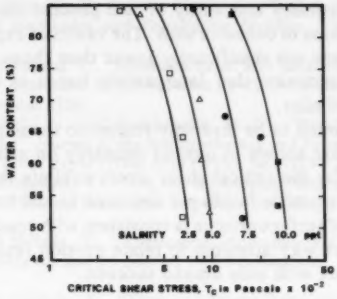

FIG. 7.—Variation of Critical Shear Stress with Salinity and Water Content (1 psf = 47.9 Pa)

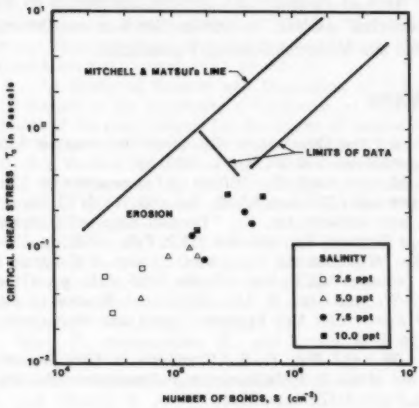

FIG. 8.—Critical Shear Stress and Shear Strength as a Function of the Number of Interparticle Bonds (1 psf = 47.9 Pa)

Alternate interpretations of these results are possible. The size of the experimental flow volumes could be used to argue that actual particles are the flow units. However, the interpretation proposed here is reasonable and consistent with the data. More importantly, these results suggest that the concepts of soil strength and deformation proposed to explain soil strength and creep behavior apply equally to surface erosion.

Conclusions

Results from a series of tests designed to test the applicability of rate process and double-layer theories for describing surface erosion of cohesive soils have been presented. These results and comparisons with earlier studies clearly

demonstrate the applicability and utility of rate process theory for qualitatively describing surface erosion of cohesive soils. The values of experimental activation energies for erosion are not significantly lower than those for soil creep. This result leads to the conclusion that interparticle bonds in both erosion and in creep are essentially similar.

Flow volumes, assumed to be inversely related to the number of interparticle bonds per unit area, are shown to depend primarily on salinity. The resistance to erosion measured by the critical shear stress exhibits the same dependency on the number of interparticle bonds per unit area as soil strength does.

This interpretation of surface erosion is consistent with concepts of soil strength. It also explains in part why attempts to relate erosion resistance to undrained shear strength have met with only limited success.

Acknowledgment

The authors are grateful for the support of the National Science Foundation through a grant "Rate of Erosion of Cohesive Sediments by Rate Process and Double Layer Theories" (ENG 76-20660). Work is continuing under a grant CME-7926297 from the National Science Foundation.

Appendix I.—References

1. Andersland, O. B., and Douglas, A. G., "Soil Deformation Rates and Activation Energies," *Geotechnique*, Vol. 20, No. 1, 1970, pp. 1–16.
2. Abou-Seida, N. M., and Arafa, F., "Effect of Temperature On Channel Resistance," *Journal of the Hydraulics Division*, ASCE, Vol. 103, No. HY3, Mar., 1977, pp. 251–263.
3. Ariathurai, R., and Arulanandan, K., "Erosion Rates of Cohesive Soils," *Journal of the Hydraulics Division*, Vol. 104, No. HY2, Feb., 1978, pp. 279–283.
4. Arulanandan, K., "Fundamental Aspects of Erosion of Cohesive Soils," *Journal of the Hydraulics Division*, ASCE, Vol. 101, No. HY5, 1975, pp. 635–639.
5. Christensen, R. W., and Das, B. M., "Hydraulic Erosion of Remolded Cohesive Soils," *Special Report 135*, Soil Erosion: Causes and Mechanisms, Prevention and Control, 1974, pp. 8–19.
6. Christensen, R. W., and Wu, T. H., "Analysis of Clay Deformations as a Rate Process," *Journal of the Soil Mechanics and Foundation Division*, ASCE, Vol. 90, No. SM6, Proc. Paper 4147, Nov., 1964.
7. Eyring, H., "Viscosity, Plasticity and Diffusion as Examples of Absolute Reaction Rates," *Journal of Chemical Physics*, Vol. 4, Apr., 1936, pp. 283–291.
8. Glasstone, S., Laidler, K., and Eyring, H., *The Theory of Rate Process*, McGraw-Hill Book Co., Inc., New York, N.Y., 1941.
9. Grissinger, E. H., "Resistance of Selected Clay Systems to Erosion by Water," *Water Resources Research*, Vol. 2, No. 1, 1966, pp. 131–138.
10. Gularte, R. C., "Erosion of Cohesive Marine Sediment as a Rate Process," thesis presented to the University of Rhode Island, at Kingston, R.I., in 1978, in partial fulfillment of the requirements for the degree of Doctor of Philosophy.
11. Kelly, W. E., Gularte, R. C., and Nacci, V. A., "Erosion of Cohesive Sediments as a Rate Process," Technical Note, *Journal of the Geotechnical Engineering Division*, ASCE, Vol. 105, No. GT5, Proc. Paper 14556, May, 1979, pp. 673–676.
12. Mitchell, J. K., "Shearing Resistance of Soils as a Rate Process," *Journal of the Soil Mechanics and Foundation Division*, ASCE, Vol. 90, No. SM1, Proc. Paper 3773, Jan., 1964, pp. 29–61.
13. Mitchell, J. K., "Temperature Effects on the Engineering Properties and Behavior of Soils," Highway Research Board, *Special Report 103*, 1969, pp. 9–38.
14. Mitchell, J. K., *Fundamentals of Soil Behavior*, John Wiley and Sons, New York, N.Y., 1976, 422 pp.

15. Mitchell, J. K., Campanella, R. G., and Singh, A., "Soil Creep as a Rate Process," *Journal of the Soil Mechanics and Foundation Division*, ASCE, Vol. 94, N. SM1, 1968, pp. 231–253.
16. Mitchell, J. K., and Matsui, T., "Implications of Soil Microstructure for Macro-Constitutive Relations" presented at the October 23–25, 1979 National Convention held at Atlanta, Ga. (Preprint 3716).
17. Mitchell, J. K., Singh, A., and Campanella, R. G., "Bonding, Effective Stresses and Strength of Soils," *Journal of the Soil Mechanics and Foundation Division*, ASCE, Vol. 95, No. SM5, Proc. Paper G786, Sept., 1969, pp. 1219–1246.
18. Murayama, S., and Shibata, T., "On the Rheological Characteristics of Clay, Part I," *Bulletin No. 26*, Disaster Prevention Research Institute, Kyoto University, Japan, 1958.
19. Murayama, S., and Shibata, T., "Rheological Properties of Clays," *Proceedings, 5th International Congress on Soil Mechanics and Foundations*, Paris, France, 1961, pp. 269–273.
20. Murayama, S., and Shibata, T., "Flow and Stress Relaxation of Clays (Theoretical Studies on the Rheological Properties of Clay—Part I)," *Proceedings, Rheology and Soil Mechanics Symposium of the International Union of Rheothetical and Applied Mechanics*, Grenoble, France, Apr., 1964.
21. Noble, C. A., and Demirel, T., "Effect of Temperature on the Strength Behavior of Cohesive Soil," Highway Research Board, *Special Report 103*, 1969, pp. 204–219.
22. Paaswell, R. E., "Causes and Mechanisms of Cohesive Soil Erosion: The State of the Art," Highway Research Board, *Special Report 135*, Soil Erosion: Causes and Mechanisms, Prevention and Control, 1974, pp. 52–72.
23. Partheniades, E., "A Study of Erosion and Deposition of Cohesive Soils in Salt Water," thesis presented to the University of California, at Berkeley, Calif., in 1962, in partial fulfillment of the requirements for the degree of Doctor of Philosophy.
24. Partheniades, E., "Erosion and Deposition of Cohesive Soils," *Journal of the Hydraulics Division*, ASCE, Vol. 91, No. HY1, Proc. Paper 4204, Jan., 1965, pp. 105–138.
25. Partheniades, E., and Paaswell, R. E., "Erodibility of Channels with Cohesive Boundary," *Journal of the Hydraulics Division*, ASCE, Vol. 96, No. HY3, Proc. Paper 7156, Mar., 1970, pp. 755–771.
26. Raudkivi, A. J., and Hutchison, D. L., "Erosion of Kaolinite by Flowing Water," *Proceedings of the Royal Society of London A.*, Vol. 337, 1974, pp. 537–554.
27. Task Committee on Erosion of Cohesive Materials, Frank D. Marsh, Chairman, "Erosion of Cohesive Sediments," *Journal of the Hydraulics Division*, ASCE, Vol. 94, No. HY4, Proc. Paper 6044, July, 1968, pp. 1017–1049.
28. Sargunam, A., Riley, P., Arulanandan, K., and Krone, R. B., "Physico-Chemical Factors in Erosion of Cohesive Soils," *Journal of the Hydraulics Division*, ASCE, Vol. 99, No. HY3, Proc. Paper 9609, Mar., 1973, pp. 555–558.
29. Taylor, B. D., and Vanoni, V. A., "Temperature Effects in Low Transport, Flat Bed Flows," *Journal of the Hydraulics Division*, ASCE, Vol. 98, No. HY8, Aug., 1972, pp. 1427–1445.
30. Vanoni, V. A., and Brooks, N., "Laboratory Studies of the Roughness and Suspended Load of Alluvial Streams, *Report No. E-68*, California Institute of Technology, Pasadena, Calif., 1957.
31. Wu, T. H., Resindez, D., and Neukirchner, R. J., "Analysis of Consolidation by Rate Process Theory," *Journal of the Soil Mechanics and Foundation Division*, ASCE, Vol. 92, No. SM6, Proc. Paper 4991, Nov., 1966, pp. 229–248.

Appendix II.—Notation

The following symbols are used in this paper:

E = experimental activation energy, Kcal/mole;
k = Boltzman's constant = 1.38×10^{-16} erg/°K;
R = universal gas constant = 1.98 cal/(°K-mole);
S = salinity, parts per thousand;

T = absolute temperature, °K;
V = volume, cm^3;
ϵ = erosion, rate, $gram/(cm^2 \cdot sec)$; and
τ = shear stress, pascals.

Ice Cover Effects on Stream Flows and Mixing

By Y. Lam Lau[1] and Bommanna G. Krishnappan[2]

Introduction

The presence of ice cover in a stream alters the flow characteristics to a great extent. The normal flow depth increases due to the increased resistance resulting from an additional solid boundary and the average flow velocity decreases. In addition, both the velocity and shear stress distributions change. Therefore, one can expect differences in the momentum and mass transfer coefficients between ice-covered stream flows and open-water stream flows.

For a two-dimensional, fully developed turbulent flow in an open channel with a free surface, for which linear shear stress and logarithmic velocity distributions are often assumed to apply, the distributions of the kinematic viscosity, ν_t, and the mass transfer coefficient, Γ_y, are parabolic, with a maximum at middepth and zero at the stream bed and at the free surface.

In analyzing the flow structure in an ice-covered stream, the flow is usually divided into two layers, separated by the line of maximum velocity, with linear shear stress and logarithmic velocity distributions within each layer (3,4,11,13). However, these distributions lead to parabolic distributions of ν_t and Γ_y in each layer with a value of zero at the location of maximum velocity. This is obviously incorrect because it implies no momentum or mass transfer across the plate of maximum velocity. To avoid this obvious deficiency, the distribution of Γ_y may be arbitrarily altered as by Shen and Harden (11) who adopted the assumption that Γ_y is constant in the central portion of the flow, as suggested by Ismail (1).

In addition to the arbitrary modification of the Γ_y distribution, Shen and Harden had to assume that the depth remains constant when the flow acquires an ice cover. This is also not correct because, given the same discharge, the depth will increase with the presence of an ice cover. In this paper, an alternate approach has been adopted to overcome the above difficulties. The "k-ϵ"

[1]Head, Environmental Hydr. Section, Hydr. Research Div., National Water Research Inst., Canada Centre for Inland Waters, Burlington, Ontario, Canada, L7R 4A6.

[2]Research Scientist, Environmental Hydr. Section, Hydr. Research Div., National Water Research Inst., Canada Centre for Inland Waters, Burlington, Ontario, Canada, L7R 4A6.

Note.—Discussion open until March 1, 1982. To extend the closing date one month, a written request must be filed with the Manager of Technical and Professional Publications, ASCE. Manuscript was submitted for review for possible publication on July 28, 1980. This paper is part of the Journal of the Hydraulics Division, Proceedings of the American Society of Civil Engineers, ©ASCE, Vol. 107, No. HY10, October, 1981. ISSN 0044-796X/81/0010-1225/$01.00.

turbulence model, described in detail by Launder and Spalding (5), is used to calculate the depth, velocity distribution, and ν_t distribution for two flows with the same given discharge, bed slope, and bottom roughness. One of these flows has a free surface at the top while the other has an ice cover of a given roughness. These results are then used in the two-dimensional mass transport equation to simulate the concentration distributions due to sources placed at different heights in the flow. The results give some indications of the effects of ice cover on the flow and on the vertical mixing.

Theoretical Considerations

In k-ϵ model of turbulence, the turbulence structure is considered to be governed by *two* characteristic parameters, namely, the kinetic energy of turbulent motion, k, and its rate of dissipation ϵ. As a result, the turbulent kinematic viscosity ν_t can be expressed as:

$$\nu_t = c_\mu \frac{k^2}{\epsilon} \quad (1)$$

in which c_μ = an empirical constant.

Eq. 1 permits the evaluation of the ν_t distribution from the distributions of k and ϵ. The distributions of k and ϵ, in turn, are determined by solving the semiempirical transport equations for k and ϵ along with the continuity and momentum equations for the flow field.

Governing Equations

For steady, two-dimensional channel flow, the equations of continuity, momentum and the transport equations for k and ϵ take the following forms:

$$\frac{\partial u}{\partial x} + \frac{\partial v}{\partial y} = 0 \quad (2)$$

$$\frac{\partial u^2}{\partial x} + \frac{\partial uv}{\partial y} = \frac{\partial}{\partial y}\left(\nu_t \frac{\partial u}{\partial y}\right) + gS - g\frac{dh}{dx} \quad (3)$$

$$\frac{\partial uk}{\partial x} + \frac{\partial vk}{\partial y} - \frac{\partial}{\partial y}\left(\frac{\nu_t}{\sigma_k}\frac{\partial k}{\partial y}\right) + G - \epsilon \quad (4)$$

$$\frac{\partial u\epsilon}{\partial x} + \frac{\partial v\epsilon}{\partial y} = \frac{\partial}{\partial y}\left(\frac{\nu_t}{\sigma_\epsilon}\frac{\partial \epsilon}{\partial y}\right) + c_1\frac{\epsilon}{k}G - c_2\frac{\epsilon^2}{k} \quad (5)$$

$$\frac{\partial u\phi}{\partial x} + \frac{\partial v\phi}{\partial y} = \frac{\partial}{\partial y}\left(\frac{\nu_t}{\sigma_\phi}\frac{\partial \phi}{\partial y}\right) + s_\phi \quad (6)$$

The coordinate system chosen is shown in Fig. 1. The x-axis is measured along the channel bed and the y-axis is measured perpendicular to the x-axis in the vertical plane. Parameters u, v = the velocity components in the x and y directions, respectively. The parameter h = the flow depth; S = the slope of the channel bed; σ_k, σ_ϵ, σ_ϕ, c_1, and c_2 = empirical constants; and G = the turbulent

energy production by the mean motion given by:

$$G = \nu_t \left[\left(\frac{\partial u}{\partial y} \right)^2 + 2 \left(\frac{\partial v}{\partial y} \right)^2 \right] \quad \ldots\ldots\ldots\ldots\ldots\ldots\ldots\ldots\ldots\ldots (7)$$

in which ϕ = a scalar quantity such as temperature in the case of heat transfer and concentration in the case of mass transfer. The term s_ϕ is the volumetric source rate of ϕ.

The empirical constants were determined by Launder and Spalding (5) who considered a variety of flows such as flows in pipes, channels, mixing layers, jets and wakes. The values arrived at by Launder and Spalding are as follows: (1) $c_\mu = 0.09$; (2) $\sigma_k = 1.00$; (3) $\sigma_\epsilon = 1.30$; (4) $c_1 = 1.43$; (5) $c_2 = 1.92$; and (6) $\sigma_\phi = 1.00$ for mass transfer and 0.50 for heat transfer.

The governing equations listed in the foregoing are derived with the assumption that the flow is predominantly in one direction (namely, along x) and that the turbulent transports of u, k, ϵ, and ϕ are negligible in that direction, i.e., the terms containing the second order derivatives in x are *not* included in the set of equations. This latter assumption modifies the equations from elliptic type

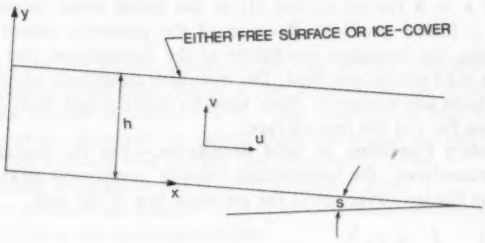

FIG. 1.—Co-Ordinate System

to parobolic type. Parabolic equations are especially suitable for numerical schemes which solve the equations for one station at a time and march forward along x. Such numerical schemes require less computer memory and are executed at a much faster rate.

The fully developed distributions of velocity and turbulent kinematic viscosity, which are required for evaluating the effects of ice cover on the flow and mixing characteristics, are obtained as asymptotic distributions resulting from the solution of the governing equations. The same results could have been obtained by solving a set or ordinary differential equations representing the fully developed flows. Indeed, for fully developed flows, the variation of flow properties along x vanishes and therefore the governing equations become:

$$\frac{d}{dy} \left(\nu_t \frac{du}{dy} \right) = -gS \quad \ldots\ldots\ldots\ldots\ldots\ldots\ldots\ldots\ldots\ldots (8a)$$

$$\frac{d}{dy} \left(\frac{\nu_t}{\partial_k} \frac{dk}{dy} \right) = \epsilon - G \quad \ldots\ldots\ldots\ldots\ldots\ldots\ldots\ldots\ldots\ldots (8b)$$

$$\frac{d}{dy}\left(\frac{\nu_t}{\sigma_\epsilon}\frac{d\epsilon}{dy}\right) = c_2\frac{\epsilon^2}{k} - c_1\frac{\epsilon}{k}G \qquad (8c)$$

The numerical schemes to solve the preceding system of ordinary differential equations are simpler in comparison to those schemes required to solve the partial differential equations. However, the prediction of concentration distributions still requires the solution of the partial differential equation (Eq. 6). In addition, the solution of the original set of partial differential equations can be applied to the investigation of jet type discharges. Therefore, it was decided to solve the governing equations as expressed by Eqs. 2–7 rather than the set given by Eq. 8.

Boundary Conditions

Eqs. 1–7 form a closed set of equations and, given values for the empirical constants and for s_ϕ, therefore can be solved simultaneously for u, v, k, ϵ, ν_t, G, and ϕ. Boundary conditions for the above parameters have to be specified: (1) At the channel bed, i.e., at $y = 0$ for all x; (2) at the upper boundary, i.e., at $y = h$ for all x; and (3) at the initial cross section, i.e., at $x = 0$ for all y (initial profiles). Because of the parabolic nature of the governing equations, the boundary conditions at the downstream end of the calculation domain need not be specified. The boundary conditions adopted for the present calculations are similar to those used by Rastogi and Rodi (8), except for the condition for ϵ at the free surface.

Boundary Conditions at Solid Boundaries.—For the boundary layer type of flows considered, the longitudinal velocity component near the channel bed, and near the ice cover obeys the universal law of the wall.

$$\frac{u_w}{V_*} = \frac{1}{\kappa}\ln\left(E\frac{v_* y_w}{\nu}\right) \qquad (9)$$

in which u_w = the x component of velocity at a distance y_w from the wall; and v_* = the shear velocity defined in terms of boundary shear stress, τ_b, and the fluid density ρ as

$$v_* = \sqrt{\frac{\tau_b}{\rho}} \qquad (10)$$

κ = the von-Karman constant, equal to 0.42; ν = the kinematic viscosity of the fluid; E = a roughness parameter which takes a value of 9.0 for hydraulically smooth turbulent flows and $(30.1/v_* K_s/\nu)$ for rough turbulent flows; and y_w = the distance from the solid boundary to the grid point nearest to the solid boundary. The symbol K_s, represents the size of the equivalent sand grain roughness for the solid boundary.

The vertical velocity component v at solid boundaries is zero.

The turbulent kinetic energy, k, and its dissipation rate ϵ near solid boundaries are evaluated using the following assumptions: (1) The production of turbulent kinetic energy is equal to the rate of dissipation (i.e., $G = \epsilon$); (2) the turbulent shear stress τ near the solid boundary is constant and is equal to the boundary

shear stress (i.e., $\tau = \tau_b$); (3) the velocity distribution in the vicinity of the solid boundary is given by Eq. 9.

Under these conditions, the kinetic energy of turbulence and its dissipation rate near solid boundaries can be evaluated as:

$$k_w = \frac{v_*^2}{\sqrt{c_\mu}}; \quad \epsilon_w = \frac{v_*^3}{\kappa y_w} \quad \ldots\ldots\ldots\ldots\ldots\ldots\ldots\ldots\ldots\ldots\ldots\ldots (11)$$

For heat or mass transfer, or both, the flux at solid boundaries is assumed to be zero.

Boundary Conditions at Free Surface.—Following the approach adopted by Rastogi and Rodi (7), the free surface is treated as a symmetry plane for u, k, and ϕ. Accordingly, the y gradients for u, k, and ϕ become zero. Rodi (8) has suggested that the presence of a free surface should have an effect of reducing the length scale of turbulence near the surface and that a symmetry boundary condition for ϵ may not be completely satisfactory. Consequently, a condition similar to that at the solid boundary is introduced and expressed as:

$$\epsilon_f = \frac{(k_f \sqrt{c_\mu})^{3/2}}{\kappa y_f} \quad \ldots\ldots\ldots\ldots\ldots\ldots\ldots\ldots\ldots\ldots\ldots\ldots (12)$$

in which k_f = the turbulent kinetic energy at the free surface calculated using the symmetry boundary condition; and y_f = the distance of the nearest grid point from the free surface in which $k = k_f$. This condition is only tentative and needs further testing. However, the results show that it does not significantly affect the comparison between free surface and ice-covered flows.

The vertical velocity component v at the free surface is zero.

For heat transfer problems the gradient of ϕ at the boundaries will be nonzero. However, this problem is not investigated here.

Initial Profiles.—At the starting cross section, i.e., at $x = 0$, the distributions of u, v, k, and ϵ are not known a priori and, certain assumptions have to be made in specifying them. The distributions used in the present work are outlined in the following:

1. *Free surface flow case*: The velocity component u follows a logarithmic distribution in the vicinity of the channel bed, i.e., Eq. 9. In the remaining part of the flow region a uniform distribution is assumed. The assumed distribution has to satisfy the requirement that it yields the specified flow rate per unit width of the channel. The distributions for k and ϵ are assumed to be uniform over the whole height of the flow field, having the values k_w and ϵ_w respectively, as given by Eq. 11. The vertical velocity component v is assumed to be zero everywhere.

2. *Ice-covered flow case*: The velocity component u follows a logarithmic distribution both near the channel bed and near the ice cover. In the central region of the flow, u is assumed to be uniform. Here again, the assumed distribution has to yield the specified flow rate per unit width of channel. Linear profiles for k and ϵ are used with the values k_w and ϵ_w evaluated both at channel bed and at the ice cover using Eq. 11. The vertical velocity component v is zero everywhere.

Numerical Scheme

For the present work, the numerical scheme proposed by Patankar and Spalding (6) is adopted. For the sake of completeness, some of the salient features of the numerical scheme are presented in this paper. The forms of Eqs. 3, 4, 5, and 6 are such that one single numerical scheme can be used to solve all the equations. Indeed, Eqs. 3, 4, and 5 can be expressed in the form of Eq. 6. As an example, Eq. 3 is identical to Eq. 6 when u is equated to ϕ and $(gS - gdh/dx)$ to s_ϕ. Therefore, in presenting the details of the numerical scheme here, only Eq. 6 is considered.

In the scheme proposed by Patankar and Spalding the finite difference equations of Eq. 6 are arrived at by integrating the differential equation term by term over small control volumes. Certain assumptions are made regarding the variation of ϕ along x and y directions. Referring to Fig. 2(a), I is the upstream grid

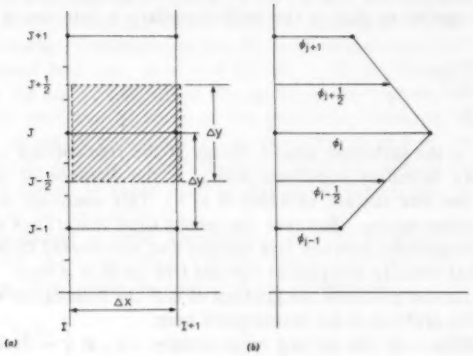

FIG. 2.—(a) Control Volume; (b) Assumed Profile for ϕ in y Direction Between Grid Points

line where the solution for ϕ is known and $I + 1$ is the downstream grid line located at a distance Δx from the upstream grid line where the values of ϕ are to be determined. The parameters $J - 1$, J, and $J + 1$ are grid lines in the y direction. $J + 1/2$ and $J - 1/2$ are the mid points between J and $J + 1$ and J and $J - 1$, respectively. The control volume over which the equation is integrated is shown by hash lines. The variation of ϕ in the y direction is assumed to be linear between grid points as shown in Fig. 2(b). The variation of ϕ along x is assumed to be stepwise. The step change occurs right at the upstream grid line. Between grid points ϕ is uniform and equal to the value corresponding to the downstream grid. Such an assumption of ϕ along x gives rise to an implicit form of the finite difference equations.

When each term of Eq. 6 is integrated over the control volume shown in Fig. 2(a), the following relation is obtained:

1. Transport velocities (u, v) and the eddy viscosity (ν_t) are defined along

the upstream grid line (I) so that the equation for ϕ is linear. Further, the transport velocity, u, is assumed to be constant with y (i.e., upstream and downstream faces of the control volume). The approximations introduced by this linearization and this representation of u, while not introducing an error for this uniform flow case, should be evaluated further before such a scheme is applied to nonuniform or unsteady, or both, flows.

$$\left\{\frac{3}{2}(P+\Omega)_J\Delta y + L_{J+1/2} - L_{J-1/2} + 2\,T_{J+1/2} + 2T_{J-1/2}^{-2s}\right\}\phi_J$$

$$+\left\{\frac{1}{4}(P+\Omega)_J\Delta y + L_{J+1/2} - 2T_{J+1/2}\right\}\phi_{J+1}$$

$$+\left\{\frac{1}{4}(P+\Omega)_J\Delta y - L_{J-1/2} - 2T_{J-1/2}\right\}\phi_{J-1}$$

$$=\left\{\frac{1}{2}P_J\left(3\phi_{I,J}\Delta y + \phi_{I,J+1}\frac{\Delta y}{2} + \phi_{I,J-1}\frac{\Delta y}{2}\right) + 2\,s_I\right\} \quad \ldots\ldots\ldots\ldots \quad (13)$$

ϕ_x, ϕ_{J+1}, $\phi_{J-1} = \phi_{I+1,J}$, $\phi_{I+1,J+1}$; $\phi_{I+1,J-1}$, respectively

in which $$P_J = \frac{u_{I,J}}{\Delta x} \quad \ldots\ldots\ldots\ldots\ldots\ldots\ldots\ldots\ldots\ldots \quad (14a)$$

$$\Omega_J = \frac{1}{\Delta y}(L_{J-1/2} - L_{J+1/2}) \quad \ldots\ldots\ldots\ldots\ldots\ldots\ldots\ldots \quad (14b)$$

$$L_{J-1/2} = v_{I,J-1/2} \quad \ldots\ldots\ldots\ldots\ldots\ldots\ldots\ldots\ldots\ldots \quad (14c)$$

$$L_{J+1/2} = v_{I,J+1/2} \quad \ldots\ldots\ldots\ldots\ldots\ldots\ldots\ldots\ldots\ldots \quad (14d)$$

$$T_{J+1/2} = \frac{\left(\frac{v_t}{\sigma_\phi}\right)_{I,J+1/2}}{\Delta y} \quad \ldots\ldots\ldots\ldots\ldots\ldots\ldots\ldots \quad (14e)$$

$$T_{J-1/2} = \frac{\left(\frac{v_t}{\sigma_\phi}\right)_{I,J-1/2}}{\Delta y} \quad \ldots\ldots\ldots\ldots\ldots\ldots\ldots\ldots \quad (14f)$$

The integral of the source term s_ϕ over the control volume is expressed in a linear form as follows:

$$s_I + s\phi_J = \int_{J-1/2}^{J+1/2} s_\phi\,dy \quad \ldots\ldots\ldots\ldots\ldots\ldots\ldots\ldots\ldots\ldots \quad (14g)$$

The values of s and s_I depend on the entity which ϕ represents. In Eq. 13, all the terms except the ones with s_I and ϕ_J represent the values at the downstream grid line $I + 1$. The subscript $(I + 1)$ is omitted for ease of writing. When Eq. 13 is written out for all values of J, a series of finite difference equations results which can be expressed as a tridiagonal matrix equation. There are several standard methods to solve such a system of algebraic equations. In

the present calculations simple successive-substitution formulae proposed by Patankar and Spalding were used.

Application of Numerical Scheme

In order to evaluate the effects of an ice cover on the flow properties and the vertical mixing characteristics in channel flows, it is necessary to solve the governing equations for both the free surface case and the ice cover case. For these two flows to be equivalent, it is assumed that both channels carry the same flow rate, have the same bottom slope and the same bottom roughness. The flow depths, of course, will be different. The flow depth in the ice-covered flow will be larger than that of the free-surface flow because of the increased resistance due to the ice cover. Since the flow depths are not known a priori, a trial and error method is required. The procedure adopted in the present work is illustrated in the following.

Calculations for Free-Surface Flow

The values of flow rate per unit width q and the channel bed roughness, K_s, are assumed to be specified. A value for the flow depth, h_o, is selected. (Subscript 0 is used to denote free-surface flow properties and i is used for ice-covered flow properties.) Because the main interest of this paper is in the

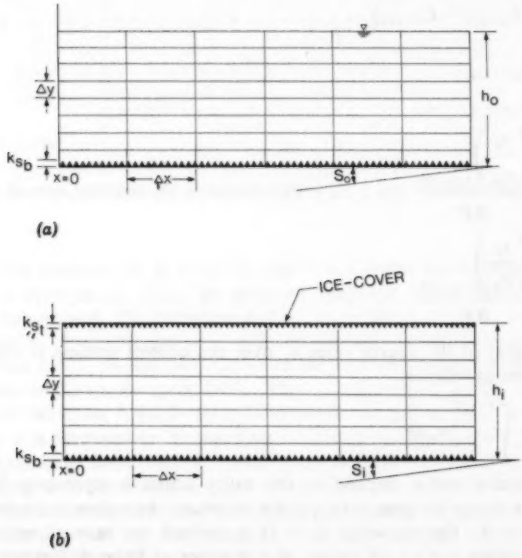

FIG. 3.—(a) Numerical Grid for Free Surface Flow Computation; (b) Numerical Grid for Ice-Covered Flow Computation

comparison between free-surface and ice-covered flows under uniform flow conditions, this flow depth is maintained constant in the longitudinal direction. Using this flow depth, a numerical grid is laid in the *x*-*y* plane as shown in Fig. 3(*a*). Therefore, the problem becomes one of finding out what the slope has to be in order to have uniform flow at the given flow depth.

From the initial profile for u_o, the shear velocity, v_*, and thus the boundary values for k_w and ϵ_w at $x = 0$ are evaluated. The ν_t distribution is obtained from Eq. 1. Eqs. 2 and 3 are then solved using the numerical scheme to obtain the *u* and *v* profiles at the downstream station $x = \Delta x$. The value of the slope *S* in Eq. 3 is evaluated using v_* and h_o, assuming uniform flow.

Using the velocity distribution at $x = \Delta x$, values for v_*, k_w, and ϵ_w are obtained. Eqs. 4 and 5 are now solved for the ϵ and *k* distributions at $x = \Delta x$. These distributions are used to calculate the ν_t distribution which is then used with Eqs. 2 and 3 to solve for the velocity distributions at the next downstream station. This procedure is continued until a certain downstream distance is reached where the profiles of *u* and ν_t no longer change from grid line to grid line, i.e., where the profiles become fully developed. At this point, the vertical velocity component is zero and the value of slope, S_0, computed becomes invariant with respect to *x*. Therefore, for the specified flow rate per unit width *q* and the bed roughness K_s, the free-surface flow with bed slope S_0 will flow at a uniform depth of h_0. This completes the calculations for open water flow.

Calculations for Ice-Covered Flow

The values of flow rate per unit width of channel and the channel bed roughness for the flow under ice cover are the same as for the free-surface flow calculated in the aforementioned.

The roughness of the ice-cover surface has to be specified. Let it be K_{s_i}. The bed roughness for the ice-covered channel is denoted by K_{s_b} and its value is equal to K_s. A value for the flow depth h_i is selected, and the computation is carried out using a procedure similar to that for the free-surface flow. The computational grid for this case is shown in Fig. 3(*b*). The value of the slope *S* appearing in the momentum equation is evaluated using the shear velocities at the channel bed and at the ice cover, v_{*b} and v_{*i}, i.e.

$$S_i = \left(\frac{v_{*b}^2 + v_{*i}^2}{gh_i}\right) \qquad (15)$$

The computations are carried out until a certain downstream distance is reached where the profiles of *u* and ν_t no longer change from grid line to grid line, i.e., where the profiles become fully developed. At this stage, the vertical velocity component v_i is zero and the shear velocities v_{*b} and v_{*i} become invariant with respect to *x*. Consequently, the slope S_i computed using Eq. 15 is also invariant with respect to *x*. For the specified flow rate, *q*, bed roughness, k_{s_b}, and ice-cover roughness k_{s_i}, the ice-covered flow becomes uniform with depth h_i for the slope S_i. Now, if this slope S_i is not the same as the slope S_0 of the uniform free surface flow previously computed, then a different value for h_i is selected and the calculations are repeated until S_i coincides with S_0. The flow depth h_i corresponding to this slope then yields an ice-covered flow equivalent to the free-surface flow.

Results and Analysis

Using the procedure outlines in the last section, fully developed profiles of u and v_t were obtained for three different flow conditions in both free-surface and ice-covered channels. The hydraulic parameters for the three flow conditions are shown schematically in Fig. 4 and are also listed in Table 1. In the first flow condition, denoted as run no. 1, the value for K_s for both channels was taken as 3 mm. The flow rate per unit width was taken as 22,300 mm^2/s for both channels. The ice cover was considered to act as an hydraulically smooth surface.

In run no. 2, the bed roughness was increased to 5 mm and the ice-cover roughness was kept the same as in run no. 1. In run no 3, the bed roughness was kept the same as run no. 2 and the ice-cover roughness was increased to 5 mm. The resulting flow depths, shear velocities and slopes are listed in Table 1 and are also shown in Fig. 4. As expected, the ice-covered flows required larger flow depths to transport the same flow rate with same bed slope. The increase in flow depth varied from 15%–31%. Calculations have also been made for a much deeper flow depth which is closer to a natural flow. In that case, the depth increased from 2.7 m–3.0 m when an ice cover was present, an increase of 11.1%. The shear velocities at the bed of ice-covered flows were smaller than those for the free-surface flows. The latter result indicates that if the bed of the stream is movable, then the sediment transporting capacity would be diminished by the presence of ice cover. Furthermore, the bed forms resulting from the movement of sediment would also be different from the free-surface flows, which in turn would alter the roughness characteristics. Therefore, the presence of an ice cover can produce significant changes to the hydraulic characteristics of natural stream flows. However, it should be noted that if the ice-covered flow is divided into an upper and a lower layer, the Darcy friction factor associated with the lower layer is actually larger than in the free surface flow, even though the bed shear stress has decreased. This is because the mean velocity in the lower layer has decreased by a proportionately larger amount.

Profiles of u for the three runs are shown in Fig. 5. Solid lines represent the ice-covered flows and the dotted lines denote the free-surface flows. In all three runs, the ice-covered flow velocities are lower than those of the free-surface flows. The u profiles in ice-covered flows resemble the ones measured by Larsen (3,4) with close to zero gradients over substantial portions of the central region. Such profiles mean that the division of the flow into two layers, as has been done by previous investigators, can be very subjective. Velocity profiles in ice-covered flows are sensitive to the roughness characteristics of both bed and ice-cover. When the bed roughness increases in comparison to the ice-cover roughness, the position of maximum velocity moves closer to the smoother surface. The profile becomes symmetrical when the roughness values of bed and ice-cover are equal as in run no. 3.

Velocity profiles for the free-surface flows are close to being logarithmic for about 75% of the flow depth for all three runs, but deviate from the logarithmic distribution for the remaining 25% near the free surface. This result is in agreement with a recent study by Song and Yang (12) who put forward the hypothesis that the flow in a wide open channel consists of three different regions: a

laminar sublayer region, very close to the channel bed; an inner turbulent region in the middle; and an outer turbulent region near the free surface. Based on the experimental work of Vanoni (14) and Sayre (9), Song and Yang argue

TABLE 1.—Hydraulic Parameters for Simulated Runs

Run Number / Flow properties (1)	Run Number 1		Run Number 2		Run Number 3	
	Open-water flow (2)	Ice-covered flow (3)	Open-water flow (4)	Ice-covered flow (5)	Open-water flow (6)	Ice-covered flow (7)
Flow rate per unit width, in square millimeters per second	22,300	22,300	22,250	22,260	22,240	22,220
Bed roughness k_{s_b}, in millimeters	30	30	50	50	50	50
Ice-cover roughness k_{s_i}, in millimeters	N/A	hydraulically smooth ice cover	N/A	hydraulically smooth ice cover	N/A	50
Shear velocity at bed v_{*b}, in millimeters per second	52.5	45.7	56.1	49.2	65.1	52.9
Shear velocity at ice cover v_{*i}, in millimeters per second	N/A	33.6	N/A	34.1	N/A	52.9
Slope of channel	00.011	00.011	00.012	00.012	00.019	00.019
Flow depth, in millimeters	257.5	300.	260.	300.	228.	300.

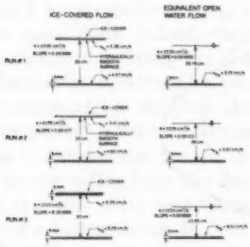

FIG. 4.—Schematic Representation of Flows Simulated

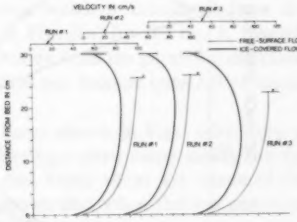

FIG. 5.—Velocity Distributions

that the logarithmic velocity distribution is applicable only to the inner turbulent region. For the outer turbulent region, they propose a parabolic distribution.

A parabolic velocity distribution in conjunction with a linear distribution for shear stress would give rise to a constant turbulent kinematic viscosity when

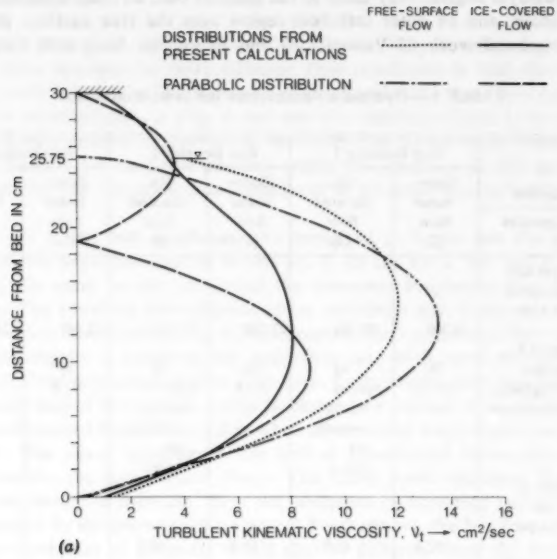

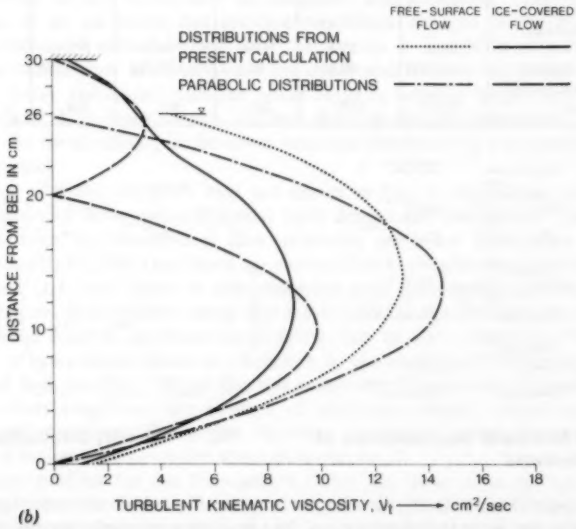

FIG. 6.—(*a*) ν_t-Distribution for Run No. 1; (*b*) ν_t-Distribution for Run No. 2

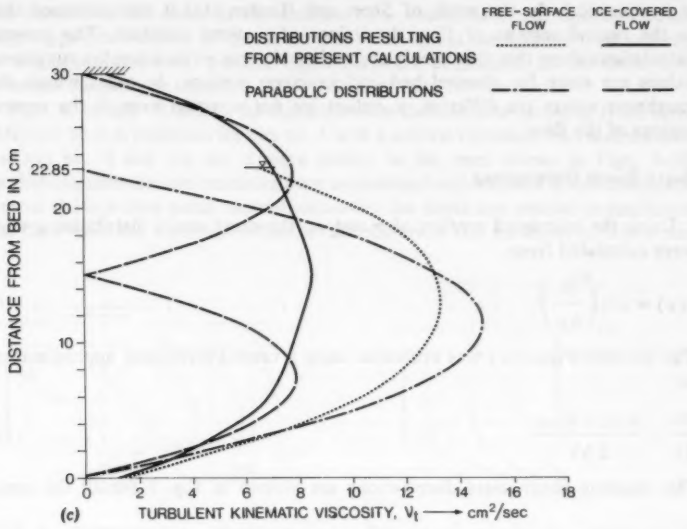

FIG. 6.—*Continued*: (c) ν_t-Distribution for Run No. 3

the Boussinesq hypothesis is invoked, whereas a logarithmic velocity distribution gives rise to a parabolic distribution for ν_t as shown earlier. Some experiments carried out to measure the turbulent kinematic viscosity [Jobson (2)] do suggest that the ν_t distribution deviates from the parabolic distribution, especially near the free surface which supports the suggestion that the velocity distribution near the free surface indeed is not logarithmic. If it is not logarithmic, then should it be parabolic as Song and Yang suggest? The answer to this question is not quite clear. Indeed, the ν_t distribution which is calculated from the k and ϵ distributions using Eq. 2 and shown in Fig. 6(*a*) for run no. 1, resembles the distribution measured by Jobson and deviates from the parabolic distribution in the upper part of the flow. However, ν_t does not become constant as required for the parabolic velocity distribution.

The ν_t distributions for the ice-covered flows shown in Figs. 6(*a*), 6(*b*), and 6(*c*) do not suffer from the drawback of having a zero value inside the flow, as in the case when logarithmic velocity and linear shear are assumed for a top and a bottom layer. In fact, Fig. 6(*c*) shows that when the top and bottom roughness are equal, ν_t is a maximum at mid-depth.

A comparison between ν_t values for ice-covered flows and free-surface flows indicates that the values of ν_t for ice-covered flows are smaller than those for the free-surface flows in all three runs. The difference increases as one moves away from the bed. The distributions of ν_t for the ice-covered flows are affected by the relative roughness of the boundaries. In runs 1 and 2, the ν_t distributions are skewed towards the rougher lower boundary whereas in run 3 for which the roughness is equal for both boundaries are the ν_t distribution

is symmetrical. In the work of Shen and Harden (11) it was assumed that in the central regions of flow the values of ν_t were constant. The present calculations show that this is only approximately true even when the roughness values are same for channel bed and ice-cover surface. In cases where the roughness values are different, ν_t values are not constant even in the central regions of the flow.

Shear Stress Distributions

Using the calculated profiles of u and ν_t, the shear stress distributions $\tau(y)$ were calculated from

$$\tau(y) = \rho \nu_t \left(\frac{\partial u}{\partial y}\right) \quad \ldots \ldots \ldots \ldots \ldots \ldots \ldots \ldots \ldots \ldots \quad (16)$$

The derivative $(\partial u/\partial y)$ was evaluated using a central difference approximation as:

$$\frac{\partial u}{\partial y} = \frac{u_{J+1} - u_{J-1}}{2\Delta y} \quad \ldots \ldots \ldots \ldots \ldots \ldots \ldots \ldots \ldots \ldots \quad (17)$$

The resulting shear-stress distributions are plotted in Fig. 7 for all the runs.

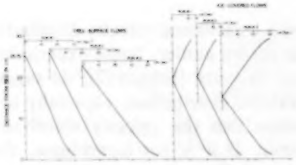

FIG. 7.—Shear Stress Distributions

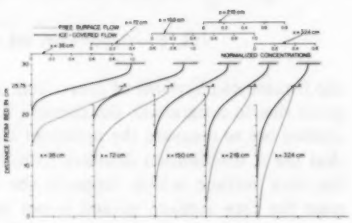

FIG. 8.—Concentration Distributions for Run No. 1 (Surface Injection)

From Fig. 7 it can be seen that the shear-stress distribution is very close to linear for all the runs. Very close to the solid boundaries, the distributions seem to deviate from the linear profile; this may be due to the approximations in calculating the derivative of u by Eq. 17 and the k-ϵ model.

Distribution of Neutrally Buoyant Tracker

After calculating the fully developed distributions of u and ν_t, calculations were performed to obtain concentration distributions of a neutrally buoyant tracer by solving Eq. 6 with $\sigma_\phi = 1$. After the flow has been fully developed, tracer was introduced in the x-direction (parallel to the flow). The sources were of finite height (50 mm) and of uniform concentrations. Three different vertical positions for injections were considered: (1) Surface injection; (2) middle injection; and (3) bottom injection. The injections were either neutral, (the velocity of

the tracer was the same as the ambient flow velocities at the injection point) or jet-type (the velocity of the tracer was twice that of the ambient flow velocity at the injection point). Neutral injections were considered for all three runs whereas the jet-type injection was considered only for run no. 1.

Figs. 8, 9, and 10 depict the concentration distributions resulting from three different source positions for run no. 1 with a neutral injection. The distributions for run no. 2 and run no. 3 were similar to the ones shown in Figs. 8–10. In these figures the concentrations are normalized with respect to the concentration at the injection point. Actual values for the depth are plotted to emphasize the fact that the equivalent depths are different for ice-covered flows and

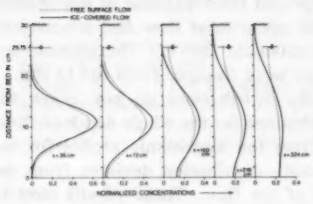

FIG. 9.—Concentration Distributions for Run No. 1 (Middle Injection)

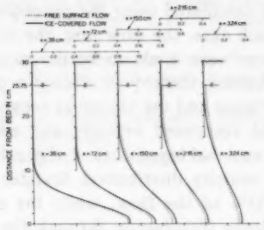

FIG. 10.—Concentration Distributions for Run No. 1 (Bottom Injection)

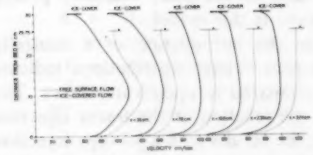

FIG. 11.—Velocity Distributions for Jet-Type Tracer Injection

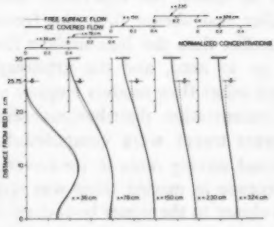

FIG. 12.—Concentration Distributions for Jet-Type Tracer Injection

free-surface flows. The center line of the middle injection was at a depth of 11 cms in both types of flow.

These figures show that the reduction in the maximum concentration values is more rapid in the free-surface flows than in the ice-covered flows. This result indicates that an ice cover tends to reduce the mixing rate. The difference in the mixing rate is the largest when the injection is at the surface. As the position of injection was moved towards the channel bed, the difference in the mixing rate diminishes.

Figs. 11 and 12 show the velocity and concentration distributions for a jet-type injection. Fig. 11 shows that the velocity distribution changes along the length of the channel from the injection location and becomes invariant with x at

about 300 cms from the injection point. The concentration distributions shown in Fig. 12 indicate that the mixing is much faster in the jet-type discharge than in the neutral discharge and that the difference between the mixing rates in the free-surface flow and the ice-covered flow was not significant.

Summary and Conclusions

In this paper, a procedure was been outlined to calculate the uniform, two-dimensional flows in channels with and without ice covers using the k-ϵ turbulence model proposed by Launder and Spalding (5) and a numerical scheme proposed by Patankar and Spalding (6). Three different fully developed flows were calculated using the procedure for open-water and ice-covered conditions. In each case, the flow rate, the channel slope and the roughness of the channel bottom were made to be the same for both open-water flow and ice-covered conditions, thereby producing a pair of "equivalent flows." The channel-bed roughness and the ice-cover roughness values were changed from run to run.

The computed velocity and eddy viscosity distributions do not follow the conventional logarithmic and parabolic distributions for the whole depth of flow. The velocity distribution deviates slightly from the logarithmic profile for the top 25% of the flow, while the eddy viscosity distribution deviates from the parabolic distribution through the top half of the flow. These results tend to agree with the results from recent investigations of the velocity distribution (11) and measurements of the eddy viscosity distribution (2), and give confidence to the calculations from the k-ϵ model.

In all cases, the equivalent ice-covered flows have larger flow depths and smaller bed shears then the free-surface flows. The resulting eddy viscosity is smaller than the free-surface flow values. However, the eddy viscosity does not go to zero, and the arbitrary modification of the eddy viscosity profile which other flow models employ is not required in this model.

Concentration distributions resulting from the introduction of a neutrally buoyant tracer were computed for all the runs. These distributions indicate reduced mixing rates in ice-covered flows compared to open-water flows. The difference in mixing rates was larger when the location of the tracer injection was closer to the upper boundary. However, the results with a jet-type injection gave approximately the same concentrations for the ice-covered and free-surface flows, and indicate that the effects of jet mixing outweigh the difference in the eddy viscosity between the flows.

Appendix I.—References

1. Ismail, H. M., "Turbulent Transfer Mechanism and Suspended Sediment in Closed Channels," *Transactions*, ASCE, Vol. 11, 1952, pp. 409–446.
2. Jobson, H. E., "Vertical Mass Transfer in Open Channel Flow," thesis presented to Colorado State University at Fort Collins, Colo., in 1968, in partial fulfillment of the requirement for the degree of Doctor of Philosophy.
3. Larsen, P. A., "Head Losses Caused by an Ice Cover on Open Channels," *Journal of the Boston Society of Civil Engineers*, Vol. 45, No. 1, 1968, pp. 45–67.
4. Larsen, P. A., "Hydraulic Roughness of Ice Covers," *Journal of the Hydraulics Division*, ASCE, Vol. 99, No. HY1, Proc. Paper 9498, Jan., 1973.
5. Launder, B. E., and Spalding, D. B., "The Numerical Calculation of Turbulent Flows," *Computer Methods in Applied Mechanics and Engineering*, Vol. 3, 1974, pp. 269–289.

6. Patankar, S. V., and Spalding, D. B., "Heat and Mass Transfer in Boundary Layers," Intertext Publishers, London, England, 1970.
7. Rastogi, A. K., and Rodi, W., "Predictions of Heat and Mass Transfer in Open Channels," *Journal of the Hydraulics Division*, ASCE, Vol. 104, No. HY3, Proc. Paper 13639, Mar., 1978, pp. 397–000.
8. Rodi, W., "Turbulence Models and Their Application in Hydraulics—A State-of-the-Art Review," *Technical Report No. SFB 80/T/127*, University of Karlsruhe, Karlsruhe, Germany, May, 1978.
9. Sayre, W. W., "Dispersion of Mass in Open Channel Flow," *Hydrology Paper No. 75*, Colorado State University, Fort Collins, Colo., 1975.
10. Sayre, W. W., and Song, G. B., "Effects of Ice Covers on Alluvial Channel Flow and Sediment Transport Processes," *IIHR Report No. 218*, Iowa Institute of Hydraulic Research, University of Iowa, Ames, Iowa, 1979.
11. Shen, H. T., and Harden, T. O., "The Effects of Ice Cover on Vertical Transfer in Stream Channels," *Water Resources Bulletin*, American Water Resources Association, Vol. 14, No. 6, 1978.
12. Song, C. C. S., and Yang, C. T., "Velocity Profiles and Minimum Stream Power," *Journal of the Hydraulics Division*, ASCE, Vol. 105, No. HY8, Proc. Paper 1478, Aug., 1979, pp. 981–998.
13. Uzuner, M. S., "The Composite Roughness of Ice-Covered Streams," *Journal of Hydraulics Research*, IAHR, Vol. 13, No. 1, 1975, pp. 79–102.
14. Vanoni, V. A., "Transportation of Suspended Sediment by Water," *Transactions*, ASCE, Vol. 111, Paper 2267, 1946, pp. 67–102.

Appendix II.—Notation

The following symbols are used in this paper:

c_1, c_2, c_μ = empirical constants;
E = roughness parameter;
g = acceleration due to gravity;
G = rate of production of turbulent energy;
h = flow depth;
i = subscript denoting ice-covered flow;
I = grid location in longitudinal direction;
J = grid location in vertical direction;
K_s = equivalent sand grain roughness;
k = kinetic energy of turbulent motion;
0 = subscript denoting free surface flow;
q = per unit width;
S = slope of channel bed;
s = source term;
u = velocity component in longitudinal direction;
v = velocity component in vertical direction;
v_* = shear velocity;
w = subscript denoting values close to wall regions;
X = longitudinal distance where flow attains fully developed state;
x = cartesian co-ordinate in longitudinal direction;
y = cartesian co-ordinate in vertical direction;
Γ_y = mass transfer coefficient in y direction;
Δx = distance between grid points in x direction;
Δy = distance between grid points in y direction;
ϵ = rate of dissipation of turbulent energy;

κ = Von-Karman constant;
ν_t = turbulent eddy viscosity;
ν = kinematic viscosity of fluid;
ρ = fluid density;
$\sigma_t, \sigma_\epsilon, \sigma_\phi$ = empirical constants;
τ = shear stress; and
ϕ = scalar quantity.

Model-Prototype Comparison of Free Surface Vortices

By George E. Hecker,[1] M. ASCE

Introduction

Free surface vortices continue to be of interest to hydraulic engineers due to the combination of incomplete mathematical or even physical understanding of vortex characteristics with new situations in which the occurrence of vortices are of concern. The detrimental effects of strong free surface vortices such as flow reductions, vibrations, and loss in efficiencies of pumps and turbines, and of structural damage, prompt engineers to design intake structures to avoid vortices. Intakes of consideration include those for pumps, navigation locks, hydroelectric power, flow and level regulation, and, more recently, withdrawal from sumps in Emergency Core Cooling Systems (ECCS) of nuclear power stations. A fundamental problem is that it is not yet possible to analytically predict whether or not a free surface vortex will occur at a particular "intake" for a given flow and water level. Therefore experiments, primarily reduced scale hydraulic models, continue to be used to investigate the susceptibility of an intake to free surface vortices. However, considerable confusion and controversy exist as to the importance of scale effects in such model studies due to the apparently conflicting results of past investigations.

This paper reviews some of the past research on vortices and scale effects, and attempts to provide some order and relationship between the various studies as a background to a new summary of model versus prototype observations regarding vortex intensity. Such a comparison itself provides a critical test of scale effects due to the large change in scale and in the associated fluid mechanic parameters known to influence vortices.

Conclusions from this review and summary are intended to help define the current state of knowledge on modeling free surface vortices.

Need for Model Studies

Various investigators have proposed guidelines for designing vortex-free intakes. The more practical of these guidelines give the required submergence

[1]Dir., Alden Research Lab., and Assoc. Prof., Civ. Engrg., Worcester Polytechnic Inst., Holden, Mass.

Note.—Discussion open until March 1, 1982. To extend the closing date one month, a written request must be filed with the Manager of Technical and Professional Publications, ASCE. Manuscript was submitted for review for possible publication on April 8, 1981. This paper is part of the Journal of the Hydraulics Division, Proceedings of the American Society of Civil Engineers, ©ASCE, Vol. 107, No. HY10, October, 1981. ISSN 0044-796X/81/0010-1243/$01.00.

in terms of the intake diameter (23), flow (17), velocity (6,12), or a withdrawal Froude number (26,25) without explicitly including a measure of circulation. Basic guidelines, such as by Anwar (1), require explicit knowledge of the circulation, a factor not known *a priori*. The acceptable versus unacceptable pumped storage intakes presented by Pennino and Hecker (22) were tested against the available practical guidelines with essentially no correlation, particularly with regard to the concept of a required submergence. The inefficacy of the available practical guidelines has also been mentioned by Dhillon (8), and such guidelines are not intended to apply in cases of strong local circulation such as generated by offset intakes or screen blockage in ECCS sumps.

Despite decades of work, therefore, the present state of knowledge is such that reduced scale hydraulic model studies or some other experiment is required for each case where it is important that no strong vortices occur. A possible difficulty with scale models, however, is that free surface vortices are subject to prediction errors due to the impossibility of reducing all pertinent forces by the same factor. Although the predominating inertial and gravitational forces are reduced similarly in the Froude-scaled models used in such studies, viscous and surface tension forces cannot simultaneously be reduced as much, and the extra influence of these forces on modeling air-core vortices is called a "scale effect." Considerable research has been conducted on the magnitude of scale effects in modeling air core vortices and on developing techniques to compensate for such effects.

Techniques to Overcome Scale Effects

As with other flow phenomena subject to viscous scale effects, it is important that the model Reynolds number be sufficiently high. Both Anwar (1) and Daggett and Keulegan (4) give a minimum suggested Reynolds number of about 3×10^4, based on inlet flow and submergence or intake diameter, respectively. These investigators indicate that viscous scale effects on air core vortices are absent when the Reynolds number is above this limit, thereby implying that models satisfying this criteria can be operated at Froude-scaled flows. That this is a sufficient criteria has not been universally accepted, although an early study by Quick (24) suggests Froude scaling is adequate as long as the Reynolds number influence on vorticity generation is taken into account. A recent study by Dhillon (8) indicates good model-prototype agreement of vortex strength for a 1:20 scale model, satisfying the Reynolds number criteria, operated at Froude-scaled flow.

Testing at higher than Froude-scaled intake velocities (flows) to overcome scale effects of modeling air core vortices, including operating models up to prototype intake velocities, has been proposed by various investigators. All such tests maintain the geometrically scaled water depth, such that approach flow velocities are increased in the same proportion as the intake velocities. Haindl (13) and Jain et al. (19) reached such conclusions based on experiments using various sized circular tanks, while Denny (5), Iversen (18), Dicmas (9,10), Zajdlik (28), and Chang (3) have reached the same conclusion using various sizes of a particular pump intake geometry. Both types of studies show that the required increase in flow above Froude scaling is related to geometry and relative submergence, such that a constant factor for such flow increases has

not been found. A generalized approach to such flow increases and a technique to project results to the prototype have, however, been presented by Durgin and Hecker (11). Conclusions derived from such studies regarding the usefulness of testing at higher than Froude-scaled flow are based on a limited change in facility size, typically by a factor of about 3, although larger changes in scale, such as by a factor of 8, were achieved in some cases using rather small outlet diameters. Denny and Young (6), based on one observation of a prototype pump previously modeled at a 1:16 scale ratio, also concluded that using prototype velocities in models of such a scale ratio may be proper. For some scale ratios, the use of the equal intake velocity concept would seriously undermine the primary Froude-scaling criterion used to achieve proper approach flow patterns and the resulting circulation at the intake. A recent series of comparative model studies by Dhillon (8) indicates that use of prototype velocities in models produced highly exaggerated vortices, incompatible with prototype observations. Similar results were apparent in an earlier study by Linford (20). In some circumstances, increased wave action and turbulence at flow rates considerably higher than dictated by Froude scaling would tend to dissipate rather than increase vorticity.

The concept proposed by Jain et al. (19), of correcting the critical submergence predicted by the model to a relatively higher prototype value, has the inherent difficulty that ambient circulation may change with geometric differences at higher elevations, and such a technique would, therefore, be most applicable to two-dimensional geometries. In addition, other studies have shown that the required correction is a function of the basic geometry involved and of the mechanisms which generate vorticity. In particular, the influence of vorticity generated in the approach flow boundary layer, as mentioned by Hattersley (14) and Quick (25), is often not evaluated, whereas this mechanism is paramount in cases in which no boundary discontinuities exist.

A clear demonstration that the vortex air core characteristics are not affected by a meaningful change in the Weber number—all other factors (particularly the Reynolds number) being constant—is difficult to provide. To investigate this point, Daggett and Keulegan (4) and Jain et al. (19) have used fluids with various degrees of surface tension but constant viscosity. Daggett and Keulegan indicated that flow characteristics (discharge coefficient) varied little for a threefold variation in surface tension, although the relationship between the discharge coefficient and the vortex air core characteristics was questioned by Hughes (15), who also provided some rationale for the constant velocity modeling concept by considering the effects of surface tension on air core vortices. Jain et al., showed that the critical submergence for incipient air entrainment was essentially constant when the surface tension was reduced by about 50% for any given value of intake velocity, outlet diameter, and circulation (peripheral vane angle).

However, the range in Weber number given in both references comes mainly from changing the velocity and outlet diameter, either of which also changes the Reynolds number and, therefore, the vortex core. Isolation of Weber number effects would require plotting a vortex-related parameter versus the Weber number for constant values of circulation, geometry, and Reynolds number. Such a plot, however, would be difficult to generate due to the stated interrelationship between the Reynolds and Weber numbers. Also, it is not clear that the commonly

used intake velocity and diameter are the relevant parameters in the Weber number as compared, for example, with the maximum tangential velocity and the radius of the air core tip, respectively. Since these latter parameters may not scale directly, the difference between model and prototype Weber numbers may be difficult to determine. The recent analysis of Yildirim and Jain (27) indicates that the effect of surface tension on air core vortices may not be negligible, and, in view of the above comments, the question of surface tension effects is considered unresolved.

Irrespective of the relative influence of surface tension and viscous forces on the air core, it seems evident that vortices with air cores extending near to or into the inlet are more subject to scale effects than surface dimples. And corresponding subsurface swirl which can be made visible by injecting dye into the dimple. In a full-size installation, due to the absence of scale effects, the transition from a dimple and coherent subsurface swirl to an air core will be relatively more rapid with increasing swirl intensity compared with a model. And the initial condition of coherent swirl from the surface to the intake, a *dye core vortex*, would be a reasonably safe limiting condition for cases in which air core vortices would be detrimental. Based on experience at the Alden Research Laboratory, the delineation of dye core vortices as part of the normal model testing program is not a difficult task.

Given the small change in size used in most experiments to define the required flow increased above Froude-scaled flows, and considering the general neglect of such factors as the transient nature of vortices, the relative effect of boundary layer vorticity compared with other sources of vorticity, and the effects of ambient flow turbulence on vorticity, the concept of increased model flows above Froude scaling could be further examined. However, the past emphasis on quantifying scale effects of modeling air-core vortices is somewhat perplexing in that few final designs developed by using scale models have such strong vortices. Perhaps a more pertinent concern is the reliability of models as predictors of weak vortex activity. For example, does a model dye core filament and surface dimple at Froude-scaled flow represent an air core vortex in the prototype? This matter is addressed by comparing information on vortex activity from model studies with similar information for the prototype.

Model-Prototype Comparisons

The ultimate test of the ability of a reduced scale hydraulic model to predict free surface vortex characteristics is to compare model data to corresponding prototype observations. Because of the inherent difficulties with field observations and the influence of other factors besides scale effects which can contribute to differences between model and prototype vortices, a significant number of such comparisons are needed before general conclusions are warranted.

Included within the first category of inherent difficulties with field observations is a natural tendency for an observer to be impressed with the size and intensity of prototype vortices, and a belief may develop that they are more severe than those predicted by a hydraulic model. This belief may be partly due to the increased levels of surface turbulence and noise, which undoubtedly do not scale directly. The difference in time scale also makes it appear that the prototype vortex is more persistent, whereas the prototype may, in reality,

be viewed for a relatively shorter time period compared with the model. It is also difficult to distinguish between various strengths of vortices in the field, and the depth of the air core cannot usually be determined. Other factors which can contribute to model-prototype differences in vortex activity are as follows:

1. Insufficient attention to approach topography and boundary roughness in the model, (vorticity approaching the inlet has a first order effect on the resulting vortex strength).
2. Viscous scale effects on modeling appurtenant flow devices such as screens, baffles, and vortex suppressors.
3. "Minor" prototype topographic or structural change from that tested in the model. Typical are construction roads, quarries and spoil areas, remaining cofferdam cells, and wing walls.
4. Wind induced currents.
5. Ambient density stratification.

A number of model-prototype comparisons of vortex intensity have been published, and, as sufficient information was made available for an independent reevaluation, the following will be included in this summary. A study by Linford (20) using a 1:200 scale model of the Kariba Dam and powerhouse intakes showed that air core vortices were produced in the model when operated near prototype velocities, whereas no air core vortices were observed in the field. Reasonable comparison of vortex strength was achieved at near Froude-scaled flows. Nelson and Johnson (21) published photographs comparing model and prototype vortices at the upstream intakes of the Eisenhower and Snell navigation locks, and concluded that the prototype vortices were larger than in the model. Such a conclusion is not, however, obvious from the photographs since the exposure times were long enough to create streaks of white floating objects.

A similar comparison for the Demopolis lock, by Nelson and Johnson (21) and The U.S. Army Corps of Engineers (16) appeared to give a reasonable correlation between model and prototype, and this was confirmed by viewing a movie with comparable scenes of both the model and prototype vortices. These lock models were all operated at Froude-scaled flows. Recently, Dexter and Ziegler (7), using a 1:120 scale model of the Grand Coulee Third Power Plant, predicted weak vortex action at the penstock intakes whereas no vortices have been observed in the field. This comparison is based on model flows of about four and one half times the Froude-scaled flows which occurred during the prototype observations. However, there are questions as to whether the approach flow circulation was properly simulated and about the detail of the field observations, so the apparent exaggeration of the model vortices has not be confirmed.

To obtain the larger data base required for a reasonable analysis, questionnaires requesting specific information on projects for which model-prototype vortex activity was observed were sent to 65 organizations, both domestic and foreign, which have had occasion to be concerned with vortices from a design, testing, or operational perspective.

The returned questionnaires were reviewed to determine which provide useful model-prototype comparisons of vortex activity and information on prototype operating problems, or the known lack thereof, while vortices occurred. The

TABLE 1.—Model—Prototype Comparison

		Vor
Project and type (1)	Intake (2)	Model (3)
Bear Creek flood control outlet (TVA)	single sluice gate, cylindrical tower	dimple ~ 0.1 ft diameter, $L_r = 1/20$ $F_r = 1$
Bear Swamp pumped storage, upper structure (New England Power Company)	single 40 ft diameter open intake; $V = 9$ ft/s, $S = 50$ ft	intermittent, some pulling air bubbles at $F_r = 1$, $L_r = 1/50$
Cabin Creek pumped storage; upper intake (Public Service of Colorado)	single covered intake, $V = 4$ ft/s, $S = 36$ ft	slow circulation, $F_r = 1$, $L_r = 1/100$
Dardanelle Lock (USC of E)	upper; multiport side intake $V \sim 2.5$ ft/s, $S_e = 24$ ft	none, $F_r = 1$, $L_r = 1/25$
Demopolis Lock (USC of E)	multiport (8) at upper gate sill, $V \approx 13$ ft/s (max), $S = 25$ ft	strong vortices, no description, $L_r = 1/33$, $F_r = 1$
Dover Dam (USC of E)	18 adjacent sluices, $0 < S < 54$ ft, $0 < V < 47$ ft/s	none reported
Eisenhower Lock (USC of E)	upper gate	swirl, $F_r = 1$, $L_r = 1/24$
Ffestiniog pumped storage; lower reservoir structure (CEGB)	four horizontal intakes, 32 ft × 22 ft, $S = 40$ ft, $V = 1.5$ ft/s	no vortices for $F_r = 1$ (air drawing vortices for $V_m = 0.9\ V_p$) $L_r = 1/60$
Foyers pumped storage, upper reservoir structure (Scotland Hydro Board)	four adjacent openings, total 68 ft × 24 ft, $S_e = 23$ ft, $V = 4.5$ ft/s (1.4 m/s)	no dimple at $F_r = 1$; deep depression at $2 < F_r < 4$, $L_r = 1/36$
Grand Coulee Third Power Plant (USBR)	six adjacent penstock intakes, each 33 ft × 45 ft, $V = 20$ ft/s, $S = 180$ ft	dye core vortices no air entrainment, $L_r = 1/120$, $F_m = 3.5\ F_p$
Heart Butte Dam (USBR) spillway	morning glory spillway, $V \approx 3$ ft/s, $0 < S < 54$ ft	negligible, $L_r = 1/22$, $F_r = 1$; none reported
Jocassee pumped storage, upper structure (Duke Power Company)	two tower intakes, $V = 6.5$ ft/s, $S_{\mathbb{C}} = 30$ ft	small vortices between gate guide piers, $L_r = 1/50$, $F_r = 1$

of Vortex Intensities

tices

Prototype (4)	Operation (5)	Comments and Key[a] (6)
~2.5 ft diameter depression.	no problems	good correlation of type and size (b)
intermittent, sometimes 3 ft diameter, pulling air and audible	—	prototype vortices seem more frequent and stable, model retested (comparison based on $F_r = 1$); see Fig. 1(*a*)
no swirls, almost no motion	—	concern for ice entrainment led to conservative design (b)
none	no problems	vortex free design developed using model (2)
two audible vortices, up to 8 ft diameter intermittent to continuous	air entrainment, possibly increased lock chamber turbulence, also hazardous	model study after prototype problems, checked initial design (16,21) (b)
none at normal submergence	—	(b)
swirl with depression	—	prototype vortex seemed larger (21) (a)
no vortex formation	—	near equal velocity exaggerated vortex in model (conditions at $F_r = 1$ used in Table 2) (b)
surface dimple at $S_r = 20$ ft	no problems	good comparison at model velocities somewhat more than Froude scale (b)
no vortices	—	comparison based on Units 19, 20, and 21; more severe model vortices may be caused by inadequate inflow simulation (c)
surface turbulence, no vortices	—	comparison based on final design with six radial crest piers to minimize vortices (b)
small, 1 in.–2 in., transient vortices	no problems	(2)

TABLE 1.—

(1)	(2)	(3)
Kariba Hydroelectric scheme (Zimbabwe and Zambia)	six adjacent intakes in sloping right embankment, each 54 ft × 32 ft, $V = 3$ ft/s, 50 ft $< S_i <$ 130 ft	borderline vortex at $F_r = 1$; air core at $F_r > 3$, $L_r = 1/120$
Ludington pumped storage, upper structure (Consumers Power)	six adequate horizontal inlets; each ~30 ft × 35 ft, $V = 11$ ft/s, $S_{\mathbb{Q}} = 36$ ft	minimal swirls with dimples $L_r = 1/122$, $F_r = 1$
Muddy Run pumped storage and upper structures (Philadelphia Electric Company)	four tower intakes, $V = 4$ ft/s, $S_q = 23$ ft	vortices (no air) above elevation 470; air entrainment at elevation 466 or less $L_r = 1/35$ and $1/141$, $F_r = 1$
Northfield pumped storage, upper structure (Northeast Utilities)	single horizontal inlet at end of channel, $V = 5$ ft/s, $S_{\mathbb{Q}} = 69$ ft	negligible, $L_r = 1/46$, $F_r = 1$
Oroville Dam diversion tunnels (California Department of Water Resources)	two adjacent 35-ft diameter tunnels near reservoir bottom, $0 < S < 690$ ft, $0 < V < 75$ ft/s	strong, noisy, air core, sucked scaled trees, persistent at $S < 100$ ft; transient at $S > 100$ ft, $L_r = 1/55$, $F_r = 1$
Ramaganga Project auxiliary intake (India)	shaft, 18 ft diameter, $14 < S < 47$ ft, $V = 11.5$ ft/s	air entraining, stable at $S \approx 23$ ft, $L_r = 1/40$
Reacteurs G2–G3 Marcoule cooling water intake (EDF)	three openings in sloping embankment, each $V \approx 5$ ft/s, $S = 14$ ft	large noisy aerated vortex. $L_r = 1/25$, $F_m = 2.5\ F_p$
Snell Lock (USC of E)	upper gate	swirl, $F_r = 1$, $L_r = 1/24$
Taum Sauk pumped storage, upper reservoir intake (Union Electric Company)	single shaft, expands to $D_e = 46$ ft, $V = 4$ ft/s, $S = 20$ ft	air entraining vortex at elevation 1,508 ft; less severe at higher elevations, $L_r = 1/36$; $F_r = 1$
Treasure Island Pumping Station (USC of E)	two vertical suction columns, $V = 2.4$ ft/s, $S = 2.5$ ft	air entraining vortex, $L_r = 1/12$, $F_r = 1$

[a]See Table 2.

Note: 1 ft = 0.305 m; 1 in. = 25.4 mm; 1 ft^3 = 0.0283 m^3.

Continued

(4)	(5)	(6)
swirl with white water	—	near equal velocities exaggerated vortex in model (comparison near $F_r = 1$ with Units 5 and 6 and reservoir elevation 1,549 ft (20) used in Table 2) (b)
swirls (initially had 3-ft diameter vortices during project start-up)	no problems (including initial start-up)	perforated wall used to dissipate two strong model vortices; initial vortices in prototype not observed since start-up (a)
vortices as level approaches elevation 470 ft	objectionable turbine noise at extreme low water, < elevation 470 (operate at half flow)	model predictions based on submergence; prototype structure 10 ft lower than tested (b)
minor swirls	—	(b)
persistent, strong, audible air core for 100 ft < S < 230 ft, passed trees, surface diameter = 30 ft	no problems	prototype vortices seemed more persistent at higher submergences; otherwise good agreement (a)
strong audible vortices at uncontrolled flow	vibration of adjacent hill	(b)
large noisy aerated vortex	blocked racks due to suction of debris	model tests after prototype problems; remedial design developed using model with satisfactory prototype results (b)
vortex with depressed core	—	prototype vortex seemed larger (21) (a)
air entraining vortex at elevation 1,515 ft or less	run turbine at 1/2 flow at low surface elevation to avoid rough operation	plan was to use floating grid in prototype, if necessary (b)
air entraining vortex, core diameter = 8 in.	vibration and adverse effects on machinery	good model to prototype comparison at Froude scale flow; model built to develop vortex suppressor (floating grid) (b)

information on operating problems was considered important since it is relevant to the determination of what expenses are warranted to achieve vortex-free designs.

Unfortunately, a large portion of the returned questionnaires were not useful for a variety of reasons, including provision of information on a model study only, use of imprecise or contradictory terms, or generally insufficient information. Follow-up inquiries were made regarding projects of interest and other projects previously referenced in various publications. The numerous reports, photographs, and other material collected are not referenced directly herein. The information on some projects is considerably more detailed, whereas the filled-in questionnaire was relied on for other cases. It is consequently important in this review to concentrate on basic trends rather than detailed observations. Comparisons in which the final model design and the corresponding prototype had only weak swirls and no vortices were considered meaningful in that they showed field conditions were not worse than expected.

Projects for which an adequate comparison between model and field vortices exist are listed in Table 1, which also gives a basic description of the intakes,

TABLE 2.—Number of Projects with Indicated Model-Prototype Vortex Comparison

(1)	$F_r = 1$ (2)	$2 < F_r < 4.5$ (3)	$V_m \cong V_p$ (4)	Total (5)
(a) Prototype vortices stronger or more persistent than in model.	5	0	0	5
(b) Model and prototype vortices essentially equal.	14	2	0	16
(c) Prototype vortices weaker or less frequent than in model.	0	1	0[a]	1
				22

[a]See Ffestiniog and Kariba, Table 1, and Dhillon (9).

information regarding the model tests, and any additional pertinent comments. Whenever possible, the wording is that used on the material supplied, although some changes or interpretations were made for consistency and to concisely give the general sense of the comparison. Table 1 includes various types of intakes, e.g., for navigation locks, pump intakes, or screen wells, outlet control structures and sluices, specialty intakes for diversion tunnels and water-supply-regulating tanks, cooling water intakes for steam electric stations, and a considerable number of pumped storage intakes.

A basic summary of how many projects fit the case of prototype vortices stronger than in the model (a); essentially comparable vortices (b); or vortices less intense in the prototype than in the model (c), is given in Table 2. Since such a comparison is most meaningful when related to any model testing techniques to overcome scale effects, this summary is provided according to the scaled flow rate used in the model tests. The major observation apparent from Table 2 is that most modeled vortices compared reasonably well with observed prototype vortices. Five projects seem to have stronger or more persistent prototype vortices, and one case of less severe prototype vortices was reported.

The five projects in category (a) were all tested at Froude-scaled flows and had Reynolds numbers equal to or greater than the recommended minimum values given by Anwar (1) and Daggett and Keulegan (4). Since these projects had occasional air core vortices, some scale effect for Froude models of air core vortices may be indicated. That this is a weak conclusion is indicated by the following comments. Two of the five projects are the previously mentioned Eisenhower and Snell lock intakes (21) for which no conclusive comparison could be made. A third case refers to the apparently more persistent prototype vortices at the Oroville Dam diversion tunnels at high submergences during a flood. However, few model observations were made on vortex activity at various reservoir levels, possibly because no operational problems were expected during the diversion phase, and a comparison of persistence is not based on detailed data.

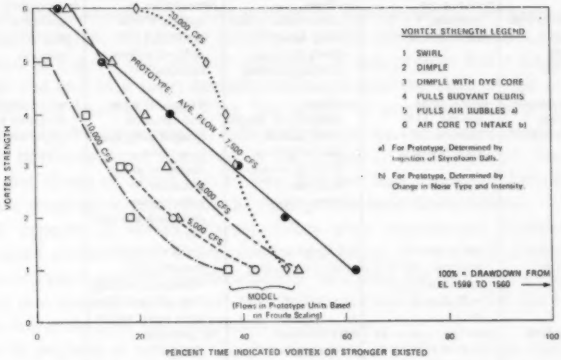

FIG. 1.—Model to Prototype Comparison of Vortex Persistance at Bear Swamp Project (1 cfs = 0.0283 m^3/s)

At the Ludington upper reservoir intake, vortex activity not predicted by the model occurred only during initial operation of two out of six units. No coherent vortices have been observed in the field for years subsequent to the initial project start-up.

This case raises an interesting point regarding scale selection and the minimum Reynolds number required to avoid scale effects. Without the perforated wall of the final design, two strong and persistent air drawing vortices existed in the model. Suppression of these vortices with the perforated wall, or with any other similar technique, involves dissipating angular momentum by form loss, as well as reorienting flow patterns. The former factor may be dependent on the Reynolds number based on the velocity and size associated with the energy dissipating element. It is possible that excess energy and vortex dissipation occurs in small-scale models in which vortex suppressors are used. When selecting a model scale ratio and when testing vortex suppressors, this should be a consideration as should the withdrawal Reynolds number.

The last case listed within category (a) is the Bear Swamp upper reservoir

TABLE 3.—Additional Projects with Vortices for Which Operation Information is Known

Project and Type (1)	Intake (2)	Prototype vortex (3)	Operation (4)	Comments (5)
Beach City Dam flood control outlet (USC of E)	tower in open reservoir, six adjacent gated openings, each 7 ft × 15 ft, $0 < S_q <$ 40 ft, V varies with head	1 ft–3 ft diameter vortex at 2,200 ft^2/s	for largest vortex, soft rumbling, very little vibration	occurs at particular gate opening
Beas Dam at Pong (India)	single bulkhead shaft for tunnel	no direct observation, inferred from model study	dislocation and damage to grating	see Dhillon (8)
Centrale hydroelectrique de Caderousse (Compagnie Nationale du Rhone)	intake to six turbines, $V = 5$ ft/s, $S = 26$ ft	no direct observation, model study showed intermittent air drawing vortices	irregularities in approach flow resulting in reduced turbine efficiency	large probability that problems are due to prototype vortices
Centrale Thermique de Cordemais, pump intake (EDF)	vertical pump column, 16 ft diameter, $V = 3.3$ ft/s, $S = 8.2$ ft	no direct observation, model study showed intermittent air drawing vortices at minimum submergence	considerable noise and vibration (judged dangerous to support structure) at minimum submergence, depriming and unit trip	large probability that problems are due to prototype vortices
Enid Dam flood control outlet (USC of E)	tower in open reservoir, two 8-ft × 16-ft intakes, $V = 30$ ft/s, $S = 43$ ft	3-ft diameter near full gate opening	reduced efficiency, possible gate vibrations, swirling flow affects stilling basin performance	—
Glen Canyon Dam (USBR)	open approach to 24 ft × 14 ft bellmouth, $V = 9$ ft/s, 23 ft $< S <$ 241 ft	near minimum submergence, two transient vortices within intake, 1 ft diameter, 6 ft core depth	No problems reported	—
Kori Nuclear Station Cooling Water Pump (Korea Electric Company)	four vertical pump columns, bell diameter = 7.5 ft, $V = 8.2$ ft/s, $S =$ 15 ft	no direct observation, inferred from model study	excessive noise and vibration, contributed to gearbox failure	large probability that problems due to prototype vortices
Mohicanville Dam flood control outlet (USC of E)	tower in short forebay, three 7 ft × 12 ft gates, no conduit, $0 < S_q <$ 25 ft, V varies with head	small eddy near right gate	slight vibration	occurs at particular gate opening and submergence
Nimbus Dam power intake (USBR)	open approach to 41 ft × 15 ft powerplant intake in dam face, $V =$ 3.6 ft/s, $S_q = 10$ ft	5-ft diameter air-entraining vortex	rough operation of turbines during vortex	raft used to dissipate vortices, satisfactory operation achieved
St. Anthony Falls Lock (USC of E)	multiport (4) in upper gate sill, $V = 6$ ft/s maximum, S = 14 ft	strong air entraining, audible	hazardous flow condition, resulted in fatality	subsequent to field problems, model study was initiated; no comparison with original design

TABLE 3.—*Continued*

(1)	(2)	(3)	(4)	(5)
Shadehill Dam Spillway (USBR)	Morning Glory Spillway $V \approx 3$ ft/s, $0 < S < 40$ ft	2-ft diameter, audible vortex; pulled in ice sheets and 50 gal drums	no apparent ill effects on structures or operation, no vibrations	similar to Heart Butte Dam Spillway, but Shadehill has shorter vertical piers and no outlet structure incorporated in spillway

Note: 1 ft = 0.305 m, 1 ft/s = 0.305 m/s; 1 ft^3/s = 0.0283 m^3/s; 1 gallon = 378 liters.

intake, for which considerable model and prototype data were recently made available by Castro (2), including the percent of time (persistence) that vortices of various strengths occurred. The method of differentiating between vortices of varying strengths, which was developed at the Alden Research Laboratory, is indicated in Fig. 1. The vertical penstock of this project has a single round opening at the end of a short approach channel near the edge of the reservoir. Basic results of carefully retesting the model, in conjunction with prototype observations by the same person, indicated that prototype vortices were stronger and more persistent than occurred in the model at Froude-scaled flows. Fig. 1 shows that flows of about two or two and one half times the Froude-scaled flows were required to reproduce the field persistence observations.

Not all aspects of vortex characteristics were reproduced, however, with the increased model flow. For example, the trend of vortex intensity versus reservoir elevation was not identical despite modeling the entire upper reservoir, indicating that factors such as relative differences in friction for the reservoir flow may have changed the generation of vorticity.

Of the 16 projects in category (b) showing good model-prototype comparison, two compared well when the model flows were increased from 2–4 times Froude scale, and the remaining 14 comparisons all being based on Froude-scaled flows. Of the latter group, 11 concern good comparison of negligible or weak vortices, a significant finding in that negligible scale effect for weak swirls or dimples is implied. The remaining three cases concern good comparisons of air core vortices, and these cases are not as instructive in that any scale effects would dictate that an air core model vortex certainly represents an air core prototype vortex.

The single case in category (c) is the previously discussed tentative conclusion regarding the Grand Coulee Third Power Plant (7).

In general, final intake designs which were developed from Froude-scale model tests to be vortex-free were indeed vortex-free in the prototype, and those that had weak vortices in the model had weak prototype vortices. In particular, there is no reported case in which a negligible model vortex corresponded to a sufficiently strong prototype vortex that it produced operating problems. The operating problems to be discussed below were either predicted by the model or were for projects for which no initial model study was conducted.

Prototype Operating Problems

In addition to the projects in Table 1 for which information on operating

conditions related to vortices is known, information on this topic was received on projects which lacked model-prototype comparison of vortices. These various additional projects and a brief description of the intake types and the operating problems, or lack thereof, are listed in Table 3. A summary of project operating conditions related to vortices, from both Tables 1 and 3, is provided in Table 4.

It does seem that prototype vortices have produced sufficient operating problems that reasonable measures should be taken to avoid strong vortices. Of the 20 projects which are known to have (or have had) reasonable sized vortices, 14 have experienced the various types of problems listed in Table 4. A considerable amount of operating difficulty is associated with prime movers, particularly for "wet-pit" pumps. Pumped storage projects for which air core vortices were observed in the model at low water levels produced unacceptable turbine operation in the field at corresponding conditions, thus requiring flow reductions to avoid the vortex condition (e.g., Taum Sauk and Muddy Run). Air entrainment may also be a problem in navigation locks in which the release

TABLE 4.—Summary of Projects with Information Regarding Effect of Vortices on Operation

A. Prototype Operating Problems[a] (1)	Number (2)
Vortex reduced flow, or flow reduction required to avoid vortex induced problems	2
Vibration (structure or pump)	5
Other pump or turbine operating problems (i.e., rough operation, objectionable noise, lower efficiency)	2
Clogging of and damage to trashracks	2
Detrimental effects on stilling basin performance	1
Hazard to personnel	2
No operating problems with vortices	6

[a]For each project, the major problem, if any, is selected and no project is listed more than once.

of air in the chamber leads to excess turbulence. Also to be noted is that six projects have experienced no problems while vortices occurred.

Summary and Conclusion

The possible occurrence of vortices has generally defied analytic prediction, and experiments, usually scale model tests, are needed to ensure vortex-free designs. Such scale models should have Weber and Reynolds numbers above published critical values to minimize scale effects (1,4).

To help clarify apparently contradictory information previously published regarding scale effects of modeling free surface vortices, comparisons were made between model and prototype vortex characteristics of various intake structures. Since scale effects axiomatically have only a secondary influence, a large change in scale was considered desirable to make any such effects

more obvious. The projects compared herein cannot encompass all available information, but together with other previously published data, provide enough information to reach the following conclusions:

1. Sufficient operating problems due to vortices have occurred to warrant reasonable efforts to minimize vortices at intakes of various types.
2. Hydraulic models operated at Froude-scaled flows to predict vortex intensity have some scale effects when simulating air core vortices. Compensation for these scale effects is possible by some increase in model flows above Froude-scaled values, but large increases are not justified and may distort the approach flow pattern. The concept of equal velocity modeling seems relevant only to large models for which small flow increases yield prototype inlet velocities.
3. Negligible scale effect was evident in models with Froude-scaled flows which predicted that only swirls and surface dimples, but no air core vortices, would occur in the prototype. A possible exception involved a vortex dissipator itself subject to scale effects.

In addition, the following recommendations are made:

1. Considerable attention must be given to scaling the approach topography and boundary roughness so that the vorticity flux approaching the intake is correctly modeled. The difference in Reynolds number and friction factors between model and prototype boundary flow should, therefore, be evaluated.
2. Model tests should include a careful delineation of various vortex types, including dimples and dye cores, and notation should be made of vortex type, location, and, in particular, persistence.
3. A dye core from the surface to the inlet is a reasonable demarcation between acceptable and unacceptable vortex conditions since this represents the initiation of coherent subsurface swirl. Since modeling such a dye core and surface dimple involves essentially no scale effect, models can be operated at Froude flows to detect such flow patterns. Dye cores should be present for less than 50% of the time.
4. When vortex suppression devices are used in scale models, consideration should be given to possible excessive energy dissipation due to low model Reynolds numbers based on the characteristic velocity and dimension of the dissipator.

Acknowledgments

This effort was initiated to assist in meeting the objectives of the ASCE Task Committee on Intake Vortices. The information and comments supplied by H. O. Anwar and G. A. J. Young of the committee are appreciated. Considerable assistance and information was supplied by a number of organizations listed in Table 1, and the help of D. L. King of the U.S. Bureau of Reclamation, E. B. Pickett of the U.S. Corps of Engineers, and Messrs. J. Chevalier and L. Pugnet of Electricité de France are especially acknowledged.

Appendix I.—References

1. Anwar, H. O., Weller, J. A., and Amphlett, M. B., "Similarity of Free Vortex at

Horizontal Intake," *International Association of Hydraulic Research, Journal of Hydraulic Research*, Vol. 16, No. 2, 1978, pp. 95–105.
2. Castro, P., "An Investigation of Scale Effects in Vortex Modeling by Model to Prototype Comparison," thesis presented to the Mechanical Engineering Department, Worcester Polytechnic Institute, at Worcester, Mass., 1979, in partial fulfillment of the requirements for the Master's Degree.
3. Chang, E., "Scaling Laws for Air-Entraining Vortices," *British Hydromechanic Research Association Report RR1519*, Jan., 1979.
4. Daggett, L. L., and Keulegan, G. H., "Similitude in Free-Surface Vortex Formations," ASCE, *Journal of the Hydraulics Division*, Vol. 100, No. HY11, Nov., 1974, pp. 1565–1581.
5. Denny, D. F., "An Experimental Study of Air-Entraining Vortices in Pump Sumps," *Journal of The Institution of Mechanical Engineers*, London, England, Vol. 170, No. 2, 1956, pp. 106–116.
6. Denny, D. F., and Young, G. A. J., "The Prevention of Vortices and Swirls at Intakes," *Proceedings of the Seventh International Association of Hydraulic Research Congress, Paper No. C-1*, Lisbon, Portugal, 1957.
7. Dexter, R. B., and Zeigler, E. R., "Penstock Intake Vortex and Related Turbine Operation Model Studies," *Proceedings of the ASCE/ASME/International Association of Hydraulic Research Joint Symposium on Design and Operation of Fluid Machinery*, Colorado State University, Fort Collins, Colo., Vol. 1, June, 1978, pp. 425–436.
8. Dhillon, G. S., "Vortex Formation at Pipe Intakes and Its Prediction—A Status Report," *Report No. HY/R/4/79*, Irrigation and Power Research Institute, Punjab, India, July, 1979.
9. Dicmas, J. L., "Development of an Optimum Sump Design for Propeller and Mixed-Flow Pumps," *ASME Paper 67-FE-26*, presented at the Fluids Engineering Conference, Chicago, Ill., May, 1967.
10. Dicmas, J. L., "Effect of Intake Structure Modifications on the Hydraulic Performance of a Mixed Flow Pump," *Proceedings of the ASCE/ASME/International Association of Hydraulic Research Joint Symposium on Design and Operation of Fluid Machinery*, Colorado State University, Fort Collins, Colo., Vol. 1, June, 1978, pp. 403–412.
11. Durgin, W. W., and Hecker, G. E., "The Modeling of Vortices at Intake Structures," *Proceedings of the ASCE/ASME/International Association for Hydraulic Research Joint Symposium on Design and Operation of Fluid Machinery*, Colorado State University, Fort Collins, Colo., June, 1978, Vol. 1, pp. 381–391.
12. Gordon, J. L., "Vortices at Intakes," *Water Power*, Vol. 22, No. 4, Apr., 1970, pp. 137–138.
13. Haindl, K., "Contribution to Air Entrainment by a Vortex," *Eighth Congress of IAHR*, Montreal, Canada, 1959, *Paper 16-D*.
14. Hattersley, R. T., "Hydraulic Design of Pump Intakes," *Journal of the Hydraulics Division*, ASCE, Vol. 91, No. HY2, Mar., 1965, pp. 223–249.
15. Hughes, R. L., "Discussion of 'Similitude in Free-Surface Vortex Formation,' by Daggett and Keulegan," *Journal of the Hydraulics Division*, ASCE, Vol. 101, No. HY9, Sept., 1975, pp. 1287–1284.
16. "Intake Manifolds for Demopolis and Warrior Locks, Tombigbee River, Alabama, and Jim Woodruff Lock, Apalachicola River, Florida—Hydraulic Model Investigation," *Hydraulic Laboratory Report No. 70*, U.S. Army Corps of Engineers, Apr., 1961.
17. *Hydraulic Institute Standards for Centrifugal, Rotary and Reciprocating Pumps*, 13th ed., Hydraulic Institute, Cleveland, Ohio, 1975.
18. Iversen, H. W., "Studies of Submergence Requirements of High Specific-Speed Pumps," *Transactions*, ASME, Vol. 75, No. 4, May, 1953, pp. 635–641.
19. Jain, A. K., Raju, K. G. R., and Garde, R. J., "Vortex Formation at Vertical Pipe Intakes," *Journal of the Hydraulics Division*, ASCE, Vol. 104, No. HY10, Oct., 1978, pp. 1429–1445.
20. Linford, A., "The Application of Models to Hydraulic Engineering, Part 2: Air-Entraining Vortices," *Water and Water Engineering*, Mar., 1965, pp. 105–110.
21. Nelson, M. E., and Johnson, H. J., "Vortex Problems at Intakes for Lock Hydraulic Systems," *Proceedings of the Eighth Congress of International Association for Hydraulic Research*, Montreal, Canada, Aug., 1959, *Paper 12-B*.
22. Pennino, B. J., and Hecker, G. E., "A Synthesis of Model Data for Pumped Storage

Intakes," D. Webb and C. Papadakis, eds., *Pump Turbine Schemes: Planning, Design, and Operation, Proceedings of the Joint ASME/CSME Applied Mechanics, Fluids Engineering and Bioengineering Conference*, June, 1979.
23. Prosser, M. J., *The Hydraulic Design of Pump Sumps and Intakes, Report No. ISBN 0-86017-027-6*, British Hydromechanics Research Association/Construction Industry Research and Information Association, July, 1977.
24. Quick, M. C., "Scale Relationships Between Geometrically Similar Free Spiral Vortices," *Civil Engineering and Public Works Review*, Part 1, Sept., 1962, p. 1135 and Part 2, Oct., 1962, p. 1319.
25. Quick, M. C., "Efficiency of Air-Entraining Vortex Formation at Water Intakes," *Journal of the Hydraulics Division*, ASCE, Vol. 96, No. HY7, July, 1970, pp. 1403–1416.
26. Reddy, Y. R., and Pickford, J. B., Vortices at Intakes in Conventional Sumps," *Water Power*, Vol. 24, No. 3, Mar., 1972, pp. 108–109.
27. Yildirim, N., and Jain, S. C., "Surface Tension Effect on Profile of a Free Vortex," *Journal of the Hydraulics Division*, ASCE, Vol. 107, No. HY1, Jan., 1981, pp. 132–136.
28. Zajdlik, M., "New Checking Mode of Model Parameters for Vortex Formation in Pump Tanks," *International Association of Hydraulics Research, 17th Congress*, Baden-Baden, West Germany, Vol. 5, Aug., 1977, pp. 379–386.

Appendix II.—Notation

The following symbols are used in this paper:

F_m = Froude number in model;
F_p = Froude number in prototype;
F_r = Froude number ratio, model to prototype;
L_r = length ratio, model to prototype;
S = submergence (if available, minimum is given);
$S_{\mathcal{C}}$ = submergence to center line of opening (if available, minimum is given);
S_i = submergence to invert (if available, minimum is given);
S_s = submergence to soffit (if available, minimum is given);
V = average intake velocity;
V_m = average model intake velocity; and
V_p = average prototype intake velocity.

TECHNICAL NOTES

Note.—Discussion open until March 1, 1982. To extend the closing date one month, a written request must be filed with the Manager of Technical and Professional Publications, ASCE. This paper is part of the Journal of the Hydraulics Division, Proceedings of the American Society of Civil Engineers, ©ASCE, Vol. 107, No. HY10, October, 1981.

Technical Notes

To provide a place within ASCE for publication of technical ideas that have not advanced, as yet, to the point where they warrant publication as a Proceedings paper in a *Journal*, the publication of Technical Notes was authorized by the Board of Direction on October 16–18, 1967, under the following guidelines:

1. An original manuscript and two copies are to be submitted to the Manager of Technical and Professional Publications, ASCE, 345 East 47th Street, New York, N.Y., 10017, along with a request by the author that it be considered as a Technical Note.
2. The two copies will be sent to an appropriate Technical Division or Council for review.
3. If the Division or Council approves the contribution for publication, it shall be returned to Society Headquarters with appropriate comments.
4. The technical publications staff will prepare the material for use in the earliest possible issue of the *Journal*, after proper coordination with the author.
5. Each Technical Note is not to exceed 4 pages in the *Journal*. As an approximation, each full manuscript page of text, tables, or figures is the equivalent of one-half a *Journal* page.
6. The Technical Notes will be grouped in a special section of each *Journal*.
7. Information retrieval abstracts and key words will be unnecessary for Technical Notes.
8. The final date on which a Discussion should reach the Society is given as a footnote with each Technical Note.
9. Technical Notes will not be included in *Transactions*.
10. Technical Notes will be included in ASCE's annual and cumulative subject and author indexes.

The manuscripts for Technical Notes must meet the following requirements:

1. Titles must have a length not exceeding 50 characters and spaces.
2. The author's full name, Society membership grade, and a footnote reference stating present employment must appear on the first page of the manuscript. Authors need not be Society members.
3. The manuscript is to be submitted as an original copy (with two duplicates) that is typed double-spaced on one side of 8-1/2-in. (220-mm) by 11-in. (280-mm) white bond paper.
4. All mathematics must be typewritten and special symbols must be properly identified. The letter symbols used must be defined where they first appear, in figures or text, and arranged alphabetically in an Appendix.—Notation.
5. Standard definitions and symbols must be used. Reference must be made to the lists published by the American National Standards Institute and to the *Authors' Guide to the Publications of ASCE*.
6. Tables must be typed double-spaced (an original ribbon copy and two duplicate copies) on one side of 8-1/2-in. (220-mm) by 11-in. (280-mm) paper. An explanation of each table must appear in the text.
7. Figures must be drawn in black ink on one side of 8-1/2-in. (220-mm) by 11-in. (280-mm) paper. Because figures will be reproduced with a width of between 3 in. (76 mm) to 4-1/2 in. (110 mm), the lettering must be large enough to be legible at this width. Photographs must be submitted as glossy prints. Explanations and descriptions must be made within the text for each figure.
8. References cited in text must be typed at the end of the Technical Note in alphabetical order in an Appendix.—References.
9. Dual units, i.e., U.S. Customary followed by SI (International System) units in parentheses, should be used throughout the paper.

Uncertainties in Water Distribution Systems

By Derrick A. Clarke,[1] Edward A. McBean,[2] and S. A. Al-Nassri,[3] M. ASCE

Introduction

Water distribution networks require a major share of the capital investment of water works. As a result, over the years the analysis of water distribution networks has been the interest of many researchers. While these activities resulted in the development of general computer programs which can handle the analysis of a large network in a matter of seconds at nominal cost, in contrast, little work has been done on the uncertainties associated with the analysis of water distribution networks. Hudson (6) states that

> Unfortunately the design of water distribution systems, based on poor data, looks just as good in the computer printout as a design based on the most accurate data that can be obtained.

As a means of examining the uncertainties, the objective herein is to examine the sensitivity of the pressure difference, ΔP, in the analysis of a distribution network as a result of uncertainties in the parameters involved in the basic equation describing the flow. The First Order Analysis method developed for evaluating the pressure sensitivity is used to assess the required pressure measurement accuracy for field tests.

Development of Equations

Hazen-William's formula can be rearranged to express ΔP in terms of all the other parameters as:

$$\Delta P = \frac{\lambda_E \gamma Q^n L}{C_{HW}^n D^{2.63n}} \quad \ldots\ldots\ldots\ldots\ldots\ldots\ldots\ldots\ldots\ldots\ldots\ldots\ldots\ldots\ldots\ldots (1)$$

in which λ_E = the model error term which is introduced to account for additional pressure differences due to fittings within the network; γ = the specific weight;

[1]Engr. Jamaican Water Authority, Jamaica.
[2]Assoc. Prof., Civ. Engrg., Univ. of Waterloo, Ontario, Canada, N2L 3G1.
[3]Visiting Prof., Civ. Engrg., Univ. of Waterloo, Canada; and Vice-Pres., Univ. of Tech., Baghdad, Iraq.

Note.—Discussion open until March 1, 1982. To extend the closing date one month, a written request must be filed with the Manager of Technical and Professional Publications, ASCE. Manuscript was submitted for review for possible publication on January 21, 1981. This paper is part of the Journal of the Hydraulics Division, Proceedings of the American Society of Civil Engineers, ©ASCE, Vol. 107, No. HY10, October, 1981. ISSN 0044-796X/81/0010-1263/$01.00.

Q = the flow; n = the reciprocal of the exponent of the hydraulic slope; L = the length; C_{HW} = the Hazen-William's coefficient; and D = the internal diameter (ID). Noteworthy is that Hazen-William's equation has been utilized as the fundamental equation describing the flow in a pipe. The arguments and conclusions to follow are equally applicable to any other equivalent formula. The application of first order analysis to Eq. 1 gives (see Refs. 3 or 10 for further details)

$$\overline{\Delta P} = \frac{\gamma\bar{\lambda}\bar{Q}^{\bar{n}}\bar{L}}{\bar{C}_{HW}^{\bar{n}} D^{2.63\bar{n}}} \quad \ldots \quad (2)$$

and $$\Omega^2_{\Delta P} = \Omega^2_{\lambda E} + (\bar{n})^2\Omega^2_Q + \Omega^2_L + (\bar{n})^2\Omega^2_{C_{HW}} + 6.9169(\bar{n})^2\Omega^2_D$$

$$+ (\log_e \bar{Q} - \log_e \bar{C}_{HW} - \log_e \bar{D})^2(\bar{n})^2\Omega^2_n$$

$$- (\bar{n})^2\rho_{C_{HW},Q}\Omega_{C_{HW}}\Omega_Q + 2.63(\bar{n})^2\rho_{C_{HW},D}\Omega_{C_{HW}}\Omega_D - 2.63(\bar{n})^2\rho_{D,Q}\Omega_D\Omega_Q \quad \ldots \quad (3)$$

in which the bar (¯) in Eqs. 2 and 3 = the mean value of the parameter; Ω = the coefficient of variation of the parameter; and ρ_{ij} = the coefficient of correlation between the parameters noted as subscripts.

The last three terms in Eq. 3 account for correlation between the parameters C_{HW} and Q, C_{HW} and D, and D and Q, respectively. Therefore, if the mean and variance of the parameters in the basic equation describing the flow in each pipe and the model error are known, Eqs. 2 and 3 can be used to evaluate the mean and coefficient of variation of the pressure differential ΔP.

Application of First Order Analysis to Sample Network

In order to illustrate the application of the methodology of first order analysis (FOA), a simple, 11-pipe network is considered. The sensitivity of pressure differences, ΔP, for a specific pipe in the network will be examined, as a result of uncertainties in both the parameters involved and the mathematical model.

Consider, e.g., one pipe of the 11-pipe network, 305 m in length and 304.8 mm in diameter. For a pipe that has been in service for 20 yr, the mean value of C_{HW} is 105, and the standard deviation, $\sigma_{C_{HW}}$, is 10, as obtained with the aid of Hudson's data (5).

After 20 yr in service the diameters of the pipes are subject to change due to the deposition of materials or corrosion. The change cannot be easily predicted, as it is very much a function of the quality of the water surveyed, the filtering efficiency in the water treatment facility, and the design of the network system. However, from the writers' experience, a 5% change is reasonably normal, which will give for the pipe under consideration a standard deviation σ_D of 15 mm.

The variation in the inverse of the hydraulic slope of the Hazen-Williams formula (Eq. 1) is assumed, for the present problem, within the range 1.82–1.88, with a mean value of 1.85. [This assumption is on the conservative side and applicable to a certain zone of flow, between turbulent smooth and turbulent rough, of the Moody diagram. Moore (8) introduced a modified Moody diagram with lines of constant exponent "n" varying from 1.7–2.0.] For a given relative roughness e/D and range of flow, "n" can be easily obtained.

The numerical value for the model error term, λ_E, is determined by considering all the fittings (e.g., valves, fire hydrants, and bends). The additional head loss can be accounted for by considering an equivalent pipe length being created by these fittings. The recommended fittings (7) for the pipe under consideration are: 2 Gate Valves, 3 Tees for fire hydrants, and 1 Tee piece for branch mains.

The equivalent lengths of pipe resulting from the presence of the above fittings were determined from the table produced by Hammer (4), and found to be 10.4 m, 18.3 m, and 6.1 m, respectively. Therefore, the total equivalent length is 34.8 m and the model error, λ_E, for the 305 m long pipe is $339.8/305 = 1.1$. Assuming 10% coefficient of variation, Ω_{λ_E}, will be 0.11.

Values of 0.67, −0.64, and 0.67 were obtained for the coefficient of correlation between C_{HW} and Q, C_{HW} and D, Q and D, respectively. The coefficients of correlation between both C_{HW} and Q and Q and D were determined from the values of C_{HW}, Q and D obtained from the variation of C_{HW} for the pipe, using a standard computer program for network analysis (2). The preceding second coefficient of correlation (−0.64) was determined directly from tables established by Williams (9) assuming an age of 20 yr.

Using Eqs. 1 and 2 and the aforementioned coefficient values, a mean value of 18.5 KN/m^2 was obtained for the pressure differential, ΔP, across the pipe, with a coefficient of variation, $\Omega_{\Delta P}$, of 0.337. This implies a standard deviation, $\sigma_{\Delta P}$, of 6.23 KN/m^2.

Criteria for Determining Required Accuracy in Pressure Measurement Devices

From the results obtained using FOA principles, the following criteria are proposed for the determination of the required instrument accuracy for measuring pressure in a field testing program:

1. If the standard deviation of the pressure differential, $\sigma_{\Delta P}$, obtained from FOA is less than the additional pressure differential, $\Delta(\Delta P)$, resulting from the length of time the pipe has been in service, then the measurement devices should have an accuracy capable of providing values in the range of the mean value of the pressure differential, ΔP, ± the standard deviation of the pressure differential, $\sigma_{\Delta P_M}$, obtained from FOA. Expressed mathematically this states:

$$\text{If: } \sigma_{\Delta P_{FOA}} < \Delta(\Delta P)_{FOA} \quad \ldots\ldots\ldots\ldots\ldots\ldots\ldots\ldots\ldots\ldots\ldots\ldots (4)$$

$$\text{Then: } E[\Delta P]_M + \sigma_{\Delta P_M} < E[\Delta P]_{FOA} + \sigma_{\Delta P_{FOA}} \quad \ldots\ldots\ldots\ldots\ldots\ldots\ldots (5)$$

in which E = the expectation operator; and $\sigma_{\Delta P}$ = the standard deviation in the measurement of the pressure differential between points A and B due to errors in the measurement devices located at A and B, such that:

$$\sigma^2_{\Delta P_M} = \sigma^2_{P_A} + \sigma^2_{P_B}$$

2. If the standard deviation of the pressure differential, $\sigma_{\Delta P}$, obtained from FOA is greater than or equal to the additional pressure differential, $\Delta(\Delta P)$, resulting from the length of time the pipe has been in service, then the measurement devices should have an accuracy capable of providing values in the range of the mean value of the pressure differential, ΔP, ± the additional pressure differential, $\Delta(\Delta P)$, resulting from the period of time the pipe has been in service,

obtained from FOA application. Expressed mathematically this states:

$$\text{If: } \sigma_{\Delta P_{FOA}} > \Delta(\Delta P)_{FOA} \quad \ldots\ldots\ldots\ldots\ldots\ldots\ldots\ldots\ldots\ldots\ldots\ldots (6)$$

$$\text{Then: } E[\Delta P]_M + \sigma_{\Delta P_M} < E[\Delta P]_{FOA} + \Delta(\Delta P)_{FOA} \quad \ldots\ldots\ldots\ldots\ldots\ldots (7)$$

Consider now how the results obtained in the preceding from the application of FOA can be used to select accuracy needs in pressure measurement devices for field measurements. If "perfectly" accurate pressure recording gauges were located at the ends of the pipe then with the mean values of the parameters being considered and neglecting the model error term, the analysis of the network will indicate a value of 17.1 KN/m^2 for ΔP. Furthermore, it can be shown that the variance of the measured pressure differential $\sigma_{\Delta P_M}$ is given by (1):

$$\sigma^2_{\Delta P_M} = E^2[(P_A - \bar{P}_A) - (P_B - \bar{P}_B)] \quad \ldots\ldots\ldots\ldots\ldots\ldots\ldots\ldots (8)$$

in which P_A and P_B = the measured pressures at locations A and B respectively; $\bar{P}_A$ and $\bar{P}_B$ = the mean values of measured pressures at A and B. When a 1% accuracy is considered for each pressure gage, the value of $\sigma_{\Delta P_M}$ obtained is 2.76 KN/m^2 and for 2% accuracy, the corresponding value is 5.52 KN/m^2.

From the results plotted in Fig. 1 it follows that pressure gages having a 2% accuracy or better, will provide values of pressure differential, ΔP, within

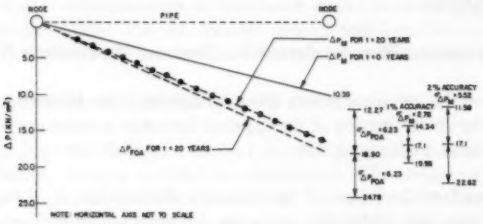

FIG. 1.—Variation of Pressure Differential, ΔP, for Example Pipe

the uncertainty range calculated by FOA (for the example pipe considered). If this accuracy is not attainable, it is recommended that the field experiment be modified, perhaps by increasing the flow through the pipes, or perhaps by modifying the lengths of pipes considered in the field testing program.

It is noteworthy to mention here that the aforementioned FOA method was applied to many existing large networks, including the City of Hamilton water distribution network (Canada). In some cases, the required accuracy for sensible pressure measurements was as high as 0.5% (see Ref. 3 for further details).

Summary and Conclusions

The application of FOA in determining the sensitivity of a particular parameter requires predetermined uncertainties. In this paper, FOA principles were utilized to examine the sensitivity of the pressure differential across a pipe due to uncertainties in the mathematical model, diameter, discharge, hydraulic slope exponent and Hazen-William's coefficient. The results obtained were also utilized to obtain a required accuracy of measurement devices for providing meaningful

results in field measurement of pressure differentials along sections of distribution mains.

In conclusion, this study shows uncertainties in the input data of water distribution networks are substantial, and therefore could lead to meaningless results in the subsequent analysis regardless of the efficiency of the computer program employed; data collection programs must be very carefully designed.

Appendix.—References

1. Benjamin, J. R., and Cornell, C. A., *Probability, Statistics, and Decisions for Civil Engineers,* McGraw-Hill Book Co., Inc., New York, N.Y., 1970.
2. Chandrashekar, M., and Stewart, K. H., "A Program for Analysis of Large Water Distribution System," *Internal Report, Dept. of System Design,* University of Waterloo, Waterloo, Ontario, Canada, Apr., 1974.
3. Clarke, D. A., "Uncertainties in the Analysis of Water Distribution Networks," thesis presented to the University of Waterloo, at Waterloo, Ontario, in 1979, in partial fulfillment of the requirements for the degree of Master of Science.
4. Hammer, M. J., *Water and Waste-Water Technology,* John Wiley & Sons, Inc., New York, N.Y., 1977.
5. Hudson, W. D., "Studies of Distribution System Capacity in Seven Cities," *Journal of the American Water Works Association,* Vol. 58, No. 2, Feb., 1966.
6. Hudson, W. D., "Computerizing Pipeline Design," *Transportation Engineering Journal,* ASCE, Vol. 99, No. TE1, Proc. Paper 9547, Feb., 1973, pp. 73–82.
7. Linsley, R. K., and Franzini, J. B., *Water-Resources Engineering,* McGraw-Hill Book Co., Inc., New York, N.Y., 1972.
8. Moore, W. L., "Relationships Between Pipe Resistance Formulas," *Journal of the Hydraulics Division,* ASCE, Vol. 85, No. HY3, Proc. Paper 1962, Mar., 1959, pp. 25–42.
9. Williams, G. S., and Hazen, A., *Hydraulic Tables,* Third Edition, Revised, John Wiley & Son, Inc., New York, N.Y., 1960, pp. 1–17.
10. Yen, B. C., and Tang, W. H., "Risk-Safety Factor Relation for Storm Sewer Design," *Journal of the Environmental Engineering Division,* ASCE, Vol. 102, No. EE2, Proc. Paper 12016, Apr., 1976, pp. 509–516.

DISCUSSION

Note.—This paper is part of the Journal of the Hydraulics Division, Proceedings of the American Society of Civil Engineers, ©ASCE, Vol. 107, No. HY10, October, 1981. ISSN 0044-796X/81/0010-1271/$01.00.

Discussions

Discussions may be submitted on any Proceedings paper or technical note published in any *Journal* or on any paper presented at any Specialty Conference or other meeting, the *Proceedings* of which have been published by ASCE. Discussion of a paper/technical note is open to anyone who has significant comments or questions regarding the content of the paper/technical note. Discussions are accepted for a period of 4 months following the date of publication of a paper/technical note and they should be sent to the Manager of Technical and Professional Publications, ASCE, 345 East 47th Street, New York, N.Y. 10017. The discussion period may be extended by a written request from a discusser.

The original and three copies of the Discussion should be submitted on 8-1/2-in. (220-mm) by 11-in. (280-mm) white bond paper, typed double-spaced with wide margins. The length of a Discussion is restricted to two *Journal* pages (about four typewritten double-spaced pages of manuscript including figures and tables); the editors will delete matter extraneous to the subject under discussion. If a Discussion is over two pages long it will be returned for shortening. All Discussions will be reviewed by the editors and the Division's or Council's Publications Committees. In some cases, Discussions will be returned to discussers for rewriting, or they may be encouraged to submit a paper or technical note rather than a Discussion.

Standards for Discussions are the same as those for Proceedings Papers. A Discussion is subject to rejection if it contains matter readily found elsewhere, advocates special interests, is carelessly prepared, controverts established fact, is purely speculative, introduces personalities, or is foreign to the purposes of the Society. All Discussions should be written in the third person, and the discusser should use the term "the writer" when referring to himself. The author of the original paper/technical note is referred to as "the author."

Discussions have a specific format. The title of the original paper/technical note appears at the top of the first page with a superscript that corresponds to a footnote indicating the month, year, author(s), and number of the original paper/technical note. The discusser's full name should be indicated below the title (see Discussions herein as an example) together with his ASCE membership grade (if applicable).

The discusser's title, company affiliation, and business address should appear on the first page of the manuscript, along with the *Proceedings* paper number of the original paper/technical note, the date and name of the *Journal* in which it appeared, and the original author's name.

Note that the discusser's identification footnote should follow consecutively from the original paper/technical note. If the paper/technical note under discussion contained footnote numbers 1 and 2, the first Discussion would begin with footnote 3, and subsequent Discussions would continue in sequence.

Figures supplied by the discusser should be designated by letters, starting with A. This also applies separately to tables and references. In referring to a figure, table, or reference that appeared in the original paper/technical note use the same number used in the original.

It is suggested that potential discussers request a copy of the *ASCE Authors' Guide to the Publications of ASCE* for more detailed information on preparation and submission of manuscripts.

CAVITATION INDUCED BY TURBULENCE IN STILLING BASIN[a]

Closure by Rangaswami Narayanan[3]

The writer wishes to thank Blazejewski for his comments. The writer accepts that the method presented is over-simplified for the obvious reason that there are so many uncertain factors. The uncertainties such as the duration of pressure below vapor pressure, the onset of cavitation coincident at p_v itself, and the others listed in the paper, make a rigrous analysis of the criterion for inception of cavitation extremely difficult. Obviously, further research is necessary before a predictive method is developed for the inception in stilling basins dealing with very fast flows. The paper is only a demonstration that spontaneous cavitation in stilling basins is probable.

The writer's assumption with respect to the mean pressure distribution in the hydraulic jump is not all that drastic. The discussor's result regarding the pressure distribution is at variance with the results of Rajaratnam (8). Rajaratnam presents static pressure distribution within the hydraulic jump to show that near the bed for about 5% of the depth the pressure is equivalent to what would be hydrostatic. If at all, the pressure is less than hydrostatic in the body of the hydraulic jump. The deviation from the hydrostatic distribution is concentrated mostly in the earlier part of the jump. But in the region where the pressure fluctuations are most active, the assumption of pressure distribution as assumed in the paper appears sensible.

The discussor argues in the main that the intermittency could be smaller than that deduced in the paper. While accepting the points raised by the discussor, the writer would like to point out that the inception of cavitation as coincident with the existence of vapor pressure is conservative. Clear evidence is now available that the inception occurs at pressures much higher than the vapor pressure at the ambient temperature. Therefore, the intermittency could be larger due to this very reason.

The writer, assuming that the duration of the instantaneous pressures below the level p_v is typically of the same order as the inverse of the dominant frequency of pressure pulsations, finds that t_{pv} could be greater than t_{cr}. Thus, it is appropriate to assume that there is enough time for the bubbles to grow.

The writer is indebted to the discussor for pointing out the errors in the example provided in the paper. Fortunately, the intermittency factor reported remains unaltered.

APPENDIX.—REFERENCE

8. Rajaratnam, N., "The Hydraulic Jump as a Wall Jet," *Journal of the Hydraulics Division*, ASCE, Vol. 91, No. HY5, Proc. Paper 4482, Sept., 1965, pp. 107–132.

[a]April, 1980, by Rangaswami Narayanan (Proc. Paper 15305).

[3]Lect., Dept. of Civ. and Struct. Engrg., Univ. of Manchester Inst. of Sci. and Tech., Manchester, England.

Errata.—The following corrections should be made to the original paper:

Page 618, line 4 from bottom of the page: Should read $y_1 = 1.63$ m; $y_2 = 33.77$ m; $l \simeq 5.7 \times 33.77 = 192$ m; and $y_m = 4.9$ m instead of $y_1 = 1.76$ m; $y_2 = 20.7$ m; $l = 124$ m; and $y_m = 5$ m.

Log Pearson Type 3 Distribution: A Generalized Evaluation[a]

Closure by Donthamsetti Veerabhadra Rao,[3] M. ASCE

The writer would like to thank Hasan for his interest in the paper and for his valuable comments. The writer concurs with the discusser's view that ever since the Water Resources Council (WRC) recommended (5) the use of LP for flood flow frequency analysis in 1967 much knowledge has been added in respect of LP and its fitting procedures.

Until Bobee (1) derived the density function of LP in 1975, the only known procedure (by moments) for fitting LP was through the logarithmic moments (LGMO). Let $Y_i = \ln X_i$, in which $X_i = i$th item of real data. Then the logarithmic SP, mean ($\bar{Y}$), variance (S_y^2), and the coefficient of skewness (CS_y) were calculated from the log data Y_i, and the parameters of LP were estimated from P. (See LGMO method, Ref. 13.) The efforts of different investigators were in the direction of improving this LGMO method; it was recognized that the sample CS_y was biased, and weighting CS_y on the basis of a generalized skew map was suggested (10). Refs. 1 and 13 show that alternative methods of moments are now available for fitting LP to data samples parameters of LP can also be estimated by the moments of real data (RLMO), or by mixing the real and log moments. In the WRC method the coefficient of variation in log space is considered accurate and the logarithmic skew is adjusted. Logically, this consideration applies also to data in real space, i.e., the coefficient of variation of real data may be considered accurate. Thus, there are four sample SP which may be regarded as accurate or less biased, viz., $\bar{X}$, S_x^2, $\bar{Y}$, and S_y^2. Since LP has three parameters to be estimated, it is possible to preserve three of the preceding SP while fitting LP to a sample. This was the concept behind the development of the methods of mixed moments (13). The method MXM1 referred to by the discusser preserves $\bar{X}$, S_x^2, and $\bar{Y}$ of the sample while fitting LP.

Further, with the derivation of the density function of LP by Bobee (1) a direct comparison of the statistical attributes of LP with those of other distributions

[a]May, 1980, by Donthamsetti Veerbhadra Rao (Proc. Paper 15391).

[3]Hydro., St. Johns River Water Management District, P.O. Box 1429, Palatka, Fla. 32077.

has become possible (15). In Ref. 15 the writer analyzed and compared some important properties of four well known three-parameter probability distributions, namely, lognormal, Weibull, *P*, and LP. In this study LP was found to possess some appealing properties (not found in other distributions) in the context of hydrologic data.

With regard to the maximum likelihood (ML) approach to LP, mathematically fitting LP to real data by ML is equivalent to fitting a *P* distribution to logarithmic data by ML. Matalas and Wallis (14) studied at length the ML estimation for the parameters of *P*, and their concluding remarks were:

> —several difficulties related to the properties of the *P* distribution were encountered in deriving both moment and ML estimates. Although these difficulties may not seriously affect the use of this distribution from the point of view of curve fitting, the difficulties are sufficiently troublesome that using other distributions warrants consideration, particularly if ML estimates are of interest.

Bobee and Robitaille (8) express that for *P* distribution ML estimates are not jointly sufficient in which case the method is not optimal for small samples.

TABLE 7.—Mean and Standard Deviation of 100-yr Flood Estimates Based on 1,000 Samples

Sample size (1)	Method (2)	Parameters Set No. 1 Mean (3)	Parameters Set No. 1 Standard deviation (4)	Parameters Set No. 2 Mean (5)	Parameters Set No. 2 Standard deviation (6)	Parameters Set No. 3 Mean (7)	Parameters Set No. 3 Standard deviation (8)	Parameters Set No. 4 Mean (9)	Parameters Set No. 4 Standard deviation (10)
20	MXM1	2.306	0.419	3.079	0.626	2.458	0.643	2.374	0.640
	ML	2.208	0.443	4.025	2.459	2.548	0.695	2.280	0.583
30	MXM1	2.302	0.349	3.074	0.528	2.475	0.538	2.406	0.565
	ML	2.217	0.364	3.298	1.459	2.599	0.622	2.358	0.519
50	MXM1	2.305	0.287	3.086	0.417	2.509	0.446	2.445	0.476
	ML	2.249	0.291	2.994	0.572	2.612	0.489	2.434	0.447
100	MXM1	2.305	0.210	3.072	0.297	2.539	0.331	2.479	0.362
	ML	2.282	0.213	2.995	0.274	2.606	0.339	2.486	0.328
Theoretic		2.315		3.082		2.583		2.559	

The writer has seen some advantages when calculations are performed by using dimensionless data (K_t) in fitting LP by ML. Parameter, c, has a positive sign when LP is bounded upwards and negative sign when bounded in the lower end. When $|c|$ is large the solution is practically equal to that obtained by the two-parameter lognormal. Such an easy interpretation of LP parameters is helpful in obtaining ML estimates. By generally following the procedure described in Ref. 14 the writer obtained ML estimates for the LP data samples generated by Monte Carlo simulation presented in Ref. 13. For the four parameter sets used in the preceding simulation experiments Table 7 presents the mean

and standard deviation (s.d.) of the 100-yr flood estimates based on 1,000 samples. Table 7 shows that for parameters set Nos. 1–2 (γ_y negative) the estimates of MXM1 are less biased and less variable than the ML estimates; for small sample sizes ($n \leq 30$) the ML estimates for several of these samples could be considered unacceptable. When γ_y is positive (parameters set Nos. 3–4) the MXM1 and ML estimates have somewhat balancing attributes. In general, the ML method gives satisfactory estimates only for large samples not commonly found in practice. Thus, MXM1 method which is simpler in its application and gives better estimates compared to the other moments methods as well as ML, is preferable for LP parameter estimation. Complete details of the writer's approach to ML method and the Monte Carlo simulation results will be presented in a separate paper.

Appendix.—References

14. Matalas, N. C., and Wallis, J. R., "Eureka! It Fits a Pearson Type 3 Distribution," *Water Resources Research*, Vol. 9, No. 2, Apr., 1973, pp. 281–289.
15. Rao, D. V., "Three-Parameter Probability Distributions," *Journal of the Hydraulics Division*, ASCE, Vol. 107, No. HY3, Proc. Paper 16124, Mar., 1981, pp. 339–358.

Errata.—The following corrections should be made to the original paper.

Page 854, line 1: Should Read "SP" instead of "of SP"
Page 859, paragraph 1, line 3: Should Read "Note that K_{lb}" instead of "Note that K_{ub}"
Page 860, paragraph 1, lines 5–6: Should read "The K_{ub} values which are less than 1,000-yr K values by LN2 and gamma distributions" instead of "The K_{ub} values, which are less than distributions"
Page 868, paragraph 3, line 7: Should read "K values for a given T; (*a*) Decrease; (*b*) increase and then decrease;" instead of "K values for T (*a*), decrease (*b*), increase and then decrease,"
Page 871, paragraph 2 (of Summary), line 8: Should read "For the upper quantiles," instead of "For the upper quantities.

Characteristics of Low Flows[a]

Closure by the Task Committee on Low Flow-Evaluation, Methods, and Needs of the Committee on Surface-Water Hydrology of the Hydraulics Division

North states that the paper clearly emphasizes the urgency of developing alternatives to the M-day, T-year low flow approach, and he describes a method of characterizing low flow by the duration of negative daily flow runs. That

[a]May 1980, by Task Committee on Low-Flow Evaluation, Methods, and Needs of the Committee on Surface-Water Hydrology of the Hydraulics Division (Proc. Paper 15400).

method should be further developed so that its utility can be assessed. One weakness appears to be that few runs are available for defining the frequency curves of runs for low values of threshold flow.

A study report by the Institute of Hydrology (43) defines a low flow spell either as the length of period that the flow is continuously below a threshold or as the deficit volume that would be required to maintain the flow at threshold. Frequency curves of these are prepared for various threshold discharges.

Alternatives to the M-day, T-year low flow are needed because no one descriptor of low flow characteristics is suitable for all hydrologic applications. Our paper pointed out, conclusion 4, that hydrologists should determine the most suitable ways of using low flow information for various applications and then provide that information in suitable form. First identify the needs and then develop the tools.

We appreciate North's contribution to the Task Committee report.

Appendix.—Reference

43. *Reports 1–3,* Institute of Hydrology, Low Flow Studies, Institute of Hydrology, Wallingford, Oxon, England, 1979, 143 pp.

Boundary Layers in Developing Open Channel Flow[a]

Closure by Edward Silberman,[3] F. ASCE

Wilson may have misread the problem posed in the paper. The analysis was undertaken to deal with cases where conventional boundary layer calculation methods are not applicable; some examples of such flows were cited in the paper. The analysis specifically applies when the discusser's Eqs. 9 and 10 cannot be used. (It is also applicable when they can be used.) Also, despite the discusser's claim to the contrary, displacement thickness as given by Eq. 2 is positive definite under the conditions stated on the third line from the bottom of page 1237 of the paper. Displacement thickness enters into the definition of critical depth via Eqs. 1 to 4 and not because the writer added it arbitrarily.

As mentioned in the final paragraph of the paper, if one wishes to calculate the drop in the specific energy line, then it is necessary to use coefficients like those used by Jaeger (10). However, for estimating changes in depth and mean velocity in complex developing flows, it is much simpler to guess a value of displacement thickness than it is to guess these other coefficients; this is the crux of the argument in the paper. If the discusser believes he can treat complex developing flows by the method he advocates, let him reproduce Kindsvater's data (8) as was done by the writer and shown in the inset of Fig. 2.

[a]July, 1980, by Edward Silberman (Proc. Paper 15516).

[3]Prof., St. Anthony Falls Hydraulic Laboratory, University of Minnesota, Minneapolis, Minn. 55414.

Bar Resistance of Gravel-Bed Streams[a]

Discussion by James C. Bathurst[7]

The authors are to be congratulated on tackling the problem of flow resistance at low flows in gravel-bed rivers since so often previous work has concentrated on conditions at bankfull flows. However, while the authors' approach makes a useful start on the problem the result is, as noted, an empirical formulation for a bulk bar resistance which is subject to uncertainties, typified by the scatter in Fig. 5 and by the slightly arbitrary criterion that, once sediment movement begins, bar resistance is negligible. In order to produce a more generally applicable equation it will eventually be necessary to consider the processes by which bar resistance is generated and this writer would therefore like to comment on the processes most likely to be of importance.

Firstly, in addition to the bar and grain resistances there are resistance components related to channel cross-sectional shape, secondary circulation and nonuniform shear stress distribution (10,40). Consequently, it is an approximation to assign all the resistance other than grain resistance to the influence of bars, as the authors have done. However, at low flows bar resistance may well be the most important of the nongrain resistances so the approximation may be acceptable.

Secondly, it may be conjectured that there are two main processes by which bars increase the flow resistance. The first is the ponding effect of the bars or riffles which, because the longitudinal bed profile is nonuniform, can act as controls on the flow in the pools, keeping those flows deeper and slower than would otherwise be the case. The second resistance is the result of the shallow flow over the bars or riffles which is characterized by features of large-scale roughness and an increased resistance to flow. As pools are usually longer than riffles and as ponding usually retards the flow more than does large-scale roughness, the contribution of the riffle flow to the overall resistance of a river reach is less than that of the ponding effect in the pools, although of course the grain resistance of the riffles is higher than that of the pools. Both resistance effects diminish as depth increases.

Means of accounting for large-scale roughness are discussed elsewhere (39) so only the ponding effect is considered here. It is proposed that this be quantified using the residual depth, or the depth in a pool when discharge is zero. Because this residual depth exists, the depth at a given discharge is greater than it would be for the same discharge over the same bed material with a uniform bed profile, while the mean velocity is lower. However, as discharge and depth increase, the ratio of residual depth to actual depth decreases and consequently the relative effect of the residual depth (i.e., the degree of ponding) decreases.

The possibility of using residual depth to account for the major portion of

[a]October, 1980, by Gary Parker and Allan W. Peterson (Proc. Paper 15733).

[7]Sr. Scientific Officer, Inst. of Hydrology, Wallingford, Oxon, United Kingdom.

bar resistance is illustrated here using data from the upper River Swale in England (38). The data were collected from a reach of channel 1,100 m (3,609 ft) long (containing 8 pool/riffle units) at three discharges. Average value of D_{84} for the bed material [based on 19 Wolman-style samples (41)] is 132 mm (0.433 ft), average channel slope is 0.0027 and channel width is in the range 17 m–20 m (55.8 ft–65.6 ft). The reach-averaged residual hydraulic radius I_0 (or hydraulic radius at zero discharge) was obtained by back extrapolation on a linear plot of average reach hydraulic radius I against discharge Q, giving the value of I (=0.2 m or 0.656 ft) at which Q = zero. This method is rather approximate given only three data points but the value so derived is suitable for illustrative purposes.

Following the authors assumption that flow resistance in the absence of bars consists mainly of grain resistance, hypothetical values of discharge Q_G were calculated for the three flows as if only grain resistance were present. For this calculation the Hey equation (10), rather than Eq. 2, was used since it has given good results in the field:

$$Q_G = 5.62\, A\,(gIS)^{1/2} \log\left(\frac{aI}{3.5\, D_{84}}\right) \quad \ldots\ldots\ldots\ldots\ldots\ldots\ldots\ldots \quad (22)$$

in which A = flow cross-sectional area; g = acceleration due to gravity; S = channel slope; and a = a channel shape parameter. If bar resistance were negligible it would be expected that Q and Q_G would be approximately equal, so the ratio Q/Q_G was calculated as a rough (inverse) measure of the effect of bar resistance. Also, if bar resistance does depend largely on residual depth it would be expected that the magnitude of the resistance would be an inverse function of the ratio $(I - I_0)/I$. Then, assuming that other resistances are negligible the two ratios (given in Table 1) should vary in a related manner, although not necessarily at the same rate. Thus, with $Q = 0$, and therefore $I = I_0$, both ratios are zero. As discharge rises, the bars become drowned out (i.e., $I_0 << I$), grain resistance becomes the most important resistance (i.e., $Q \rightarrow Q_G$) and both ratios should tend to unity. The results in Table 1 support this hypothesis as far as they go but, as the data are few, the possible influence of other reistances cannot be gauged. Nevertheless there seems to

TABLE 1.—Average Flow Parameters for River Swale Field Site

Measured discharge, Q, in cubic meters per second (1)	Calculated discharge, Q_G, in cubic meters per second (2)	Reach-averaged hydraulic radius, I, in meters (3)	Q/Q_G (4)	$(I - I_0)/I$ (5)
0.70	2.38	0.31	0.30	0.35
4.36	8.25	0.54	0.53	0.63
7.84	11.24	0.62	0.70	0.68

Note: 1 m = 3.281 ft; 1 m^3 = 35.3 cu ft.

be a good possibility that bar resistance could be calculated directly from the residual depth (the primary source of the resistance), which would be more satisfactory than deriving it from shear stress criteria which are less directly related to the process involved. Considerably more experimental data, though, will be needed to bring this idea to fruition.

Appendix.—References

38. Bathurst, J. C., "Resistance to Flow in Rivers with Stony Beds," thesis presented to the University of East Anglia, at Norwich, England, in 1977, in partial fulfilment of the requirements for the degree of Doctor of Philosophy.
39. Bathurst, J. C., "Flow Resistance of Large-Scale Roughness," *Journal of the Hydraulics Division*, ASCE, Vol. 104, No. HY12, Proc. Paper 14239, Dec., 1978, pp. 1587–1603.
40. Bathurst, J. C., "Theoretical Aspects of Flow Resistance," presented at the 22–28 June, 1980, University of East Anglia (United Kingdom)/Institute of Hydrology (United Kingdom)/Colorado State University International Workshop on Engineering Problems in the Management of Gravel-Bed Rivers, held at Gregynog, Newtown, Wales, United Kingdom. (Proceedings in press with John Wiley and Sons, Inc., New York, N.Y.)
41. Wolman, M. G., "A Method of Sampling Coarse River-Bed Material," *Transactions*, American Geophysical Union, Vol. 35, No. 6, Part 1, Dec., 1954, pp. 951–956.

Approximate Analysis of Unsteady Laminar Flow[a]

Discussion by Mario F. Letelier S.,[3] and Hans J. Leutheusser,[4] M. ASCE

The authors address a problem which has already received some attention in the recent technical literature (e.g., 7). In particular, they propose an approximate method of analysis for unsteady laminar closed-conduit flow based on the classical assumption of quasi-steady friction. According to this assumption, the flow is at any instant subject to the corresponding steady-state friction.

In order to properly assess the validity of the authors' equation of motion, viz. Eq. 5, it is convenient to write it in nondimensional form, i.e.

$$8Q^* + \Omega \frac{dQ^*}{dt^*} = \Delta p^* \quad \ldots\ldots\ldots\ldots\ldots\ldots\ldots\ldots\ldots\ldots\ldots\ldots \quad (32)$$

in which $Q^* = Q/Q_0$; $t^* = t/T_0$; $\Delta p^* = \pi R^4 \Delta p/\rho L \nu Q_0$; and Q_0 and T_0 are reference values of Q and t, respectively. Furthermore,

$$\Omega = \frac{R^2}{\nu T_0} \quad \ldots\ldots\ldots\ldots\ldots\ldots\ldots\ldots\ldots\ldots\ldots\ldots\ldots\ldots \quad (33)$$

---

[a]December, 1980, by David Stavitsky and Enzo Macagno (Proc. Paper 15922).

[3]Prof., Departamento de Mecánica, Facultad de Ingeniería, Universidad Técnica del Estado, Santiago, Chile.
[4]Prof., Dept. of Mech. Engrg., Univ. of Toronto, Toronto, Ontario, M5S 1A4, Canada.

is an "unsteadiness number," which can, for instance be interpreted as the ratio between some "pipe-fluid" time, i.e., R^2/ν, and an external "forcing" time T_0. Clearly, when $\Omega \to 0$, Eq. 1 reduces to its steady-state equivalent.

A more general and exact form of the one-dimensional momentum equation than Eq. 32 can be deduced from the Navier-Stokes equation. Thus, for parallel flow of an incompressible Newtonian fluid, there holds

$$\frac{\partial u}{\partial t} - \nu\left(\frac{\partial^2 u}{\partial r^2} + \frac{1}{r}\frac{\partial u}{\partial r}\right) = -\frac{1}{\rho}\frac{\Delta p}{L} \quad \ldots\ldots\ldots\ldots\ldots\ldots \quad (34)$$

in which $u = u(r,t)$ is the local axial velocity which is a function of the radial co-ordinate r and time t.

After some manipulations (5,6), Eq. 34 can be transformed into a series expression, viz.

$$Q^* + \frac{\Omega}{2^2}\frac{dQ^*}{dt^*} + \frac{\Omega^2}{2^2 \cdot 4^2}\frac{d^2Q^*}{dt^{*2}} + \ldots = \frac{1}{4}\left(\frac{\Delta p^*}{2} + \frac{\Omega}{24}\frac{d\Delta p^*}{dt^*} + \frac{\Omega^2}{768}\frac{d^2\Delta p^*}{dt^{*2}} + \ldots\right) \quad \ldots\ldots\ldots\ldots \quad (35)$$

which is valid for any value of Ω. A somewhat simpler form of Eq. 35 which, however, converges only up to certain values of Ω is the following:

$$8Q^* + \frac{4}{3}\Omega\frac{dQ^*}{dt^*} - \frac{r^2}{144}\frac{d^2Q^*}{dt^{*2}} + -\ldots = \Delta p^* \quad \ldots\ldots\ldots\ldots\ldots \quad (36)$$

The authors' model, Eq. 32 of this discussion, is obviously a shortened version of 36 with an incorrect coefficient for the first time-derivative of Q^*. In the light of Eqs. 35 or 36, this model can be expected to yield acceptable results only for small values of Ω, i.e., when all terms of second and higher order in series Eqs. 35 and 36 are negligibly small. One interesting exception exists for $\Omega = \infty$. In this case, Eq. 32 transforms into the inviscid (i.e., ideal flow) form of Eq. 34, viz.

$$\frac{du}{dt} = \frac{1}{\pi R^2}\frac{dQ}{dt} = -\frac{1}{\rho}\frac{\Delta p}{L} \quad \ldots\ldots\ldots\ldots\ldots\ldots\ldots\ldots \quad (37)$$

When applied to the case "Starting Flow in Pipe," the authors' model, Eq. 32, predicts a time of flow establishment to 99% of the ultimate, steady-state rate of flow, which is in error by 27% relative to the exact time (6). On the other hand, if this time were computed from Eq. 35, or even from Eq. 36 using only the first two terms on the left-hand side, then any error would be negligible. The reason for this behavior derives from the fact that a "starting flow" involves large acceleration at small time and, therefore, many time-derivatives are necessary to correctly describe the motion at its beginning.

In the second example given in the paper, viz. "Oscillatory Flow in Pipe," the authors' model reproduces exact results for both $\Omega \to 0$ and $\Omega \to \infty$, i.e., for "steady state" and "ideal flow," respectively. Nevertheless, for other values of Ω, Eq. 32 does entail considerable error. Thus, according to computations by the discussers, Eq. 32 yields, e.g., for $\Omega \simeq \omega^* = 64$ an amplitude which

is in error by 17% relative to the exact value. And this error can be still larger for other values of Ω (5). On the other hand, Eq. 35 reproduces the exact solution for all values of Ω, while Eq. 36 reproduces it up to $\Omega = 5.783$.

Other case studies, such as U-tube oscillations (7) and transient capillary rise (8), show that the predictions of the authors' model will invariable entail nonnegligible errors. Nevertheless, the discussers readily concede that equations of the form of Eq. 32 are very convenient for obtaining a first, rough assessment of a particular transient flow problem. However, and especially when large accelerations exist in the flow, more precise computations call for the use of equations such as Eq. 35 or 36.

Appendix.—References

5. Letelier, S., M. F., *"An Approach to the Analysis of Unsteady Parallel Flow in Circular Pipes,"* thesis presented to the University of Toronto, at Toronto, Ontario, Canada, in 1979, in partial fulfillment of the requirements for the degree of Doctor of Philosophy.
6. Letelier, S., M. F., and Leutheusser, H. J., "Unified Approach to the Solution of Problems of Unsteady Laminar Flow in Long Pipes," *Fluid Transients and Acoustics in the Power Industry*, C. Papadakis and H. Scarton, eds., The American Society of Mechanical Engineers, 1978, pp. 207–213.
7. Letelier S., M. F., and Leutheusser, H. J., "Skin Friction in Unsteady Laminar Pipe Flow," *Journal of the Hydraulics Division*, ASCE, Vol. 102, No. HY1, Proc. Paper 11867, Jan., 1976, pp. 41–56.
8. Letelier S., M. F., Leutheusser, H. J., and Rosas, Z. C., "Refined Mathematical Analysis of the Capillary Penetration Problem," *Journal of Colloid and Interface Science*, Vol. 72, No. 3, Dec., 1979, pp. 465–470.